JAERI-M
84-188

ASSESSMENT OF THE THYDE-B1/MOD 0 CODE WITH DATA FROM ROSA-III LOSS-OF-COOLANT EXPERIMENTS

October 1984

Masanori IRIKO*, Yutaka KUKITA
and Kanji TASAKA

日本原子力研究所
Japan Atomic Energy Research Institute

JAERI-Mレポートは，日本原子力研究所が不定期に公刊している研究報告書です。
入手の問合わせは，日本原子力研究所技術情報部情報資料課（〒319-11茨城県那珂郡東海村）あて，お申しこしください。なお，このほかに財団法人原子力弘済会資料センター（〒319-11 茨城県那珂郡東海村日本原子力研究所内）で複写による実費頒布をおこなっております。

JAERI-M reports are issued irregularly.
Inquiries about availability of the reports should be addressed to Information Division Department of Technical Information, Japan Atomic Energy Research Institute, Tokai-mura, Naka-gun, Ibaraki-ken 319-11, Japan.

編集兼発行　日本原子力研究所
印　　刷　いばらき印刷㈱

JAERI-M 84-188

Assessment of the THYDE-B1/Mod 0 Code with Data from ROSA-III Loss-of-Coolant Experiments

Masanori IRIKO*, Yutaka KUKITA and Kanji TASAKA

Department of Nuclear Safety Research,
Tokai Research Establishment, JAERI

(Received September 20, 1984)

The calculational capability of the THYDE-B1 (Mod 0) computer code, a fast-running best-estimate code for prediction of thermal-hydraulic response of a boiling water reactor during a loss-of-coolant accident, was assessed against test data from ten runs of ROSA-III recirculation-line break tests, where break area was changed parametrically from 0 to 200%. The overall system response during these tests was well reproduced by the code, however, the datailed response was not reproduced correctly because of various simplified assumptions in the code, e.g., neglecting the core-spray cooling effets. Discrepancy between the calculated and measured responses was observed particularly for:

(1) the time of initiation of steam discharge through the automatic depresurization system for small breaks (<5%),

(2) in-vessel steam generation due to flashing of coolant and vaporization of emergency core cooling water for intermediate and large breaks (≧5%), and

(3) rod surface heat transter regimes for large breaks (>50%).

The calculation reproduced PCTs for the small breaks, but underpredicted PCTs for the intermediate breaks. The calculated rod temperature behaviors for the large breaks were qualitatively different from the data.

Keywords: BWR, LOCA, ECCS, ROSA-III, THYDE-B1, PCT, Break Size, Code Assessment

---

* On leave from Computer Service Co. (CSK)

JAERI－M 84－188

ROSA－Ⅲ冷却材喪失実験によるTHYDE－B1／Mod Oコードの評価

日本原子力研究所東海研究所安全工学部
入子真規*・久木田豊・田坂完二

（1984年9月20日受理）

本報は，日本原子力研究所で開発された，沸騰水型原子炉の冷却材喪失事故時熱水力挙動の解析のための計算コードTHYDE－B1の性能評価に関するものである。ROSA－Ⅲ実験装置による10ランの再循環ポンプ入口側配管破断実験（破断面積＝0～200％）をTHYDE－B1コードで解析し，その結果を実験結果と比較することによりコードの性能評価を行った。

計算結果は，実験中の基本的な熱水力挙動を定性的に再現した。しかし，解析モデルが単純化されているため，以下の点について計算結果と実験結果の相違がみられた。(1) 小破断実験（＜5％）における自動減圧系の動作時刻，(2) 中・大破断実験（≧5％）における圧力容器内の減圧沸騰およびECC水の沸騰による蒸気発生，および(3) 大破断実験（＞50％）における被覆管表面伝熱様式。

被覆管最高温度（PCT）は，小破断実験では良好に再現されたが，中破断実験では一般に過小評価された。大破断実験における被覆管表面温度の計算結果は，実験結果と定性的に異る挙動を示した。

---

* 出向職員：コンピューターサービス（株）

CONTENTS

目　　次

List of Tables

List of Figures

1. Introduction

The Japan Atomic Energy Research Institute (JAERI) conducted the Rig of Safety Assessment (ROSA)-Ⅲ program from April 1978 to March 1984 to investigte thermal-hydraulic response of a boiling water reactor (BWR) during a postulated loss-of-coolant accident (LOCA). A broad spectrum of accidental conditions were tested. These tests provided a significant data base for code assessment and development.

The ROSA-Ⅲ facility was designed to simulate the BWR thermal-hydraulic response on real-time basis, however, several scaling compromises involved in the facility design may have limited the similarity between the ROSA-Ⅲ and BWR thermal-hydraulic responses and hence limited applicability of the ROSA-Ⅲ test results to an actual BWR. Such Scaling compromises included a half-length core, smaller-than-scaled initial core power, larger-than-scaled structure heat tranfer area, and distorted downcomer/jet pump geometry.

The similarity between ROSA-Ⅲ and the reference BWR has been investigated using computer codes. The approach taken has been either to compare analytical results obtained for BWR and ROSA-Ⅲ, or to compare analytical results for BWR with ROSA-Ⅲ test data.

The similarity for large (200%) and relatively small (5%) breaks has been investigated using the RELAP 4/Mod 6/U4/J3 code.[1][2] This study concluded that ROSA-Ⅲ well represented major BWR thermal-hydraulic responses.

The THYDE-B1 code[3] also has been used for the similarity study. The THYDE-B1 code is a fast-running code developed by JAERI for best-estimate calculation of BWR small- and intermediate-break LOCAs. The calculational capability of THYDE-B1 (Mod 0) has been assessed against ROSA-Ⅲ test data obtained from a 5% break test (Run 804).[4]

This report documents an extensive assessment of the THYDE-B1 (Mod 0) code. Data obtained from ten ROSA-Ⅲ tests where break area was changed parametrically from 0 to 200% are used. The assessment described herein provides a basis for, and defines limitation of, the ROSA-Ⅲ/BWR similarity study to be made using the THYDE-B1 code.

In the following Sections, first the ROSA-Ⅲ tests analyzed are outlined in Section 2. The computer code (THYDE-B1), models, and the analytical conditions are described in Section 3. Comparisons between the analytical results and ROSA-Ⅲ test data are presented in Section 4. The conclusions are given in Section 5.

2. Test Description

2.1 ROSA-Ⅲ Test Facility

The ROSA-Ⅲ facility[5] was a volumetrically scaled (1/424) model of a General Electric BWR/6-251 (1100 MWe) system.[6] The outline of the facility is shown in Fig. 2.1. The major design characteristics of the ROSA-Ⅲ facility and the reference BWR are compared in Table 2.1.

The test facility design objective was to represent, on a real-time basis, thermal-hydraulic performance of a BWR system during a psstulated LOCA. Major BWR components which would influence LOCA/emergency core cooling (ECC) phenomena were represented. The represented components included a pressure vessel, vessel internals, two recirculation lines each with a simulated recirculation pump, a feedwater system, a main steam system and emergency core cooling systems (ECCS). The simulated pressure vessel (Fig. 2.2) modeled the lower plenum, the core bundles and bypass region, the upper plenum, the steam separator, the downcomer, and the steam dome. The volumes of these regions were scaled as correctly as practicable.

The ROSA-Ⅲ core consisted of four half-length bundles. This core design enabled investigating the thermal-hydraulic interactions among the bundles, and was the basis for scaling of the test facility.

Each of the four core bundles comprised 62 electrically heated rods and two water rods spaced in a 8×8 square array as shown in Figs. 2.3 and 2.4. The prototypical rod diameter and array geometry were preserved. The axial power distribution along a heated rod was chopped-cosine with an axial peaking factor of 1.4 (Fig. 2.5). The power input to the simulated peak-power bundle (Bundle A) was 1.4 times as large as that to each of other bundles (Bundles B, C and D) which simulated average-power bundles. The radial power distribution within each bundle corresponded to a local peaking factor of 1.1.

Because of the half-length core, the steam generation rate per rod was one half of that in the reference BWR. Consequently, the upper tieplate flow area was reduced to one-half of the scaled area to approximately preserve the core exit counter-current flow limitting (CCFL) conditions.

The capacity of the core electric power supply was 4.24 MW, which was 47% of the volume-scaled (1/424) reference BWR rated core power.[6]

The jet pumps were located outside the pressure vessel, whereas the BWR jet pumps are located in the vessel downcomer. This was necessary to conserve the volume scaling and relative elevations of the jet pumps and downcomer.

The ECCS in the ROSA-Ⅲ facility simulated the high pressure core spray system (HPCS), the low pressure core spray system (LPCS), the low pressure coolant injection system (LPCI) and the automatic depressurization system (ADS). The simulated ECC systems were designed to provide scaled ECC flow rates as functions of system pressure. The ADS, a backup system of HPCS, was simulated by a valve and a flow-limiting orifice in the simulated main steam line. The ECCS trip logics were identical to those of the reference BWR.[6]

The simulated main steam line had three branches as shown in Fig. 2.6. Only the first and second branches were used in the tests analyzed herein. The first branch had a control valve (CV-130) which was used to maintain the initial steady-state system pressure and also to simulate the operation of the pressure control system, the satety relief valves (SRVs) and the main steam isolation valves (MSIVs).

2.2 Test Conditions and Experimental Procedure

The test conditions of the ten tests analyzed in this report are summarized in Table 2.2. The tests[7] were conducted changing the break area parametrically; the tested break areas were 0, 1, 2, 5, 15, 25, 50, 75, 100, and 200% of the scaled (1/424) piping crosssectional area at the recirculation pump inlet line of the reference BWR. The 1% through 100% break tests simulated a split break at the recirculation pump inlet line. The 200% break test simulated a double-ended break at the same location. The 0% break test simulated a non-LOCA transient initiated by reactor scram without piping rupture.

The test initial conditions were almost identical for all the tests. The steam dome pressure was 7.35 MPa, corresponding to a saturation temperature of 562 K. The steady state core power was ∿4 MW, corresponding to a maximum linear heat rate (MLHR) of ∿16.7 kW/m.

The downcomer liquid level signals were used to trip closure of the MSIV and to actuate ECCS as is the case in the reference BWR. The downcomer initial liquid level was ∿5.0 m above the vessel bottom. With

this liquid level, the fluid volume in the downcomer was correctly scaled to the volume below the scram level (L3 level) in the reference BWR.[6] Similarly, the L2 and L1 levels in the ROSA-III downcower were 4.76 and 4.25 m, respectively. The closure of MSIV was tripped by an L2-level signal with a time delay of 3 s. The LPCS, LPCI and ADS were actuated by an L1-level signal with delays of 40, 40 and 120 s, respectively. These time delays are those assumed in plant safety analyses.[6] The LPCS and LPCI injection pressures were 2.2 and 1.6 MPa, respectively.[6] The HPCS was assumed to be inactive. The failure of HPCS represents the severest single failure of ECCS.[8]

Reactor scram was assumed to occur at the time of break. However, as shown in Fig. 2.7, the initial core power (∿44% of the scaled BWR rated power) was maintained for approximately 9 s after the break, when the core power per unit fluid volume matched with that of the reference BWR.[6]

Recirculation pumps were tripped off at the time of break.

The feedwater line valve was throttled from 2 s after the break until it was closed completely at 4 s.

The control valve CV-130 in the main steam line was manually opened full at the time of break. This increased steam discharge flow rate to ∿15% above the initial value. Then CV-130 was automatically throttled to simulate the operation of the pressure control system which is designed to maintain the system pressure above 6.7 MPa. The valve CV-130 was automatically closed from 3 s after the generation of an L2-level signal to simulate the MSIV closure. Thereafter, CV-130 also simulated SRVs by maintaining the system pressure below 8.1 MPa. The simulated ADS valve, AV-169, was opened at 120 s after the generation of an L1-level signal.

2.3 Test Results

The system pressure transients, measured in the steam dome, are shown in Fig. 2.8 for all the ten tests with break areas ranging from 0 to 200%. The system initially depressurized due to discharge through the break and main steam line. The initial depressurization was arrested at 6.7 MPa for the breaks ≦5% by the operation of the simulated pressure control system. The system repressurized after the simulated MSIV closure, which was tripped by an L2-level signal with a time delay of

3 s. For the breaks ≧15%, MSIV closed before the system pressure decreased to the pressure control system's setpoint of 6.7 MPa. The simulated SRV opened for breaks ≦5% as system pressure exceeded the setpoint of 8.1 MPa.

For the small breaks (<5%), system depressurization started again when ADS was actuated by an L1-level signal. For the large and intermediate breaks (≧5%), system depressurization started again when the inlet of the broken recirculation line open to the downcomer was uncovered and steam began to leak from the break.

The in-vessel two-phase mixture levels measured by conductivity probes are shown in Figs. 2.9 and 2.10 for the 1% and 100% breaks, respectively. The system pressure and cladding temperatures along a peak-power rod are also shown for comparison. For the 100% break test, the downcome mixture level began to drop immediately after the break, and the level inside the shroud followed this. However, for the 1% break the downcomer mixture level stayed above the highest probe elevation (3.325 m) throughout the test.

The lower plenum fluid initiated to flash to steam when the system pressure decreased to 6.4 MPa, approximately the saturation pressure at the lower plenum fluid initial temperature. The lower plenum flashing (LPF) temporarily raised core mixture level and thus terminated the early dryout in the upper core region (see Fig. 2.10(c)).

The core mixture level decreased and the whole core was exposed eventually to steam environment as the surge of LPF weakened. The rod surface dryout and resultant temperature excursion propagated from the top to bottom of the core, as the core mixture level receded (see Figs. 2.9(c) and 2.10(c).

The low pressure core spray system (LPCS) and the low pressure coolant injection system (LPCI) operated at system pressures below 2.2 and 1.6 MPa, respectively. The LPCS sprayed water on the top of the core. The LPCI injected water into the core bypass region.

For the breaks ≦1%, the whole core was refooded by LPCS alone, before the initiation of the LPCI flow. For larger breaks (≧2%), reflooding of the whole core occurred only after the initiation of the LPCI flow. The difference between the core mixture levels in the average-power and peak-power channels was generally small.

After the LPCS flow initiated at a system pressure of ∿2.2 MPa, the system depressurization became slower because the injection of LPCS

water onto the top of the core augumented in-vessel steam generation.

Approximately at the LPCS injection pressure of 2.2 MPa, fluid in the feedwater line began to flash. This wes known from two-phase inflow detected by a flowmeter in the feedwater line. The feedwater line flashing (FLF), together with the in-vessel steam generation due to the vaporization of LPCS water, slowed the system depressurization, and therefore delayed the initiation of the LPCI flow. It is interesting to note that the core emptying was temporarily accelerated when the system depressurization rate decreased after the initiation of the LPCS flow and FLF, probably because of decrease in the steam generation rate in the mixture region.

The heater rod surface temperature was measured at seven elevations (Positions 1 through 7) indicated in Fig. 2.5. The rod surface temperatures showed clear correspandence with the core mixture level behavior as shown in Figs. 2.9(c) and 2.10(c). Namely, temperature excursion occurred as the rod surface was dried out, and was terminated as the rod surface was reflooded. The exeptions were temperatures at upper core elevations where, particularly for the smaller breaks, temperature turnaround occurred due to the spary (LPCS) flow on the top of the core, before reflooding.

Figure 2.11 shows rod surface temeratures for all the ten tests. Temperatures at thermocouple locations where PCT occurred in each test are shown. The temperature behavior after the dryout is of particular interest. The effect of LPCS was pronounced for the breaks $\leqq$25%, for which the rod surface heatup rate decreased shortly after the initiation of the LPCS flow.

Figure 2.12 summarizes the timings of major events in all the ten tests. The times of dryout (uncovering), reflooding and quenching at the location where PCT occurred in each test are shown. From this figure, the following observations are derived.

(1) For the 0 and 1% breaks, PCT occurred immediately after the initiation of the LPCS flow. The PCT occurred at position 3 (353 mm above the core midplane) on a peak-power rod. The rod surface at position 3 was quenched under the effect of the top spray (LPCS) alone, before the mixture level reached that elevation.

(2) For the 2 and 5% breaks, PCT occurred shortly before, or at the same time as, the initiation of the LPCI flow. The temperature turnaround occurred under the effect of LPCS alone, as the core power

decayed. The PCT occurred at position 4 (the core midplane). Quenching at that elevation occurred after the arrival of mixture level (reflooding) after the initiation of the LPCI flow.

(3) For the larger breaks (15, 25, 50, 75, 100 and 200%), the temperature turn-around occurred after the initiation of the LPCI flow, due to reflooding. The effect of the top spray (LPCS) cooling became less and less pronounced as the break size was increased.

The measured PCTs, the times when the PCT occurred and the locations where the PCTs occurred are listed in Table 2.3. The PCTs occurred in all the test on peak-power rods (having a local peaking factor of 1.1) in the peak-power bundle.

Table 2.1 Primary characteristics of BWR/6 and ROSA-III

	BWR*	ROSA-III	BWR/ROSA-III
Number of Recirc. Lines	2	2	1
Number of Jet Pumps	24	4	6
Number of Separators	251	1	251
Number of Fuel Assemblies	848	4	212
Active Fuel Length (m)	3.76	1.88	2
Total Volume (m^3)	621	1.42	437
Power (MW)	3,800	4.40	864
Pressure (MPa)	7.23	7.23	1
Core Flow (kg/s)	1.54×10^4	36.4**	424
Recirculation Flow (l/s)	2,970	7.01**	424
Feedwater Flow (kg/s)	2,060	4.86**	424
Feedwater Temp. (K)	489	489	1

* BWR/6-251

** Maximum Rated

Table 2.2 Test Conditions

Break Area (%)	Tect ID.	Initial Conditions					Simulation of Pressure Control System	Date of Performance
		Core Power (MW)	Lower Plenum Subcooling (K)	Core Exit Quality (%)	Core Inlet Flow (kg/s)	Downcomer Collapsed Level (m)		
0	923	3.962	10.3	15.8	16.4	5.00	YES	81. 9.25
1	921	3.976	10.4	15.8	16.4	5.09	YES	81. 9.11
2	920	3.962	10.3	15.7	16.5	5.00	YES	81. 9. 4
5	922	3.962	10.5	15.8	16.4	5.00	YES	81. 9.18
15	913	3.964	11.1	14.7	16.4	5.00	NO	81. 5.28
25	930	3.960	10.1	16.3	16.1	5.04	YES	82. 2.18
50	916	3.963	10.8	14.3	16.5	5.05	NO	81. 6.18
75	929	3.966	10.3	16.0	16.2	5.05	YES	82. 2.12
100	914	3.972	11.3	14.5	16.2	5.03	NO	81. 6. 3
200	926	3.967	10.0	16.1	16.3	5.05	YES	81.10.29

Table 2.3 List of peak cladding temperatures

Break Area (%)	PCT (K)	Time (s)	Position	Rod
0	637	696	P3[a]	A11
1	754	546	P3	A87
2	804	531	P4[b]	A68
5	835	410	P4	A17
15	846	336	P4	A82
25	872	274	P4	A71
50	925	189	P4	A82
75	885	154	P4	A71
100	832	133	P4	A11
200	785	119	P4	A71

[a] 353 mm above the core midplane.

[b] core midplane.

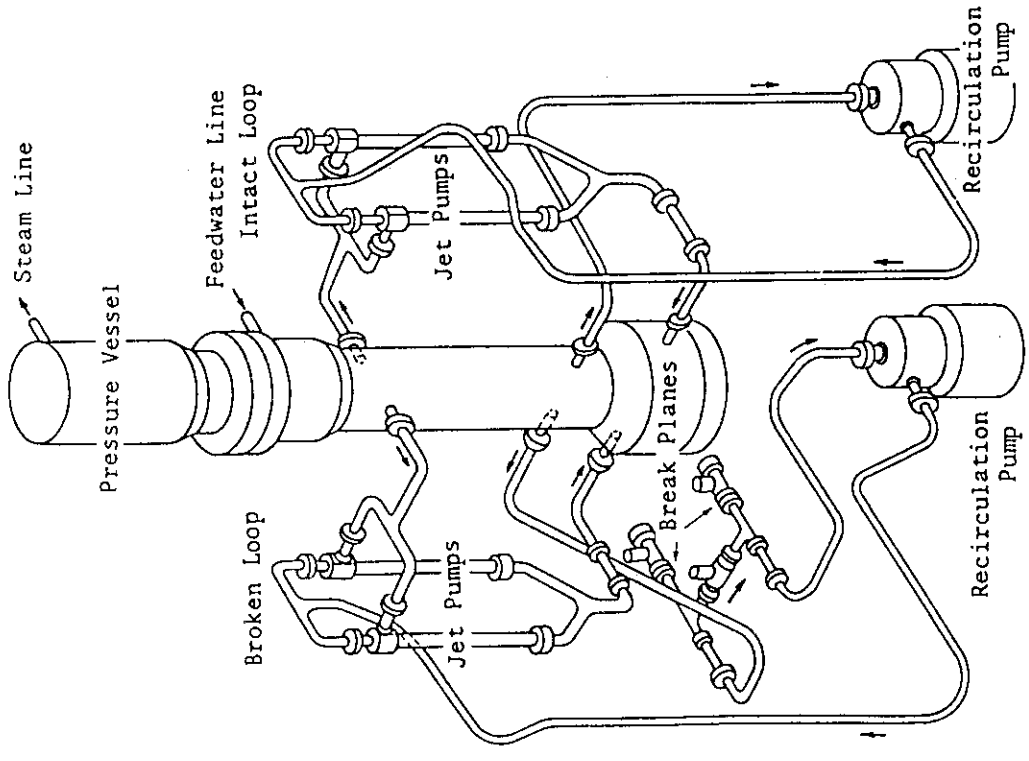

Fig. 2.1 Schematic Diagram of ROSA-III Test Facility

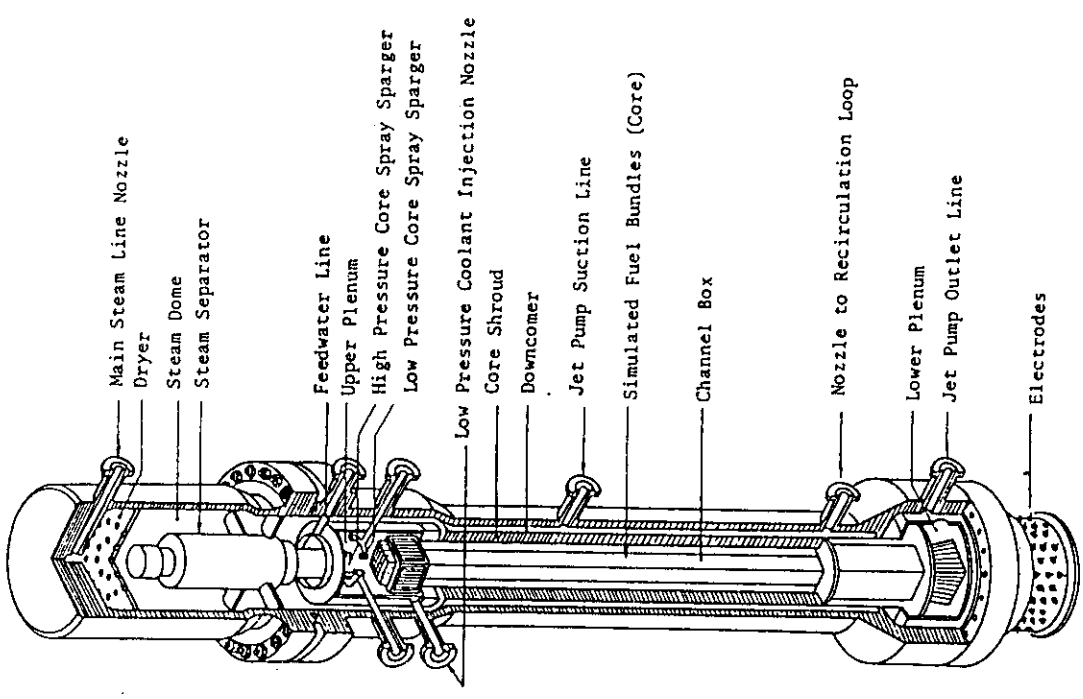

Fig. 2.2 Internal Structure of Pressure Vessel

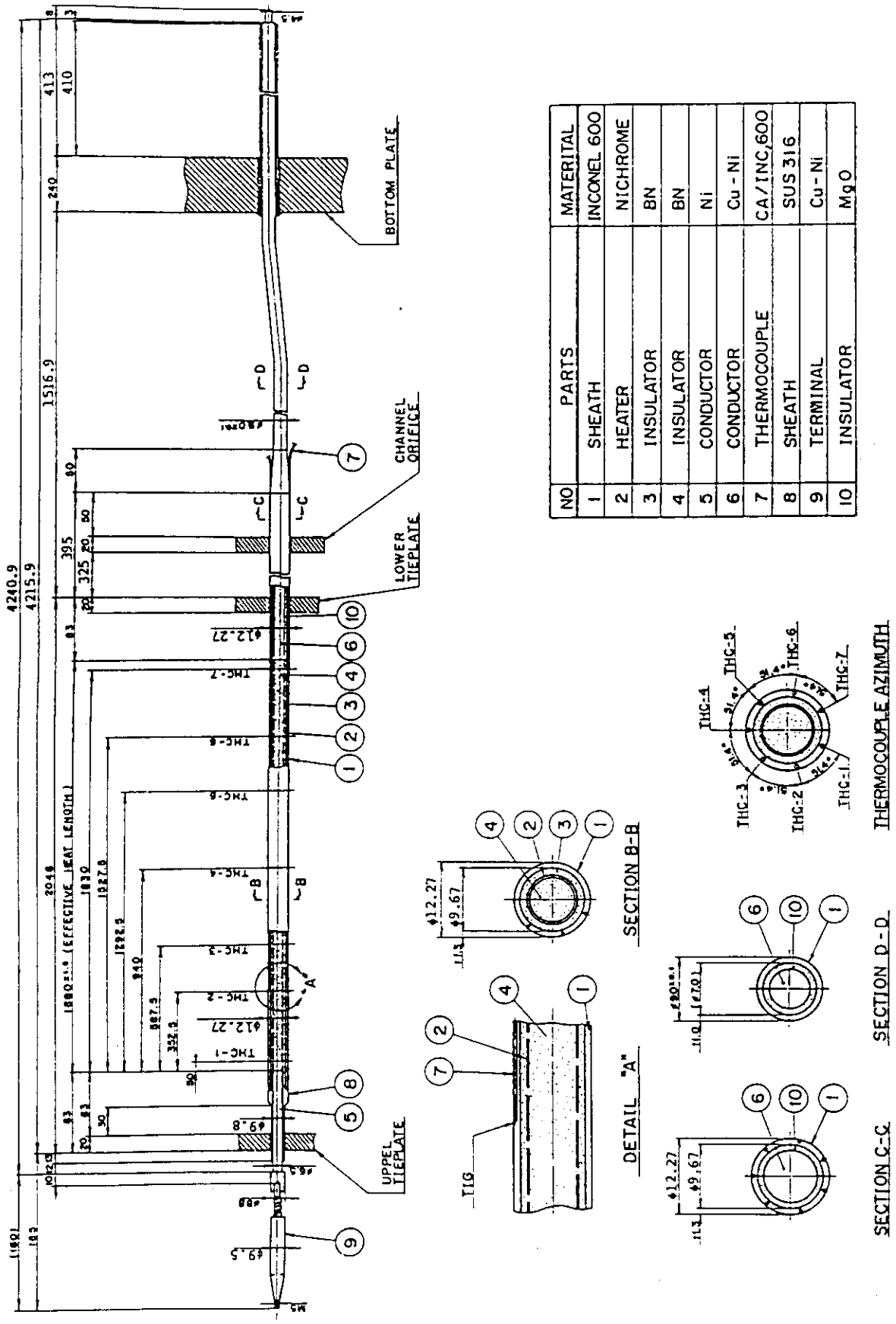

NO	PARTS	MATERITAL
1	SHEATH	INCONEL 600
2	HEATER	NICHROME
3	INSULATOR	BN
4	INSULATOR	BN
5	CONDUCTOR	Ni
6	CONDUCTOR	Cu - Ni
7	THERMOCOUPLE	CA/INC,600
8	SHEATH	SUS 316
9	TERMINAL	Cu - Ni
10	INSULATOR	MgO

Fig.2.3 Simulated fuel rod

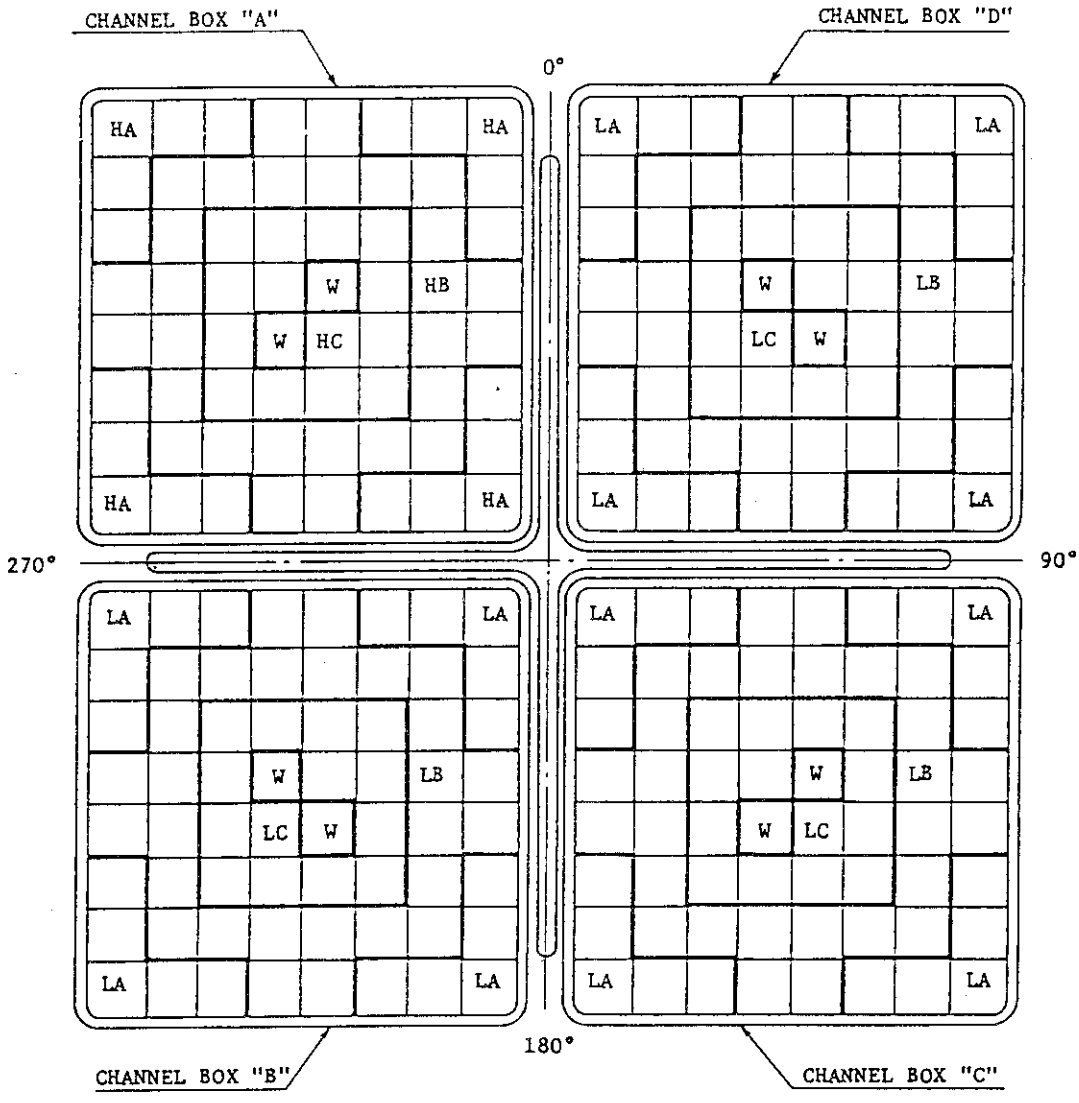

Region	HA	HB	HC	LA	LB	LC	W
Lenear Heat Rate (kW/m)	18.5	16.81	14.41	13.21	12.01	10.29	0.0
Local peaking factor	1.1	1.0	0.875	1.1	1.0	0.875	0.0
No. of Rods	20	28	14	60	84	42	8

* note : Radial peaking factor is 1.4

Fig. 2.4 Radial core power distribution

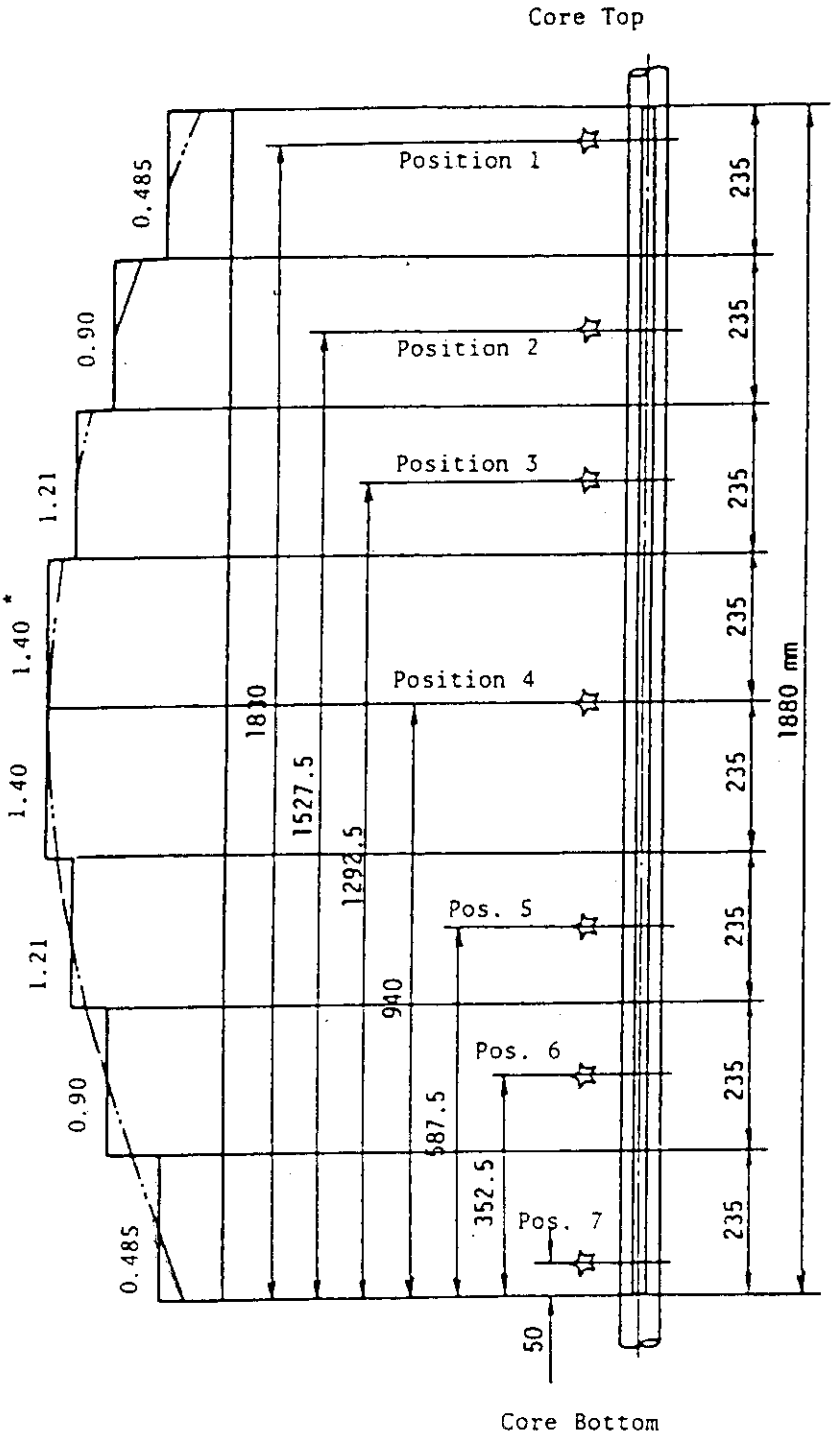

Fig. 2.5 Axial power distribution along heater rod

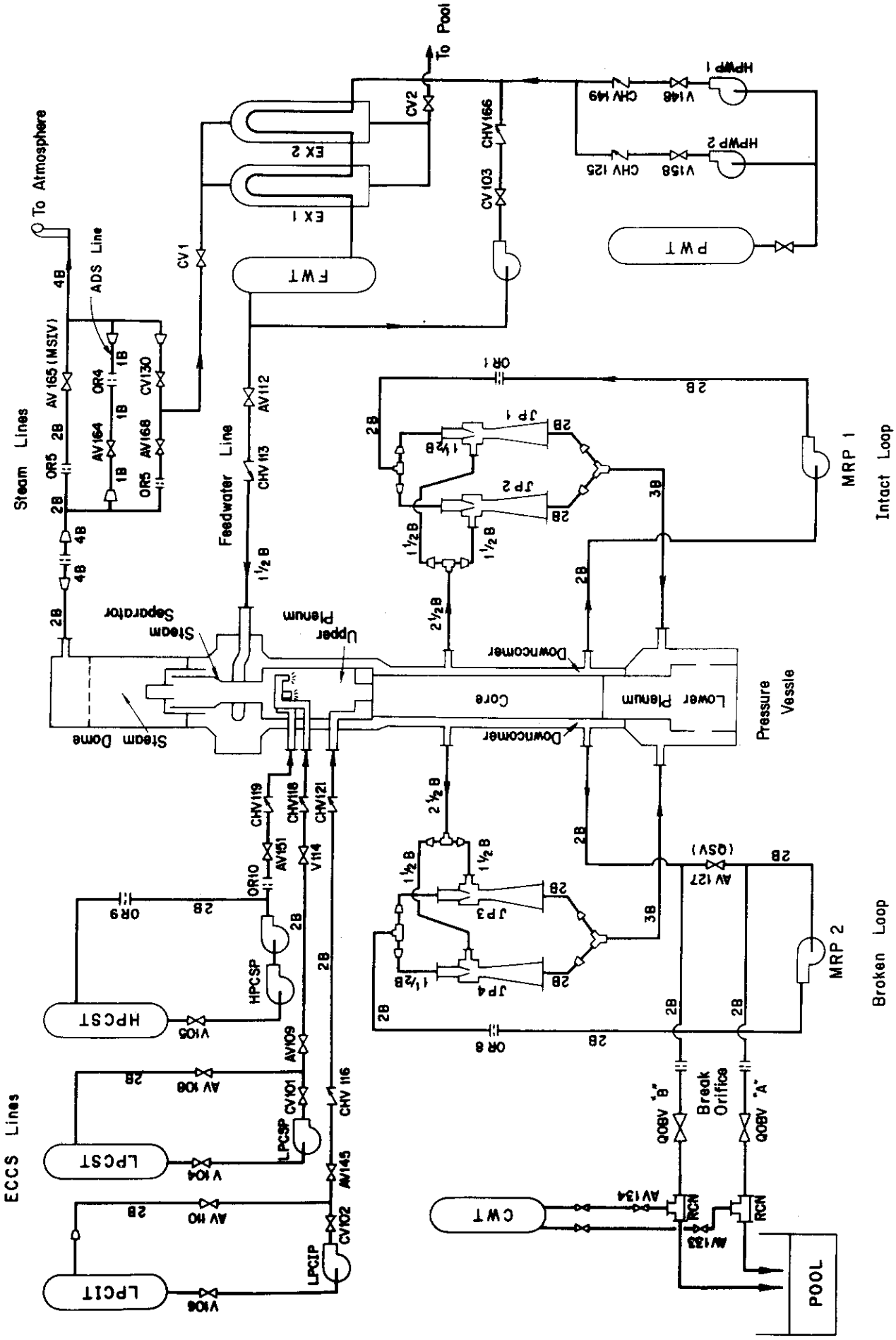

Fig. 2.6 Test facility flow diagram

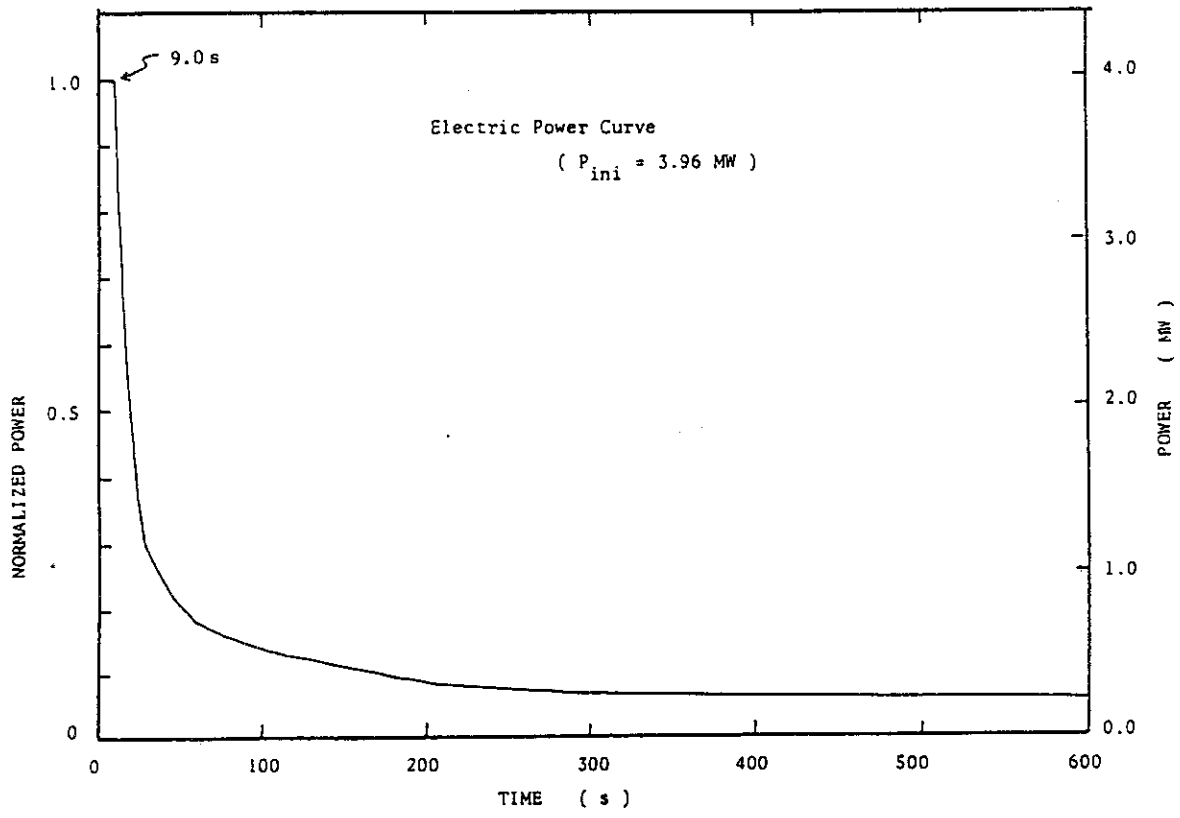

Fig. 2.7 Normalized core power transient

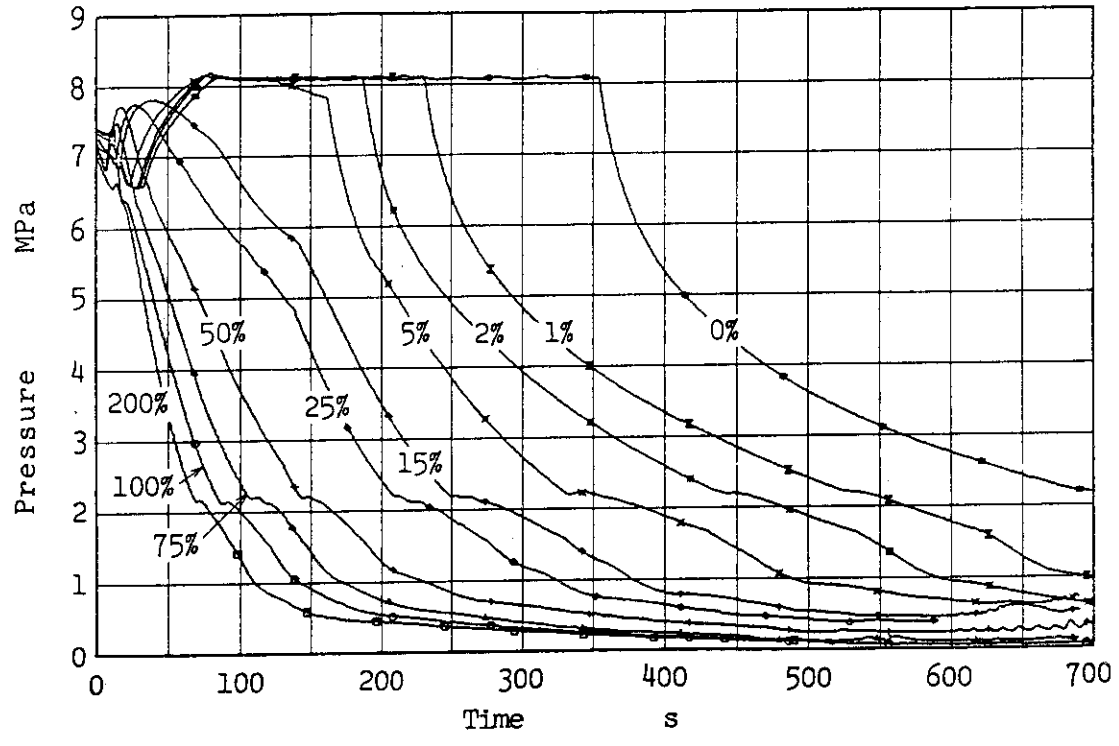

Fig. 2.8 Measured system pressures for all tests

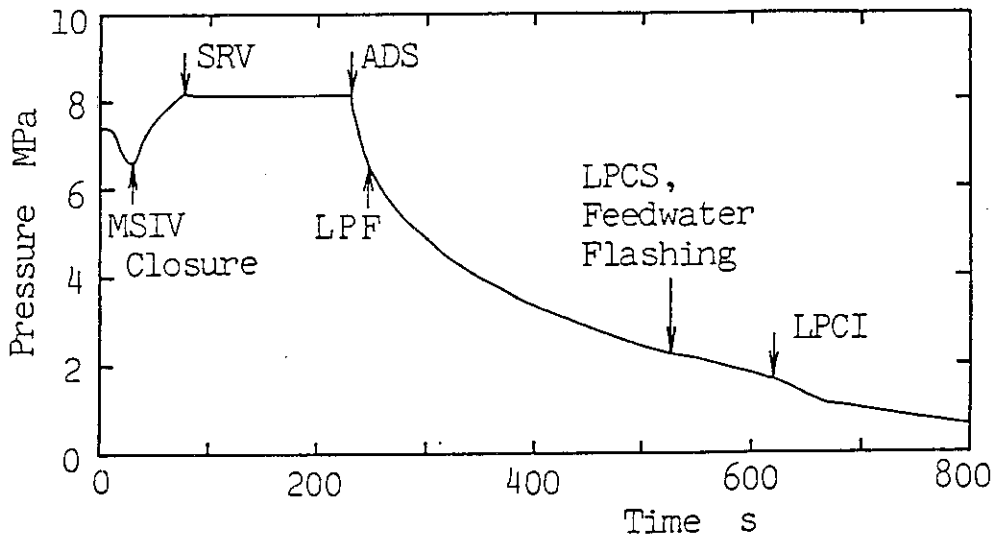

Fig. 2.9(a) Measured system pressure - 1 % break test

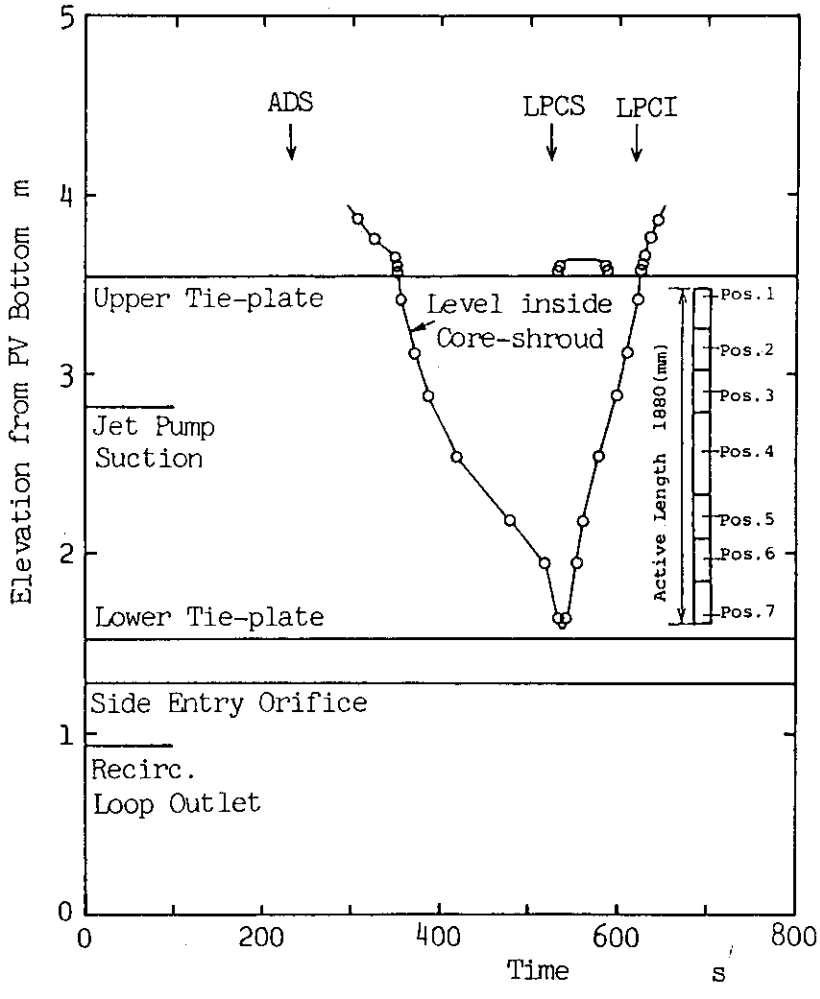

Fig. 2.9(b) Measured core mixture level - 1 % break test

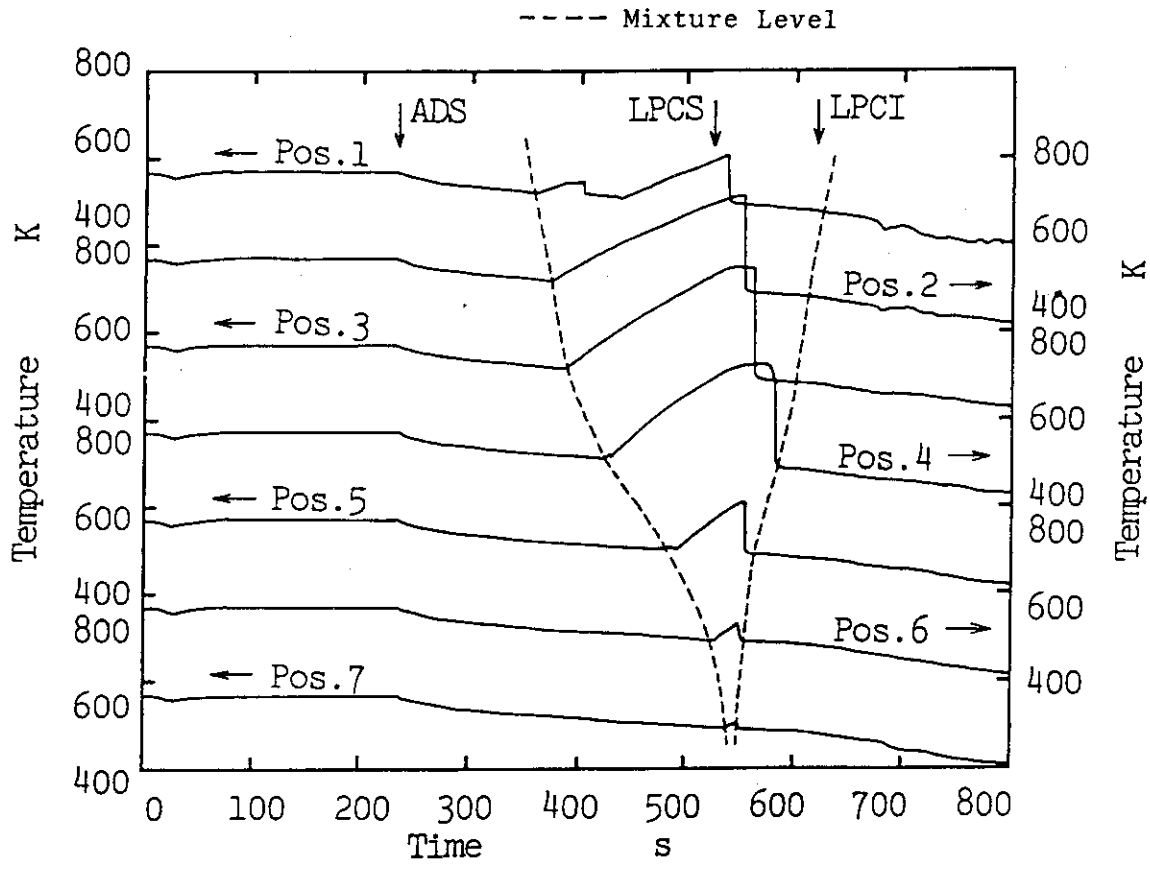

Fig. 2.9(c) Measured peak-power rod temperatures - 1 % break test

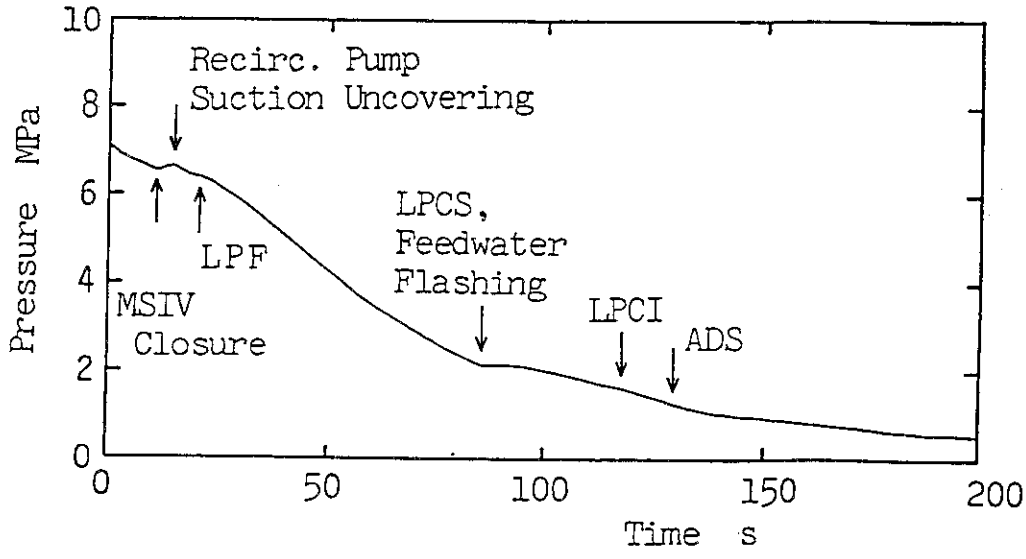

Fig. 2.10(a) Measured system pressure - 100 % break test

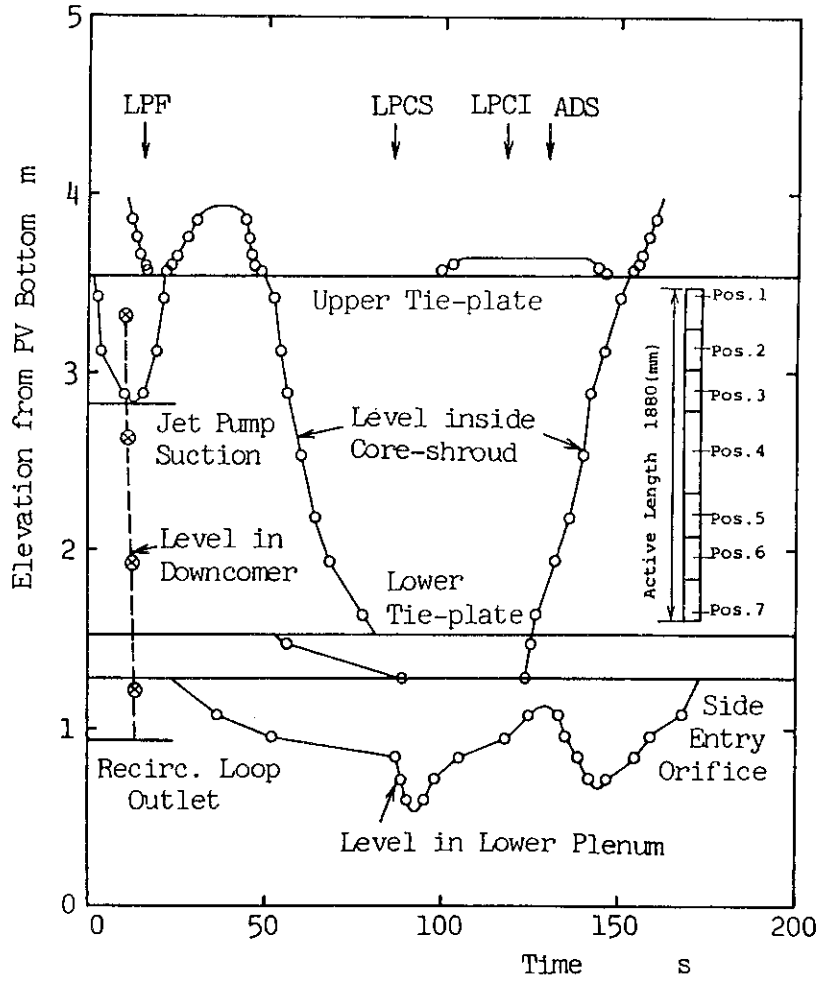

Fig. 2.10(b) Measured core mixture level - 100 % break test

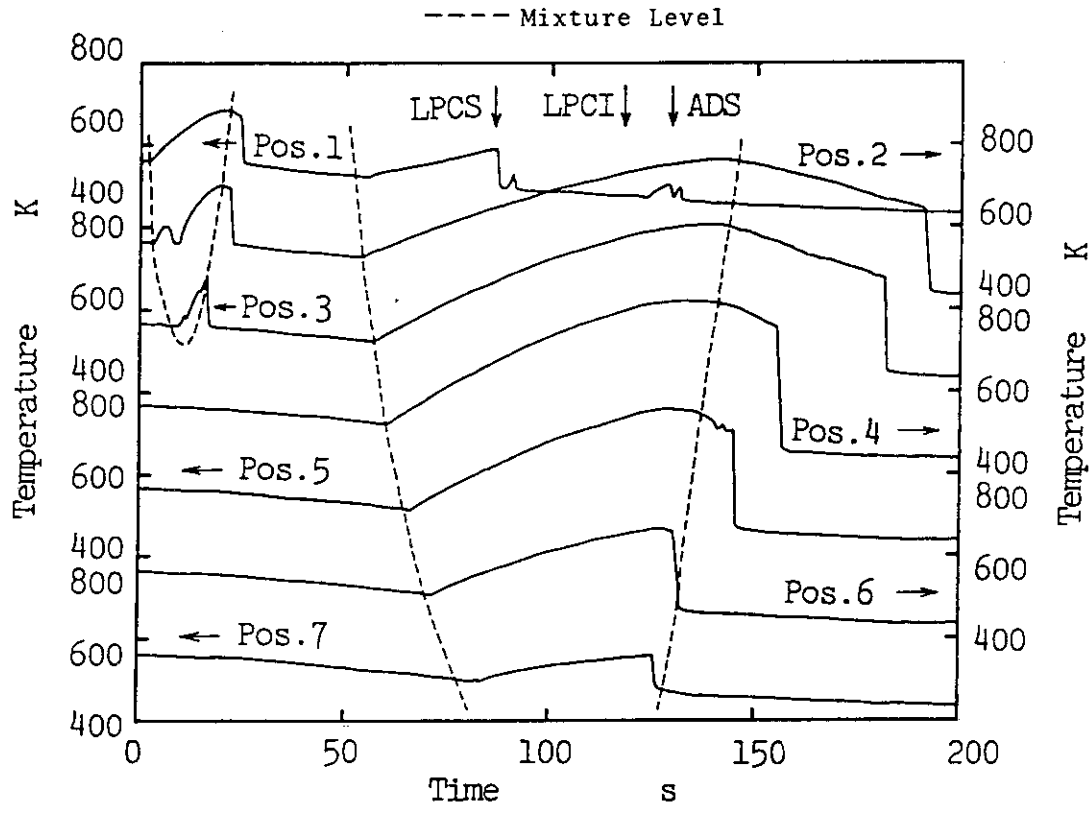

Fig. 2.10(c) Measured peak-power rod temperatures - 100 % break test

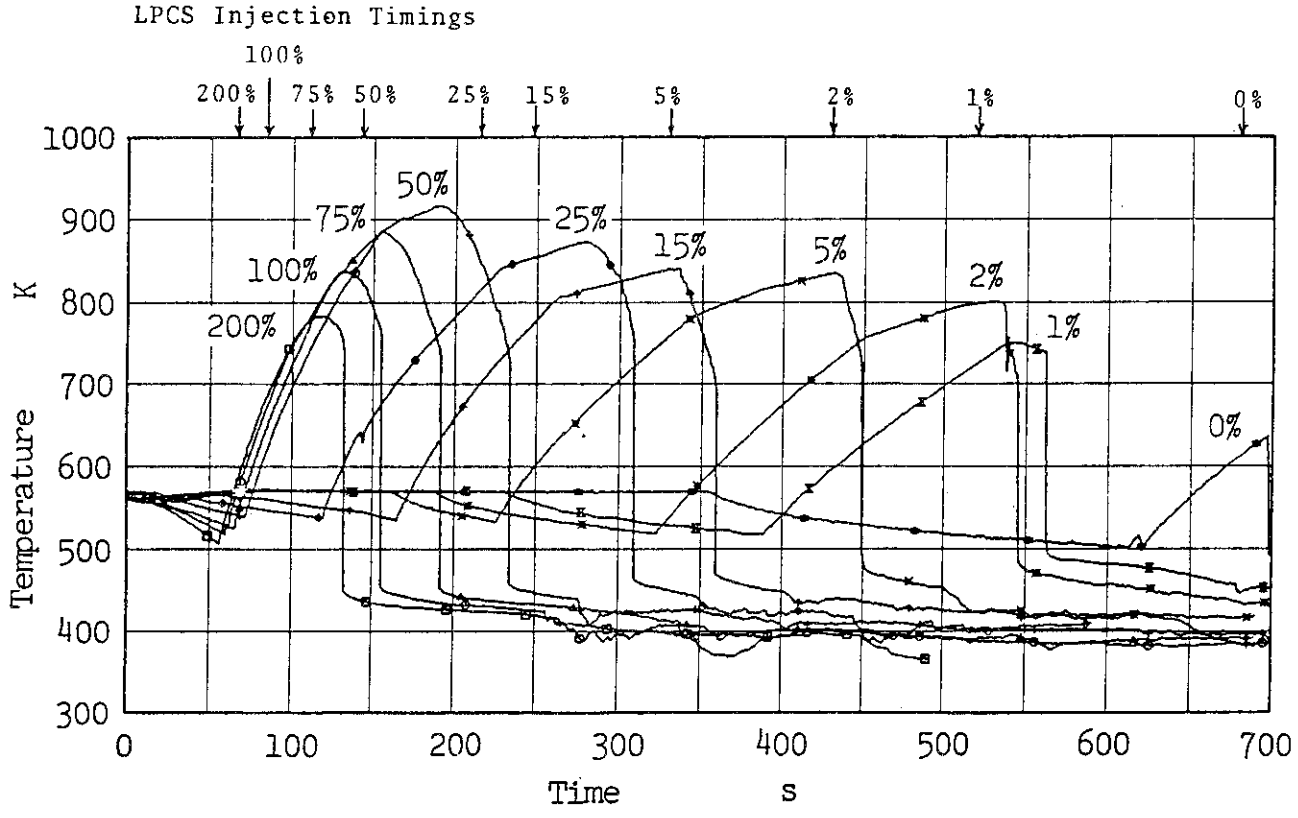

Fig. 2.11 Measured cladding temperatures at locations where PCT occurred

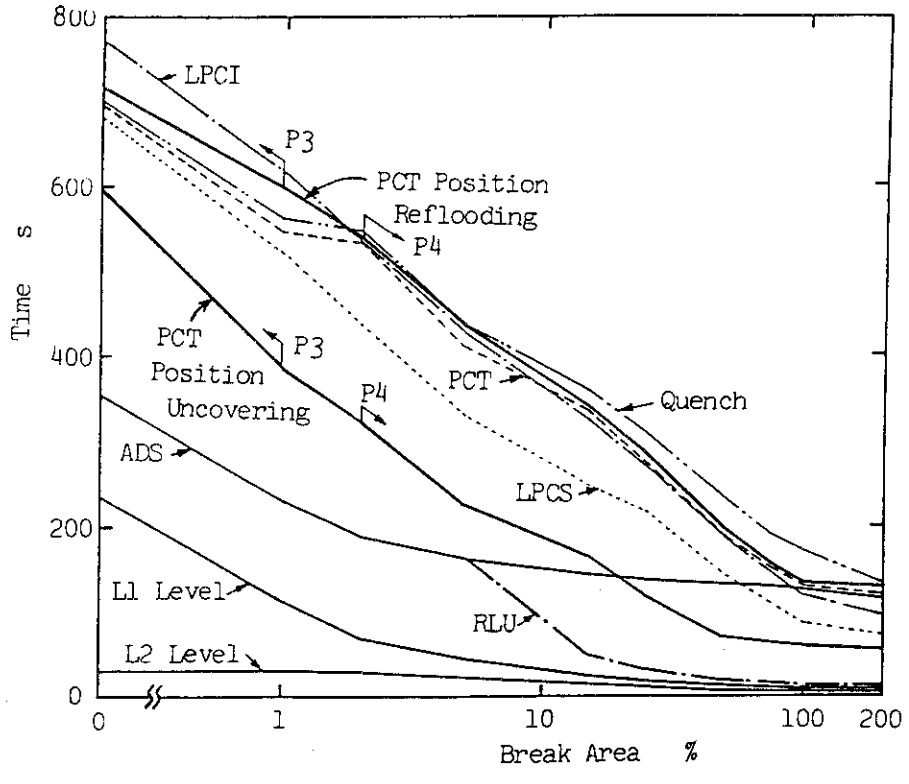

Fig. 2.12 Measured timings of events vs. break area

3. Computer code and Analytical Models

3.1 Description of THYDE-B1 Code

The THYDE-B1 code is a fast-running best-estimate computer code developed by JAERI for analyzing thermal-hydraulic response of a BWR during a LOCA. With its unique features described below, the THYDE-B1 code is particularly suitable for predicting the system pressure and core fluid behaviors during a small- or intermediate-break LOCA.

The THYDE-B1 code is a lumped parameter code. The reactor core and coolant system are represented by multiple fluid nodes. For each node the conservation laws of mass and energy apply. Fluid flow rate between nodes is determined from momentum balance along the flow path (junction). Heat transfer to fluid from the fuel or other metal structure is calculated using a one-dimensional heat slab model. The RELAP 4 heat transfer correlation package is used.

3.1.1 Node Models

Two node model options are provided in THYDE-B1: a homogeneous node model and a three-region node model.

The homogeneous node model assumes that fluids in the node are homogeneously mixed and in thermodynamic equilibrium.

The three-region node model, unique to TYHDE-B1, can consider up to three subnodes which represent a vapor region, a saturated two-phase mixture region and a subcooled liquid region, respectively. The three regions are partitioned by horizontal moving boundaries. The elevations of the boundaries are determined from mass and energy balance in each region. The three-region node model includes the following assumptions:

a) The node's pressure is represented by a pressure at a certain height in the node. The physical properties in the three subnodes are defined at that pressure. The differences in the physical properties caused by the pressure differential within a node are ignored.
b) The vapor region is assumed to be saturated. Therefore, heat added to the vapor region does not superheat the vapor region but is added to the saturated mixture region to cause phase change from liquid water to vapor.

c) The temperature distribution in the subcooled liquid region and the void distribution in the saturated mixture region are assumed to be uniform in the vertical and horizontal directions.

Mass and energy transport among the regions occurs as steam is separated from the mixture region, or as subcooled and saturated fluids are mixed. THYDE-B1 provides several options to consider such mass and energy transport among the regions.

The option used in the present calculations assume that the steam separation rate W_B is a simple function of the total steam mass in the mixture region M_B, a representative travelling distance of a steam bubble during its life time X_B, and a representative bubble rise velocity V_B. Thus,

$$W_B = \frac{M_B \cdot V_B}{X_B} \tag{3-1}$$

This equation implies that the total steam mass is replaced in a representative life time of a steam bubble X_B/V_B. The bubble travelling distance X_B, referred to as "bubble sweep-out length" in the code, is assumed to be the smaller of an input-specified length or the thickness of the mixture region. The bubble rise velocity V_B is calculated with the Wilson's correlation as a function of void fraction, hydraulic diameter, and fluid properties. The representative void fraction for the mixture region is defined as

$$\alpha = \frac{M_B}{X_B \cdot A} \tag{3-2}$$

where A is the flow area at the top of the mixture region.

(2) ECCS Mixing Model

The ECC water is injected into either the upper plenum (LPCS) or the core bypass region (LPCI). Options are provided to account for the time and distance required for complete mixing of the ECC water with saturated fluid. In the present calculations the LPCS water was assumed to be mixed either with the vapor or two-phase mixture which is present at the injection location. The LPCI water was assumed to be mixed only with two-phase mixture. Almost instantaneous mixing was assumed for either cases.

Using the three-region model enables simple nodalization without losing the accuracy of calculation. However, because of the simplicity

of the model, detailed core thermal-hydraulic responses, such as the counter-current flow limiting (CCFL) phenomenon at the core inlet and outlet, cannot be considered. Thus, the code is suitable for prediction of rather slow transients associated with small- or intermediate-break LOCAs.

3.1.2 Junction Models

THYDE-B1 has junction model options to represent various BWR hydraulic components. These options include:

(1) Homogeneous Junction

The flow rate between two adjacent nodes is given by solving a momentum equation neglecting the momentum flux terms and the effect of relative velocity between the vapor and liquid phases.

(2) Steam Separator Junction (Slip Junction)

Slip between the vapor and liquid phases is allowed to account for phase separation in the separator. The separator efficiency is to be specified as a function of the downcomer mixture level.

(3) Jet Pump Model

A jet pump is represented by a set of three special junctions where convection and mixing of momentum flux are taken into account.

(4) Leak Junction

Flow rate through breaks or relief vales can be calculated using either a flow-rate vs. time (or pressure) table or using a choked flow model.

(5) Fill Junction

Flow rate from a injection system should be specified as a function of time, or of pressure in the connected node.

3.1.3 Pump Model

The head of the recirculation pump can be included in the momentum balance of either a normal junction or the jet pump drive flow junctions. The pump head is calculated using a head vs. flow table as a function of the pump suction quality. This model is used only when the flow direction is normal; the recirculation pump is treated as a flow resist-

ance when flow direction is reversed.

3.1.4 Heat Structure Model

The fuel rods and other structures are modelled as one-dimensional heat slabs in cylindrical or rectangular geometry. The RELAP4[9] heat transfer package is used. Steam cooling after rod surface dryout is calculated using the Dittus-Boelter correlation.

3.2 Analytical Models

3.2.1 Nodalization

Two nodalization schemes were used to represent the ROSA-Ⅲ test facility. One nodalization scheme, shown in Fig. 3.1, was used for the 200% break test, and the other shown in Fig. 3.2 for other tests. The 200% break test model includes 8 nodes, 20 junctions and 21 heat slabs. The other model includes 6 nodes, 19 junctions and 21 heat slabs. The difference between the two models was in the number of nodes and break junctions. The 200% break test was a double-ended break test, and thus the model included two break junctions. THYDE-B1 input deck for the 15% break test is presented in Appendix A.

As shown in Table 3.1, a large portion of the pressure vessel was represented by a single three-region node model, node 1. It included the lower plenum, the guide tubes, the core and core bypass, the upper plenum and the jet pump discharge lines. This was intended to make the best use of the THYDE-B1 three-region node model. Similarly, the downcomer, including the jet pump suction lines, and the steam dome are represented by another three-region node, node 2. The recirculation pump suction lines and discharge lines are represented by homogeneous nodes: nodes 3 and 5 for the broken loop, and nodes 4 and 6 for the intact loop, respectively.

The THYDE-B1 heat slab models were used to represent the core electric heater rods and facility structures. Each of the ROSA-Ⅲ heater bundles contained 62 heated rods, out of which 20 had a local peaking factor (P.F.) of 1.1, 28 a P.F. of 1.0, and 14 a P.F. of 0.875.

The power per bundle for the peak-power bundle (Bundle A) was 1.4 times as large as that for each of the average power bundles (Bundles B, C and D). Thus, there were six groups of heater rods broken down by power level. As listed in Table 3.2, the heater rods were represented by two groups of heat slabs, Slabs 1 through 7 and Slabs 11 through 17. The two groups represented heater rods having average local P.F. (1.006) in average- and peak-power bundles, respectively. The total volumes, heat capacities, heat transfer areas, heat generation rates in the average- and peak-power bundles were correctly represented.

The junctions are listed in Table 3.3.

3.2.2 Break flow model

The break mass flow rates were calculated as follows:

For $x \leq 0$, use single-phase orifice flow model, i.e.,

$$W = C_1 A\sqrt{2\rho_j g_c(Po-Pb)}, \quad (3\text{-}3)$$

for $x > x_{tran}$, use the Moody's critial flow model, i.e.,

$$W = C_0 A G_M(Po,ho), \quad (3\text{-}4)$$

and for $0 < x < x_{tran}$,

use linear interpolation of Equations (3-3) and (3-4),

where,

C_0 = discharge coefficient (user input),

C_1 = contraction coefficient (user input),

A = junction flow area

$G_M(Po,ho)$ = critical mass flux determined by the Moody's slip flow model,

Pb = back pressure

ρj = fluid density at (Po,ho),

x = fluid quality at (Po,ho).

The values of C_0, C_1 and x_{tran} used in the present calculations were 0.61, 0.6 and 0.02, respectively. These values were recommended by previous analyses.[4][10]

3.2.3 Main Steam Line Model

The Moody critical flow model [Equation (3-4)] was used also for calculation of the steam flow rates through the main steam line and the automatic depressurization system (ADS).

3.2.4 ECCS Model

The HPCS, LPCI and LPCS were represented by fill junctions. The mass flow rate for each was given by a pressure vs. mass flow rate table.

3.2.5 Feedwater Line Model

The feedwater line was represented by a fill junction. The mass flow rate was given by a time vs. mass flow rate table. The volume in the feedwater line was not modelled. Thus, the feedwater line flashing (FLF) phenomenon was not calculated.

3.2.6 Steam Separation Model

The steam separation model (3.1.1 (1)) was used for node 1 and 2. The initial value of the bubble sweep-out length for node 1 was determined to be 2.4 m, as calculation with this value reproduced the steam flow rate and core mixture level measured during the steady state prior to the initiation of the tests. Thus, when the thickness of the mixture region became <2.4 m, the sweep-out length was equated to the mixture region thickness. The sweep-out length for node 2 was assumed to be the thickness of the mixture from the initiation of a calculation.

3.2.7 Recirculation Pump Model

The pump head was calculated using on input-specified head vs. flow table as a function of quality.

3.2.8 Trip Conditions

The trip conditions used in the tests were modeled exactly.

Table 3.1 Description of nodes

Node No.	component	model option
1	space inside core shroud	three-region node
2	space outside core shroud	three-region node
3	broken recirculation line from vessel to MRP	homogeneous node
(3)	broken recirculation line from break to MRP	homogeneous node
4	break side recirculation line from MRP to JP	homogeneous node
5	intact recirculation line from vessel to MRP	homogeneous node
6	intact recirculation line from MRP to vessel	homogeneous node
(7)	broken recirculation line from vessel to break	homogeneous node

Table 3.2 Description of heat slabs

Slab No.	Description
1 to 7	low power rod
8	lead rods
9	pressure vessel wall
10	pressure vessel wall
11 to 17	high power rod
18	lead rods
19	channel box
20	filler block
21	lower plenum structures
22	control rod

Table 3.3 Description of junctions

Junction No.	Component	Junction model option
1	steam separator	steam separator junction
2	recirculation line	normal junction
3	recirculation line	normal junction with pump
4	J.P. drive line	jet pump junctions
5	J.P. discharge line	
6	J.P. suction line	
7	recirculation line	normal junction
8	recirculation line	normal junction with pump
9	J.P. drive line	jet pump junctions
10	J.P. discharge line	
11	J.P. suction line	
12	high pressure core spray	fill junction
13	low pressure core spray	fill junction
14	low pressure coolant injection	fill junction
15	automatic depressurization system	leak junction
16	break 1	leak junction
17	safety relief valve	leak junction
18	feed water line	fill junction
19	main steam line	leak junction
(20)	break 2	leak junction

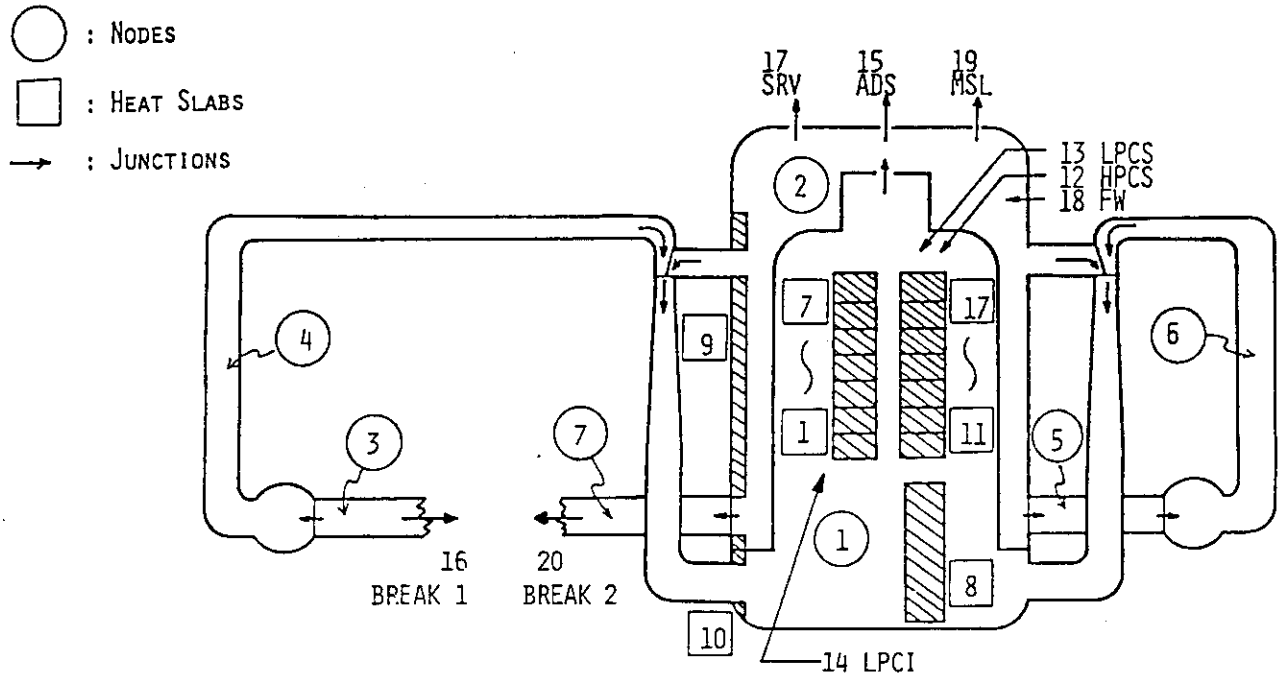

Fig. 3.1 Nodalization diagram - 200 % break test

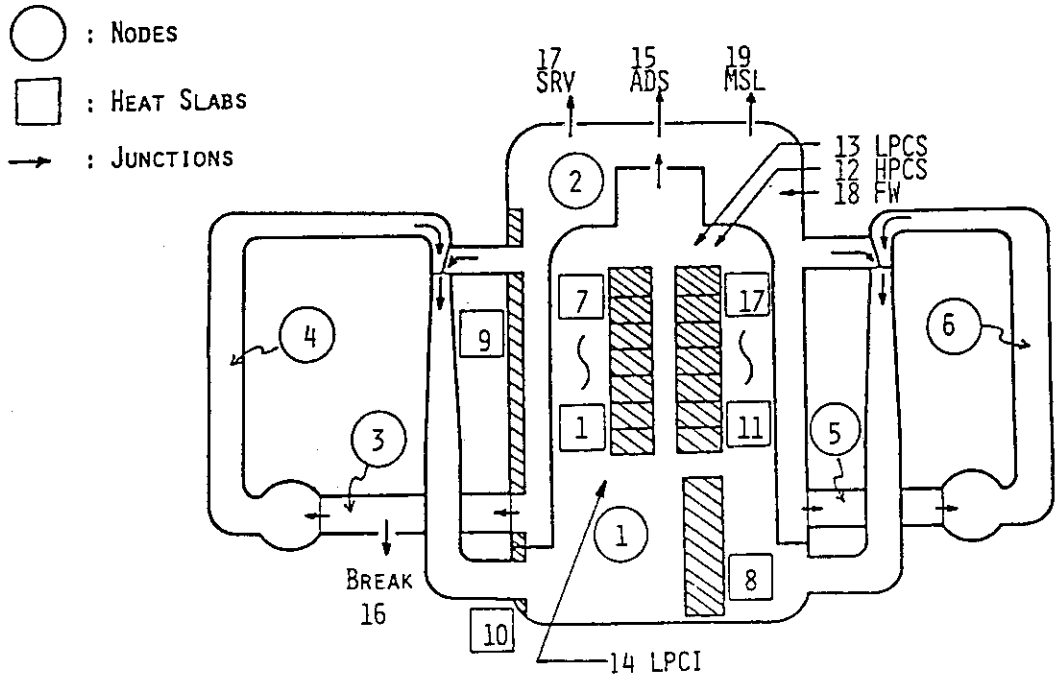

Fig. 3.2 Nodalization diagram -0 through 100 % break tests

4. Analytical Results and Discussion

In this Section, the capability of the THYDE-B1 (Mod 0) code to reproduce the ROSA-Ⅲ test results is investigated by comparing the experimental and analytical results. The ten ROSA-Ⅲ tests analyzed herein are broken down by size of break into three groups, i.e., small, intermediate and large breaks. Comparison plots between the experimental and analytical results are shown for one typical test selected from each group. Comparison plots for other tests are presented in Appendix B.

4.1 Small Break Tests (Break Areas <5%)

Three tests were conducted for this range of break area. The tested break areas were 0,1 and 2%. Figures 4.1 through 4.5 compare the major transient parameters obtained from the 1% break test and calculation.

For this range of break area, the initial system depressurization was arrested at ∿6.7 MPa, as typically shown in Fig. 4.1, as the simulated pressure control system throttled the main steam line. After the subsequent closure of MSIV, the system repressurized to the setpoint pressure of SRVs of 8.1 MPa. Then the system started to depressurize again as ADS operated. Thereafter, the steam discharge through ADS dictated the system overall behavior.

The purpose of ADS is to depressurize the system to prompt ECC water delivery. This effect was emphasized in the ROSA-Ⅲ small-break tests analized in this report. Since failure of HPCS was assumed in these tests, ECC water became first available when ADS depressurized the system to the shutoff head of LPCS of 2.16 MPa.

Thus, the time of initiation of the ADS's operation as well as the ADS flow rates were important for calculation of the system behavior during the small break tests.

The ADS was tripped on (with a time delay of 120 s) when the downcomer collapsed level decreased to the L1 level. The calculated time of the ADS initiation delayed relative to the measurement for the small breaks, as the calculated downcomer liquid level decreased more slowly than the test data.

For the 1% break test, the calculated time of the ADS initiation

delayed 15 s relative to the measurement. However, the calculated and measured behaviors of the downcomer level agreed qualitatively as shown in Fig. 4.2. It should be noted that in Fig. 4.2 the calculated two-phase mixture level is compared with test data of collapsed liquid level, because the code does not explicitly calculate the collapsed liquid level whereas mixture level was not measured at upper downcomer elevations. Thus, the comparison is meaningful until ∿250 s, when the downcomer fluid began to flash. The downcomer collapsed liquid level was measured with two transducers which measured differential pressures in the upper downcomer (between 2.814 m and 5.910 m above the vessel bottom) and the lower downcomer (between 0.938 m and 3.90 m above the bottom).

The ADS steam discharge flow rates were calculated using the Moody critical flow model with a discharge coefficient of 0.6. The calculated flow rates agreed with the test data fairlly well, but were found to be slightly (∿10%) smaller than the data as shown in Fig. 4.3.

Figure 4.4 compares the calculated and measured mixture level inside the core shroud. Core uncovery occurred both in the test and in the calculation as coolant was lost through ADS and break. The core was refilled as LPCS water accumulated in the core. Since the calculated initiation of the ADS flow delayed relative to the measurement, and hence the initiation of the LPCS flow delayed, the calculated core mixture level behavior delayed relative to the measurement. Both core uncovery and reflooding delayed, however, the delay was greater for reflooding than for uncovery. Thus, the calculated duration of core uncovery was longer than the measurement.

Figure 4.5 compares the calculated and measured peak-power rod cladding temperatures. The calculated initiation of cladding temperature excursion delayed relative to the measurement, as the calculated core uncovery delayed. The heatup rate after the dryout was calculated fairly well. Temperature turn-around and quenching propagated in the test from the top to the bottom of the core, under the effect of the LPCS injection on the top of the core. However, in the calculation the quench front moved upward, from the bottom to top of the core, as the core mixture level recovered due to accumulation of the LPCS water. This disagreement occurred because the code does not model the contact between the heater rods and the falling LPCS water. This caused dryout at the higher core elevations (positions 1 through 3) to continue longer than the test.

The calculated PCT occurred at position 3 of the peak power rod (as was the case in the test) at 634.5 s upon reflooding at the elevation (vs. 546 s, ∿45 s before reflooding in the test) before the initiation of LPCI flow (as was the case in the test). The calculated PCT was 758 K and agreed closely with the measured PCT of 754 K.

4.2 Intermediate Break Tests (5% ≦ Break Areas ≦ 50%)

Four tests were conducted for this range of break area. The tested break areas were 5, 15, 25 and 50%. Figures 4.6 through 4.10 compare the major transient parameters obtained from the 15%-break test and calculation.

The system thermal-hydraulic behavior for this range of break area was different from that for the small (<5%) breaks, in that gross system depressurization was caused by uncovery of the recirculation pump suction line inlet as typically shown in Fig. 4.6, rather than by the operation of ADS. In addition to this, the in-vessel steam generation, due to both flashing in the pressure vessel (including the feedwater line) and vaporization of ECC water, had more significant influence on the system behavior than for the small breaks.

Thus, the downcomer mixture level behavior and break mass and energy flow rates are important for the system behavior for this range of break area.

Figure 4.7 compares calculated and measured break mass flow rates for the 15% break test. The calculation and measurement agreed within the measurement uncertainty. The calculated and measured times of recirculation line uncovery (RLU) compared favorablly as well, as shown in Fig. 4.8.

However, the effect of RLU on the system pressure behavior was not correctly represented in the calculation. As typically shown in Fig. 4.6, RLU led an immediate system depressurization in the tests, however, this did not occur in the calculation. The calculated initiation of depressurization delayed relative to the test data. (The delay was greater for the smaller intermediate breaks. Also, the depressurization rate after RLU was underestimated for the smaller intermediate breaks).

These discrepancies between the measured and calculated system pressures appear to have resulted from underprediction of the break flow

rate (Fig. 4.7) and break flow quality.

The downcomer mixture level has significant influence on the break flow quality. As shown in Fig. 4.8, the downcomer mixture level was overpredicted after the initial RLU up to ∿80 s. The THYDE-B1 steam separation model (3.1.1 (1)) and the jet pump model are probably responsible for such discrepancy between the measured and calculated downcomer level behavior.

Although the calculated system depressurization delayed relative to the data, the difference between the measured and calculated pressure decreased with time, and the calculated pressure eventually became lower than the data after the LPCS injection began. This overprediction of the system depressurization rate appears to have resulted from underprediction of the in-vessel steam generation, as will be discussed in the following paragraphs.

The calculated and measured system pressures behaved differently after the initiation of LPCS flow. The system depressurization was decelerated after the initiation of LPCS flow in the tests, however this did not occur in the calculations as typically shown in Fig. 4.6. The experimentally observed decrease in the depressurization rate appears to have resulted from vaporization of LPCS water. Vaporization may have occurred as the falling LPCS water contacted with either solid surfaces heated above the saturation temperature (heater rods and vessel structures exposed to steam) or with superheated steam.

These vaporization modes for the LPCS water were not modeled in the present calculations. Direct contact between the falling ECCS water and solid surfaces was not accounted for, since the THYDE-B1 three-region node model, used to represent the core region, does not account for the presence of liquid phase above the mixture level. Vaporization due to contact with superheated steam cannot be accounted for either, because the code assumes that vapor is always saturated. As a result, the initiation of LPCS injection resulted in accelerating the system depressurization in the calculation, rather than decelerating, as saturated vapor condensed on the injected LPCS water,

In addition to the vaporization of LPCS water, there occurred in the tests flashing in the feedwater line at the system pressure of ∿2.2 MPa, which was approximately equal to the LPCS injection pressure. The steam generated by the feedwater line flashing (FLF) also contributed to the decrease in the system depressurization rate. However, the effect

of FLF was not accounted for in the present calculations where the volume in the feedwater line was not modeled.

Since steam generation due to these mechanisms was underestimated or neglected, the calculated system depressurigation was faster than the measurement during the later phase of the intermediate-break tests. The faster depressuringation led to earlier initiation of the LPCI flow than in the tests.

Figure 4.9 compares the calculated and measured core mixture level for the 15% break test. The comparison is generally favorable during the core uncovery process, although the initial core uncovery was predicted to occur slightly (∿16s) later than the test. The temporary recovery of the core mixture level at ∿115s, due to concurrent initiation of the ADS flow and lower plenum flashing (LPF), was well calculated. However, the experimentally observed formation of mixture level above the upper tieplate (from 194 to 231s, and from 252 to 264s), or above and below the channel side entry orifice (from 130 to 203s) was not calculated, because such mixture level resulted from the counter current flow limiting (CCFL) phenomenon, which was not accounted for by the code.

Despite that the core uncovery process was calculated fairly well, the reflooding was calculated to occur considerably earlier than that in the tests. This resulted from that the calculated system depressurization was faster than the measurement after the initiation of LPCS flow. The faster depressurization prompted the initiation of LPCI flow and caused greater LPCS and LPCI flow rates than in the tests. These together prompted core reflooding.

Figure 4.10 compares the calculated and measured cladding temperatures along a peak-power rod. Since the calculation well represented the core uncovery process, except for that at the upper core region, the calculated times of rod surface dryout at Positions 3 through 7 agreed well with the test data. The calculation also succeeded to reproduce the initial cladding heatup behavior after the dryout. However, since the code assumes that steam is always saturated, whereas steam actually becomes superheated as it flows along heater rods, the calculation overestimated heat transfer from the heater rod to steam environment. Thus, the calculated heatup rate became smaller than the measurement as cladding temperature increased.

It is interesting to note that such overprediction of the steam cooling effect was much less pronounced for the small breaks, because

the calculated heat transfer coefficients were smaller than those calculated for the larger breaks. The heat transfer coefficient for steam cooling was calculated using the Dittus-Boelter correlation. Thus, the calculated heat transfer coefficient depended on the steam mass flux through the core, which was induced by system discharge through the break and ADS. For the small breaks the core steam flow was induced primarily by the ADS flow, since core uncovery occurred before RLU. Since the ADS flow was relatively small because the core uncovery occurred after the system had depressurized considerably, the core steam mass flux was small and hence the calculated heat transfer coefficient was relatively small for the small breaks.

Quenching of the rod surface occurred only in the bottom-up fashion in the calculation, because of the code's limitations already mentioned. Accordingly, the top-down quench experimentally observed at the upper core region (Positions 1 through 3), was not represented. Because of this, the calculated quenching for these locations delayed relative to the measurements. However, for other locations where quenching occurred in the bottom-up fashion in the test, the calculation predicted earlier quenching than the measurements as reflooding was calculated to occur earlier than the tests.

The calculated PCT for the 15% break test occurred at position 4 of the peak power rod (as was the case in the test) at 294 s upon reflooding at that elevation (vs. 336 s in the test, also upon reflooding), after the initiation of the LPCI flow (as was the case in the test). The calculated PCT was 740 K vs. the measured PCT of 864 K.

4.3 Large Break Tests (Break Areas >50%)

Three tests were conducted for this range of break area. The tested break areas were 75, 100 and 200%. Figures 4.11 through 4.13 compare the major transient parameters obtained from the 100%-break test and calculation.

For this range of break area, the overall system behavior was similar to that for the intermediate (≦50%) breaks. However, the effects of break flow and in-vessel steam generation on the system behavior were more significant. The effect of ADS was small, because ADS operated only after the system had depressurized so that all other ECCS (LPCS

and LPCI) had begun to operate.

Although the system response was primarily governed by the break flow, the system pressure was initially affected by discharge through the main steam line until MSIV closed, since this was the only path for steam discharge until the recirculation line uncovery (RLU). Thus, the difference between the calculated and measured timings of the MSIV closure caused the difference between the initial system pressure behavior shown in Fig. 4.11. The difference between the times of the MSIV closure (tripped by an L2-signal) resulted from difference between the calculated and measured downcomer liquid level behaviors. The calculated time of the MSIV closure was generally earlier than the measurement for the large breaks, whereas it showed good agreement with the measurement for the small and intermediate breaks.

The RLU led gross system depressurization both in the experiment and calculation. The calculated RLU was more straightforward than that for the intermediate breaks in the sense that the calculated downcomer mixture level never recovered, after the initial RLU, to the elevation of the recirculation pump suction line inlet.

The effect of LPF on the system pressure behavior was to decelerate the system depressurization. This was less pronounced in the calculations than in the tests, since in the calculations LPF caused smaller increase in the core mixture level and hence smaller amount of steam generation. However, the calculated system pressure behavior agreed well with the test data until initiation of LPCS flow.

The calculated and measured system pressures after the initiation of LPCS flow behaved differently as was the case for the intermediate breaks. The LPCS injection, together with the feedwater line flashing (FLF), decelerated the system depressurization in the tests, but this did not occur in the calculations. Since the calculated depressurization after the initiation of LPCS flow was faster than the measurement, injection from LPCI was calculated to occur earlier than the tests. Major in-vessel steam generation in the calculations occurred only after the initiation of reflooding.

Figure 4.12 compares the calculated and measured core mixture levels for the 100% break test. The swelling of core mixture level due to LPF was much smaller in the calculation than in the test. Thus gross core uncovery was calculated to occur earlier than in the test. The core emptying in the calculation progressed more quickly than in the test

also because the effect of CCFL on liquid drainage at the channel side entry orifice was not accounted for by the code. Since the injection from LPCS and LPCI was calculated to begin earlier than the test, the calculated core mixture level began to recover earlier than the test.

Figure 4.13 compares the measured and calculated cladding temperatures along a peak-power rod. The measured and calculated temperature behaviors were qualitatively different. The calculation predicted early temperature excursion for positions 3 through 5, starting well before these locations were uncovered. However, such temperature excursion due to departure from nucleate boiling (DNB) did not occur in the test, and nucleate boiling continued until the rod surface was uncovered. The calculated temperature excursion continued until the rod surface was finally quenched after reflooding; although the rod surface heat transfer was improved temporarily after LPF, the rod surface at positions 3 through 5 remained dry, and temperature excursion continued as these location were uncovered above the mixture level.

The PCT was calculated to occur at the peak-power rod position 4 (as was the case in the test) at 111 s when reflooding occurred at that location (vs. 134 s in the test, upon reflooding). The calculated PCT was 846 K vs. the measured PCT was 832 K.

The prediction of unrealistic early DNB by the code was found to have resulted from iadequate calculation of the core flow. The DNB was calculated to occur for break areas ≧50% at positions 3 through 5 on the peak-power rod. The DNB occurred concurrently with the closure of MSIV, when a vapor region began to exist in node 1 (see Fig. 3.2) as the mixture level dropped from the top of the node. It was found that the code calculated the mass flux in the saturated mixture region to be zero when there existed three regions (vapor, mixture and subcooled) in a three-region node, because the order of definition of variables was inadequate. Thus, DNB was calculated to occur as soon as MSIV closed, if the rod surface heat flux exceeded the assumed critical heat flux (90000 BTU/ft^2·hr) for pool boiling. The DNB was calculated to occur only for the larger breaks (≧50%), where the above condition was satisfied.

4.4 Peak Cladding Temperature vs. Break Area

Figure 4.14 compares the measured and calculated PCTs for all the tests analyzed. Comparison of the measured and calculated PCTs, the times of PCT and the locations where the PCTs occurred are also given in Table 4.1.

The calculated PCTs were in fair agreement with the test data for the small (<5%) and large (>50%) break areas, however, for the intermediate-breaks the PCTs were underpredicted as much as 124 K.

The PCT depends much on the timing of dryout and the duration of dryout before temperature turnaround. Figure 4.19 compares the measured and calculated timings of events. The timings of dryout and reflooding are shown for the positions where PCT occurred in the calculations and tests, respectively.

For the small (0, 1 and 2%) breaks, the calculated times of both dryout and PCT were later than the measurements. The temperature turnaround was caused by the core spray (LPCS) in the tests, and by reflooding in the calculations. However, the calculated and measured PCTs agreed fairly well, because the duration of dryout was well calculated. The duration of dryout is more important for the small breaks than the timings, because dryout occurs only after the variation of core power with time has become very slow.

For the intermediate breaks (between 5 and 50%), the timing of dryout was predicted well. However, the temperature turnaround was calculated to occur earlier than the tests. Thus, the calculated duration of dryout was shorter than the measurements, and hence the calculated PCTs were lower than the measurements. The underprediction of PCT resulted also from overprediction of steam cooling after dryout, as discussed in Subsection 4.2.

For the large breaks, the calculated timings of both dryout and PCT were earlier than the measurements. However, it is difficult to discuss how such disagreement between the calculated and measured timings affected the PCT, because the calculations indicated unrealistic early DNB which may have had a considerable influence on the PCTs calculated for these tests. The calculated PCTs occurred earlier than the tests, because reflooding was calculated to occur earlier than the tests. The overprediction of steam cooling also should have affected the calculated PCTs.

4.5 Parametric Calculations

As has been discussed in the previous Subsections, the major factors which caused the underprediction of PCT appear to include the overprediction of the ECC flow rates, resulting from underprediction of the system pressure after the initiation of LPCS flow. Thus, additional parametric calculations were conducted to investigate the impact of ECC flow on the system behavior. In these calculations the ECC flow rates measured in the tests (as a function of time) were used instead of using the flow vs. pressure tables. Figure 4.16 compares calculated (baseline) and measured ECC flow rate (LPCS plus LPCI) vs. time for the 15% break test. Both in the calculation and test PCT occurred shortly after the initiation of the LPCI flow. The LPCI flow was about four times larger than the LPCS flow, and led immediately to core reflooding. The core mixture levels calculated for the 1, 15 and 100% break tests are shown in Figs. 4.17 through 4.19, respectively. The parametric calculations show much better agreement with the experimental data than the baseline calculations, for the 15 and 100% breaks (Results for other tests are shown in Appendix B). Thus, it is evident that the disagreement observed between the baseline calculations and experimental data of the core mixture level primarily resulted from the underprediction of the system pressure. Correct prediction of the system pressure is important particulary when the LPCI setpoint pressure is approached, because LPCI lead to immediate reflooding, up to the core midplane or higher, for the intermediate breaks.

Table 4.1 Measured and calculated peak cladding temperatures.

Break Area (%)	Position (No.)		Time (s)		PCT (K)		PCT occurred before LPCI injection	
	Exp.	Cal.	Exp.	Cal.	Exp.	Cal.	Exp.	Cal.
0	3	3	696	850	637	684	×	×
1	3	3	546	634.5	754	758	×	×
2	4	3	531	556.5	804	776	×	×
5	4	4	410	381	835	753	×	
15	4	4	336	294	846	740		
25	4	4	274	253.5	872	748		
50	4	4	189	177	925	821		
75	4	4	154	137	885	843		
100	4	4	133	111	832	846		
200	4	4	119	85	785	886		

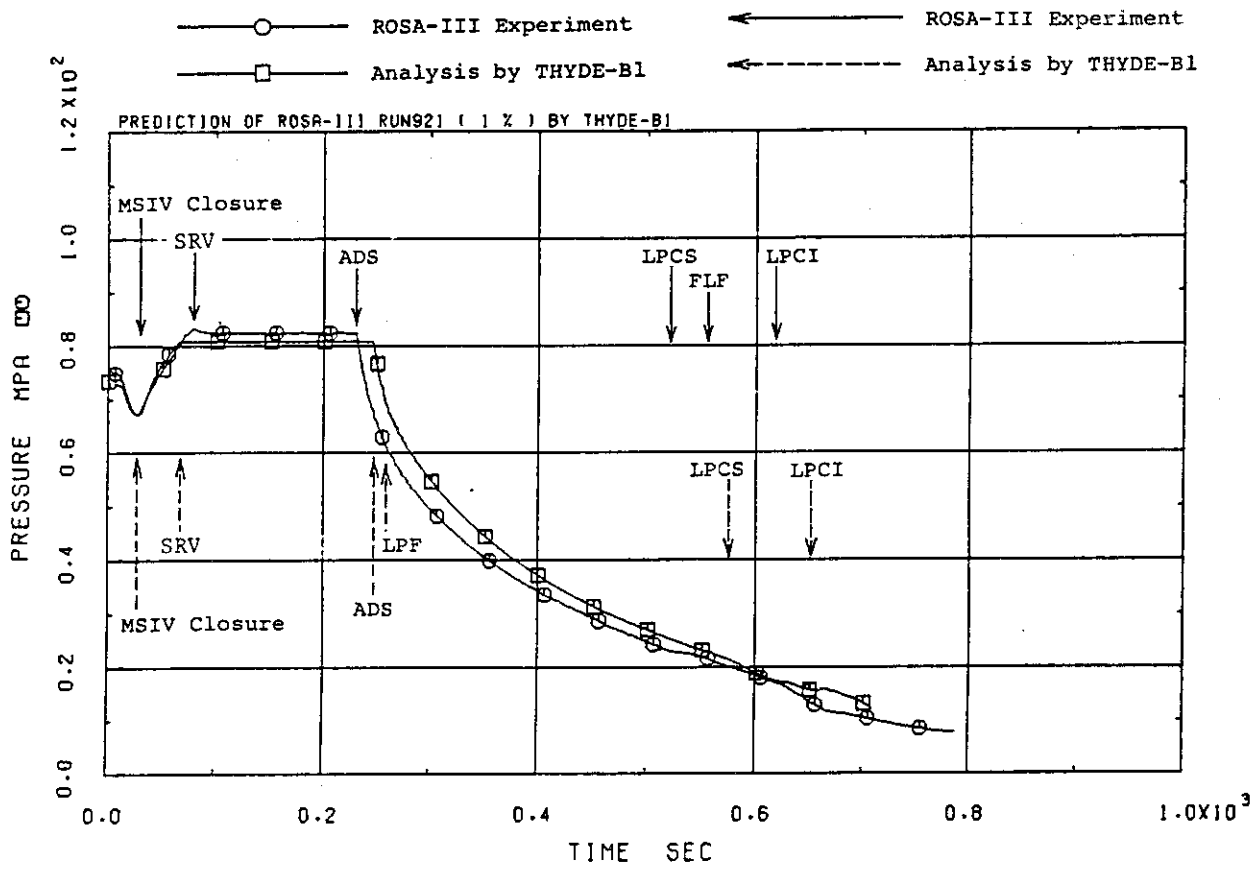

Fig. 4.1 Measured vs. calculated system pressures - 1 % break test

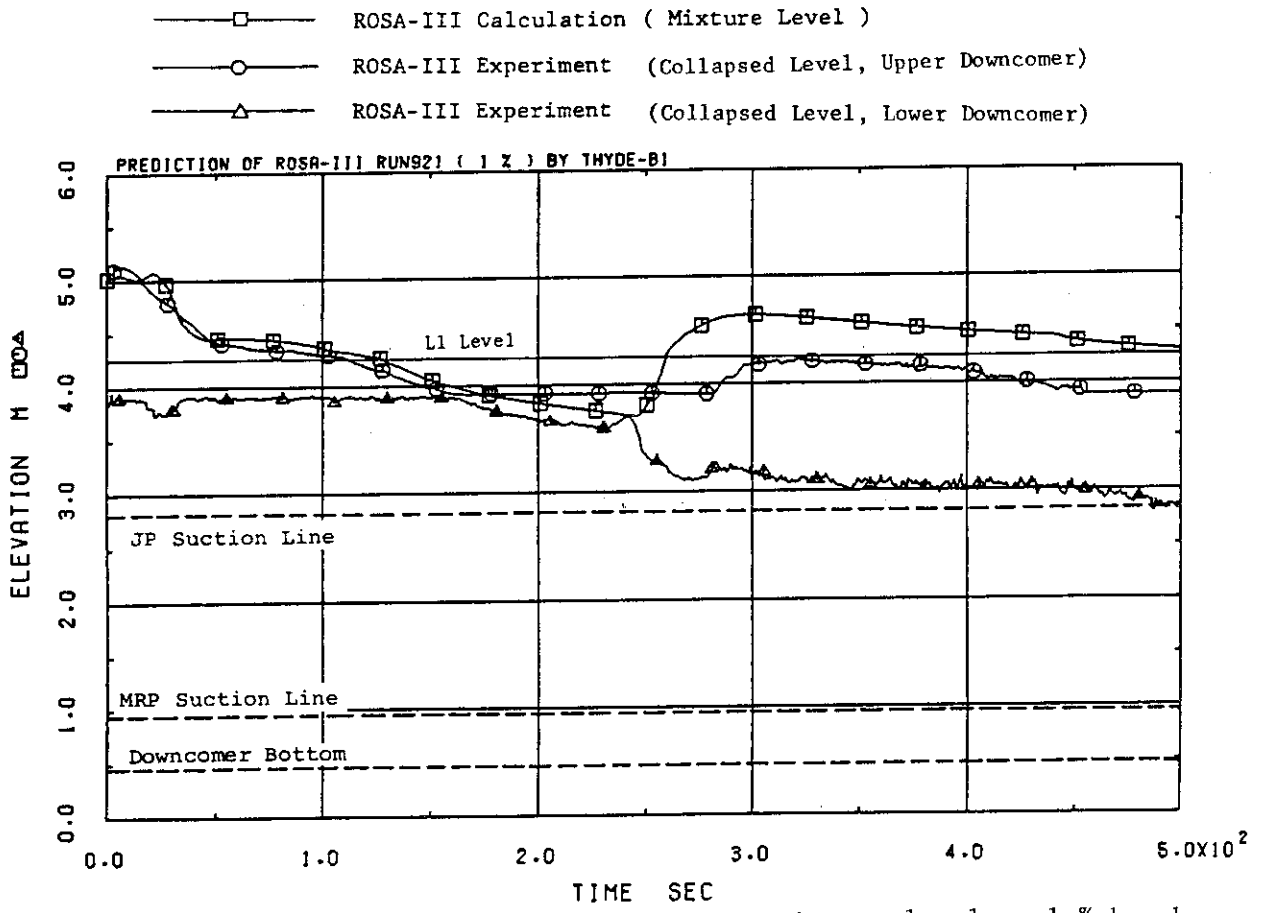

Fig. 4.2 Measured vs. calculated downcomer mixture levels - 1 % break test

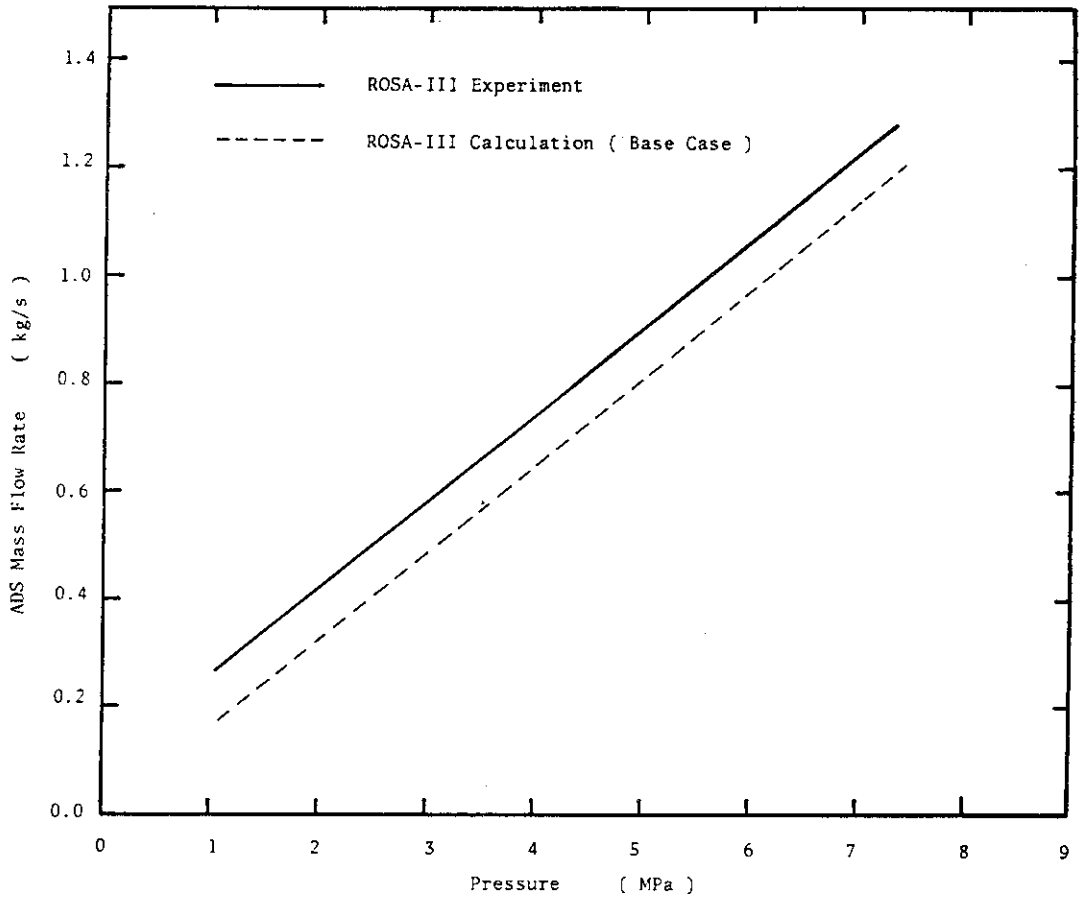

Fig. 4.3 Measured vs. calculated ADS flow rates

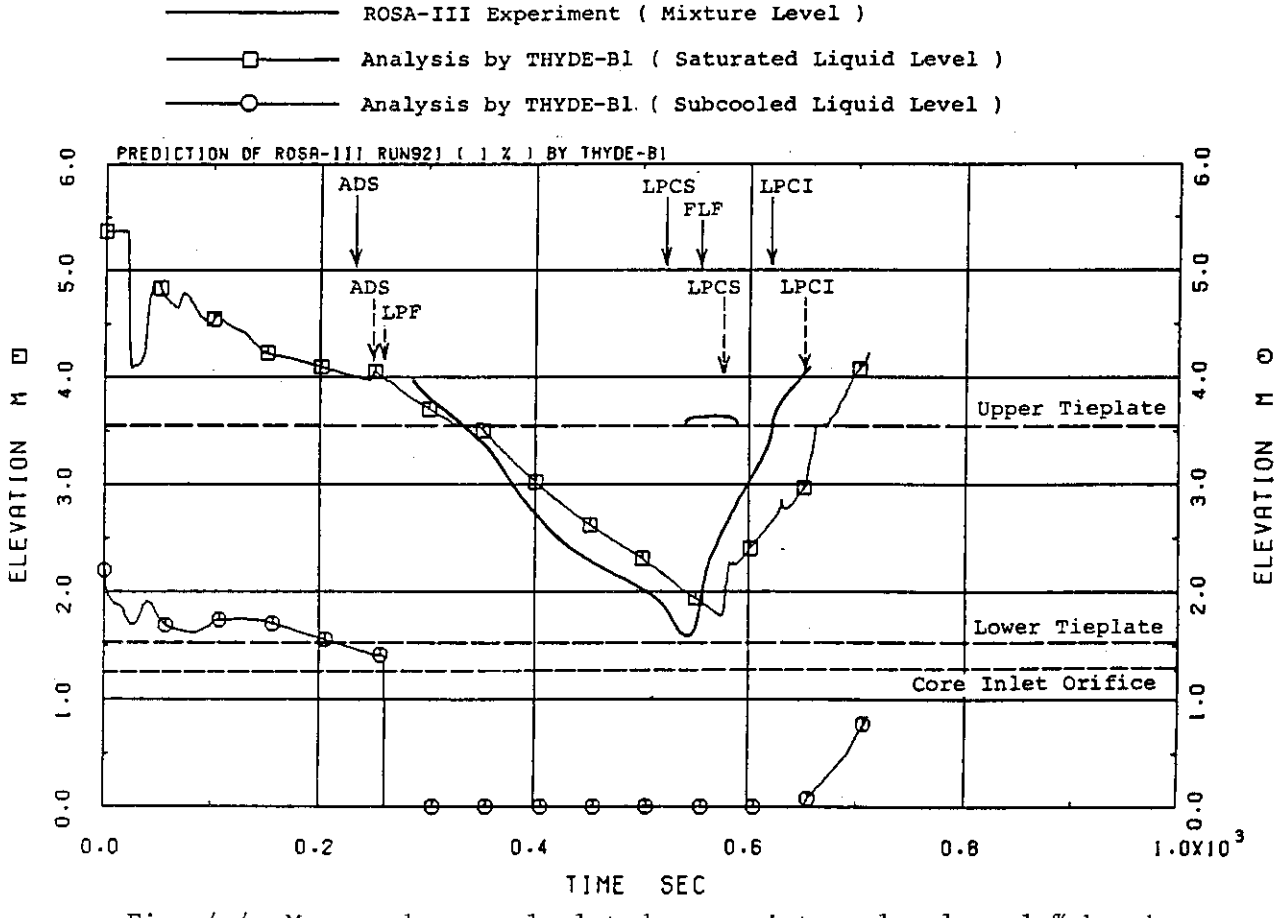

Fig. 4.4 Measured vs. calculated core mixture levels - 1 % break test

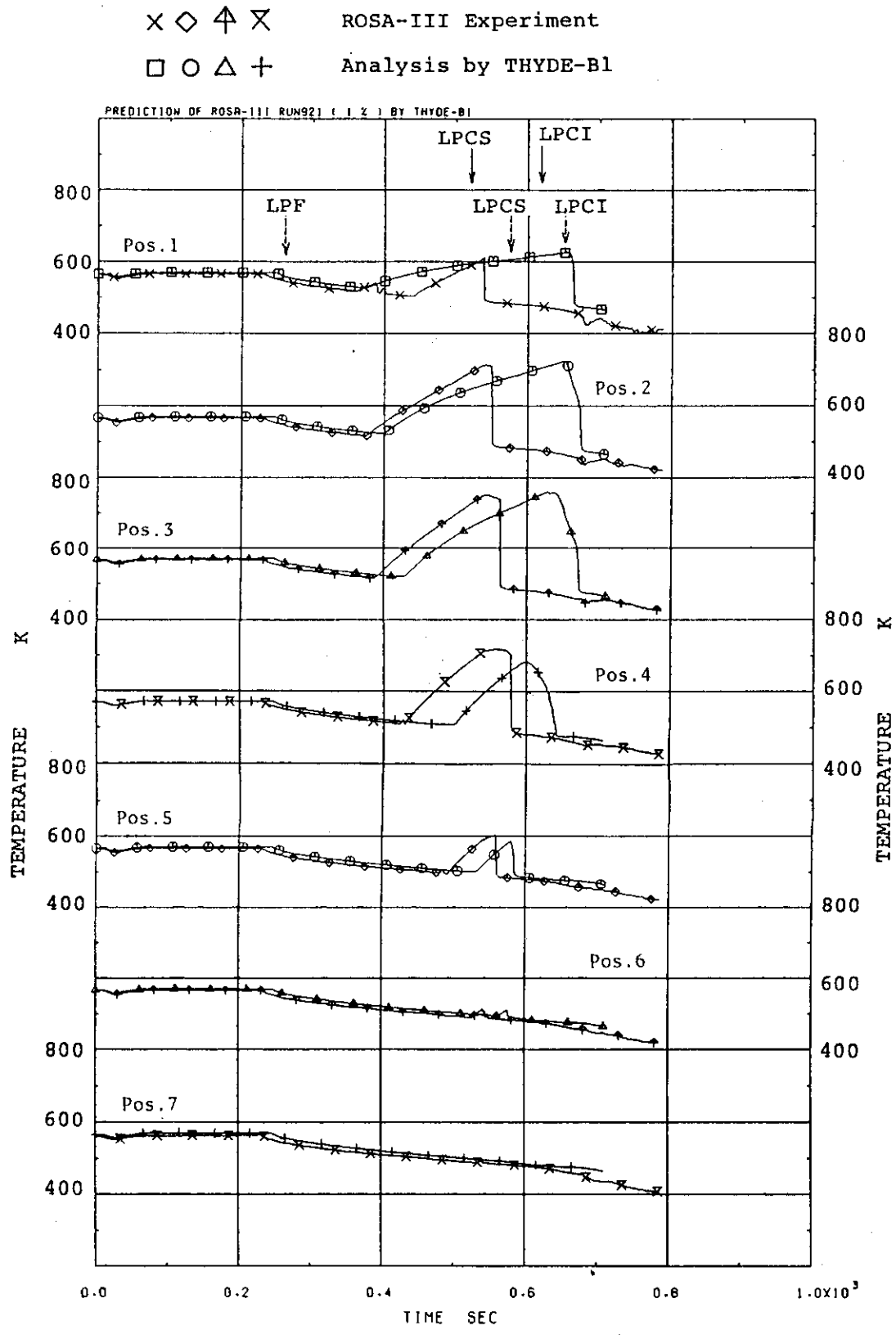

Fig. 4.5 Measured vs. calculated peak-power rod temperature - 1 % break test

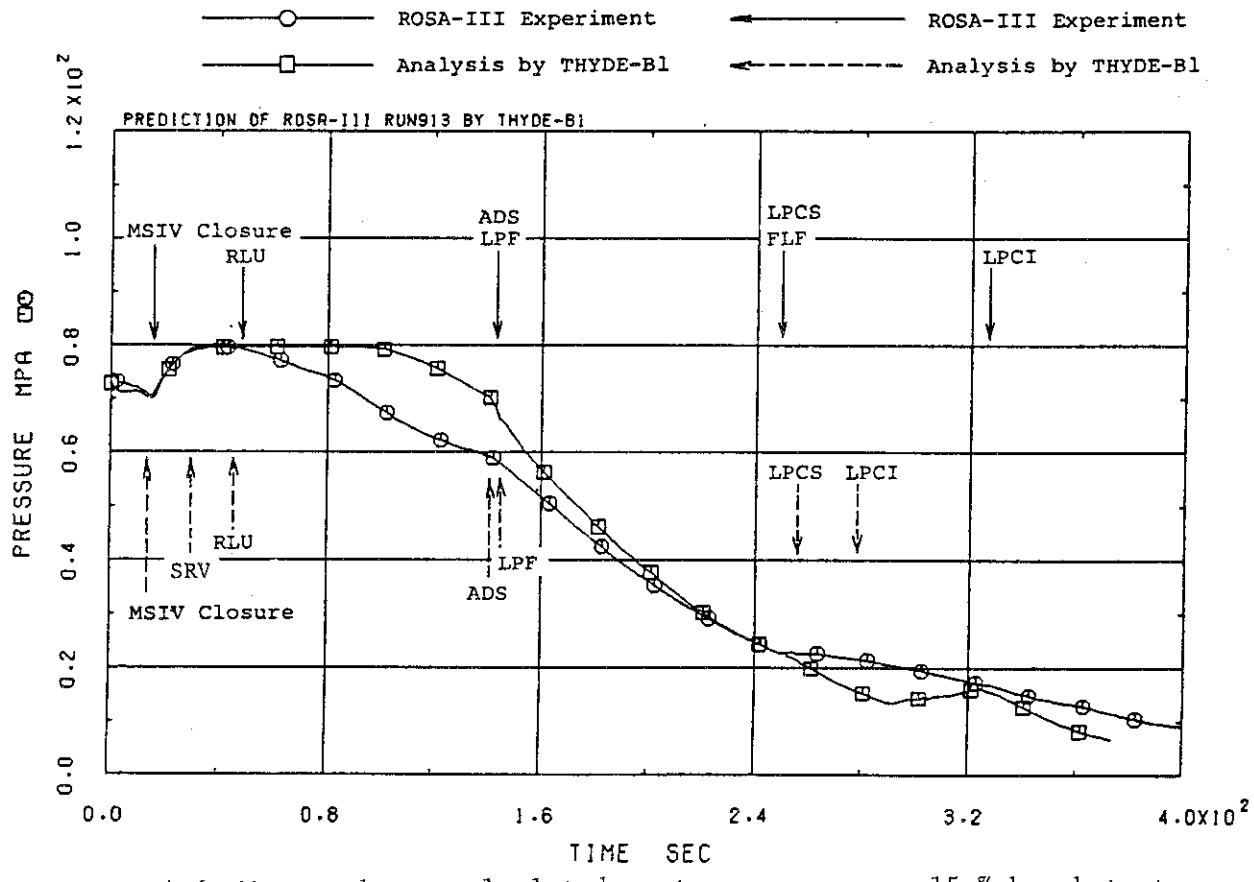

Fig. 4.6 Measured vs. calculated system pressures - 15 % break test

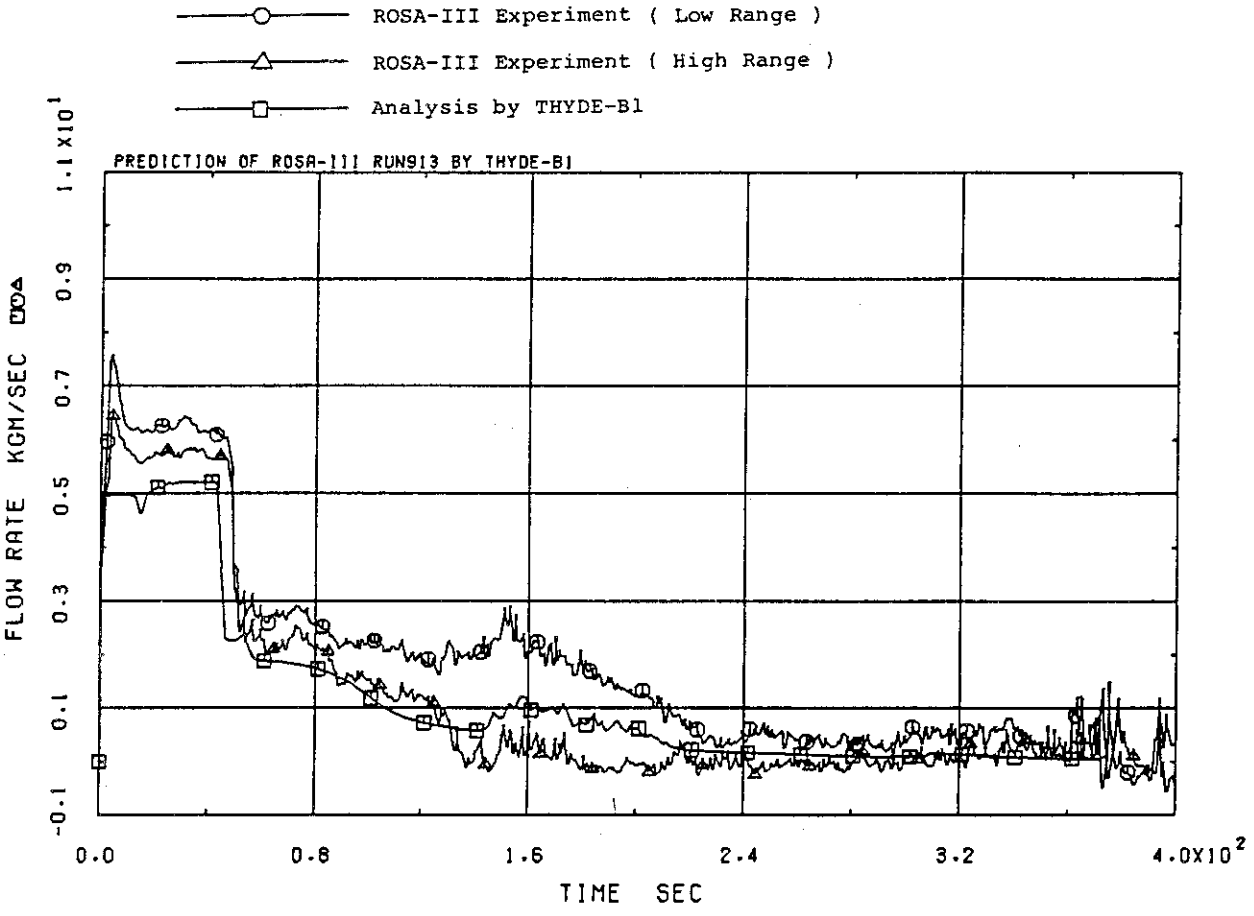

Fig. 4.7 Measured vs. calculated break flow rates - 15 % break test

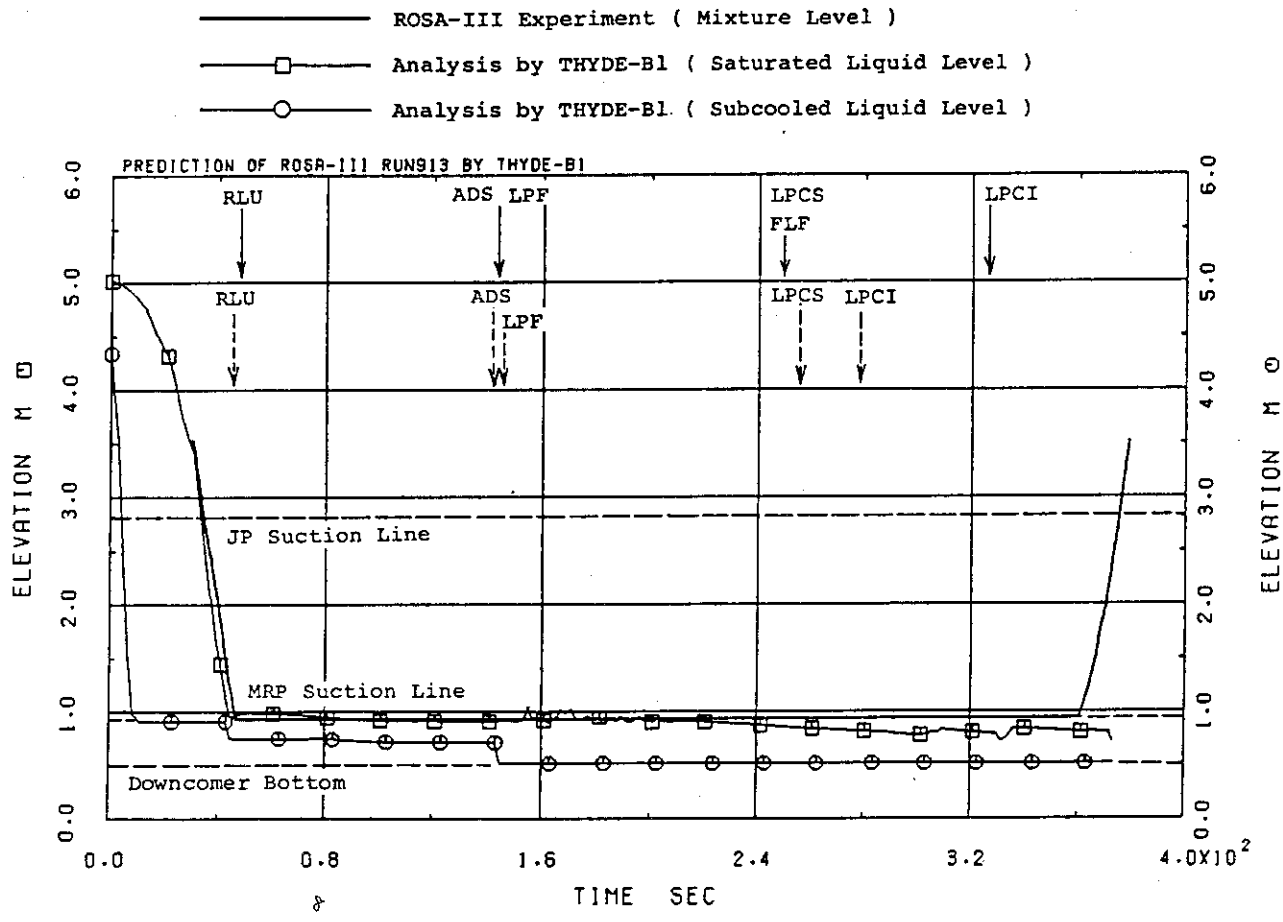

Fig. 4.8 Measured vs. calculated downcomer mixture levels - 15 % break test

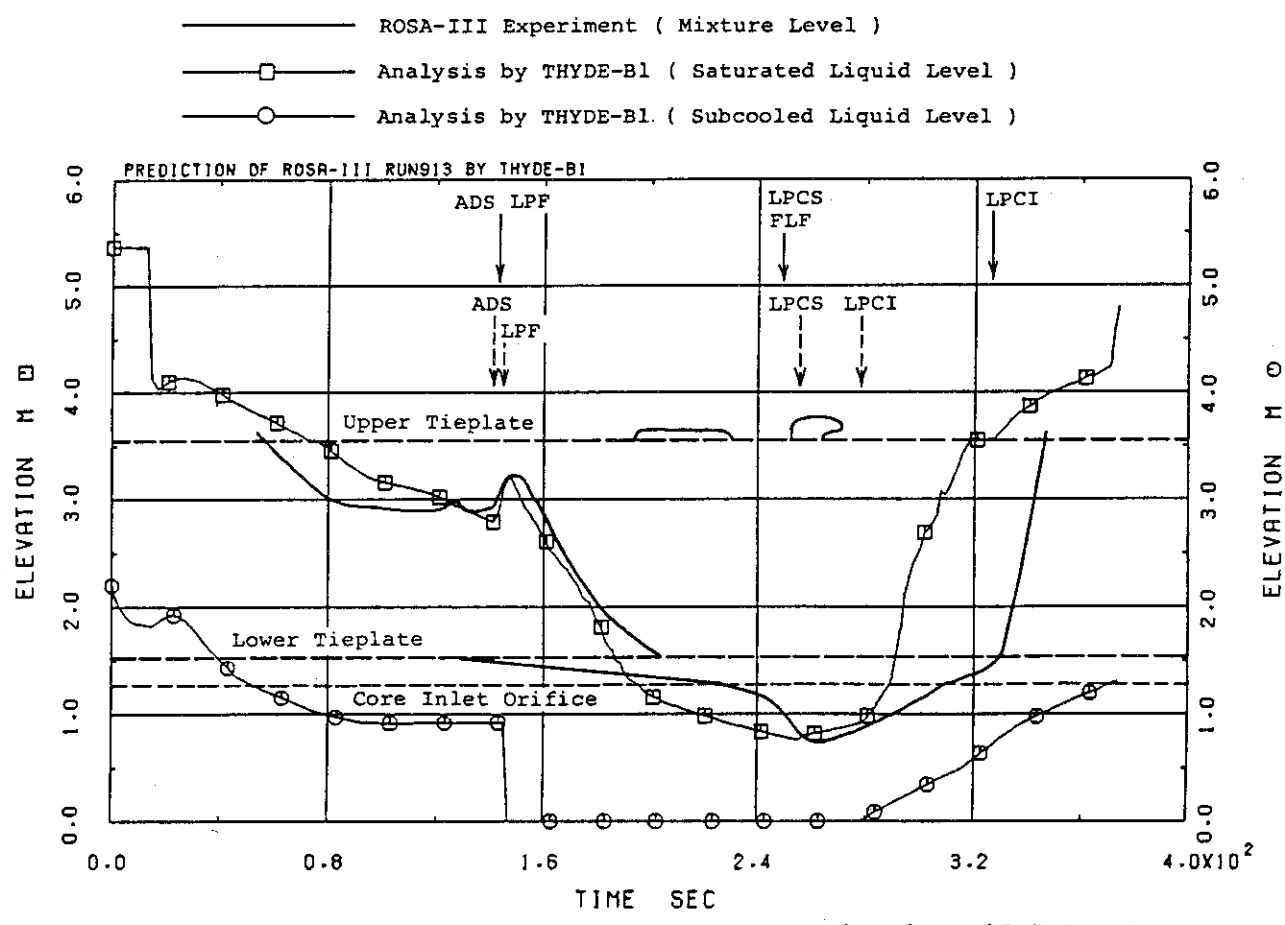

Fig. 4.9 Measured vs. calculated core mixture levels - 15 % break test

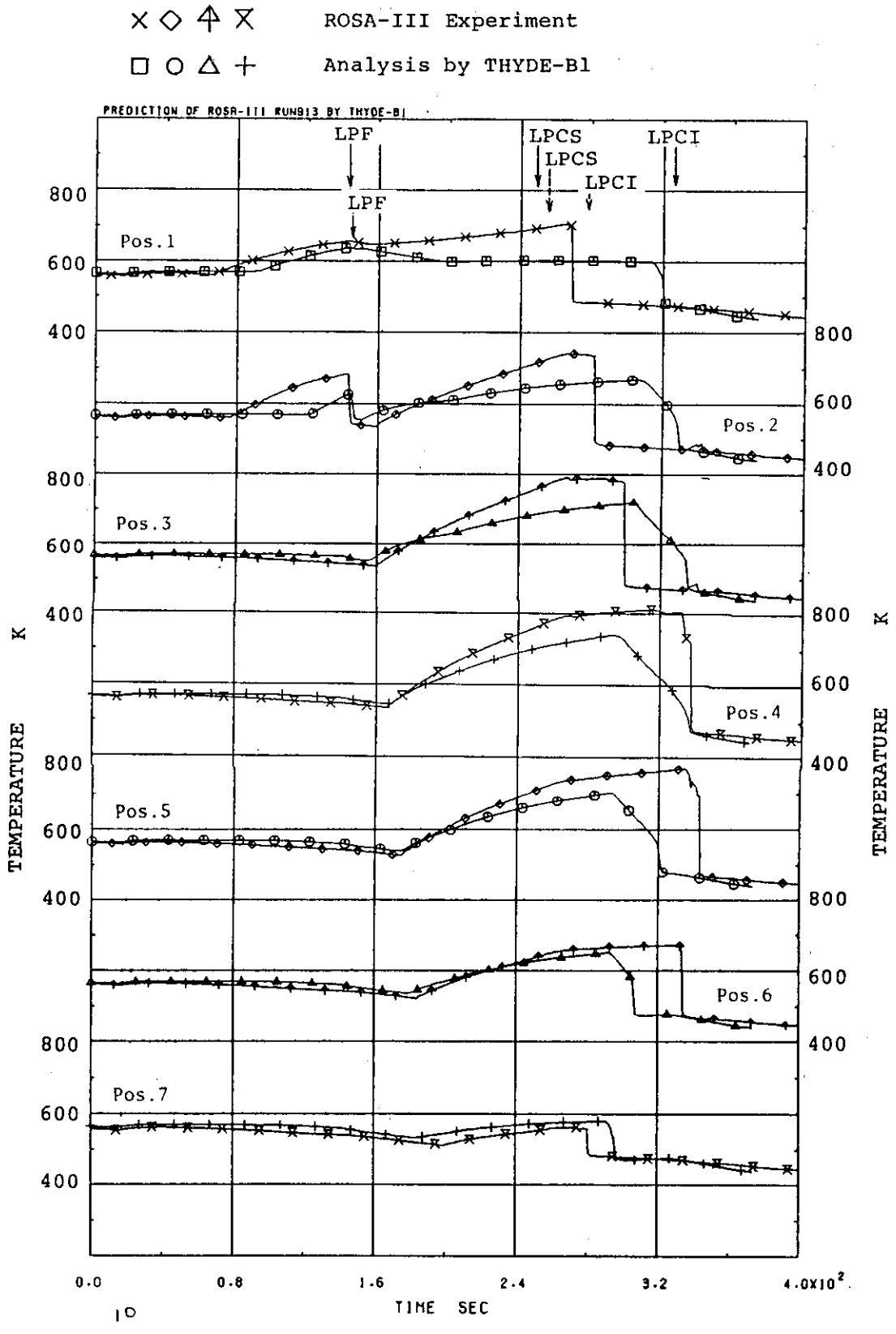

Fig. 4.10 Measured vs. calculated peak-power rod temperatures - 15 % break test

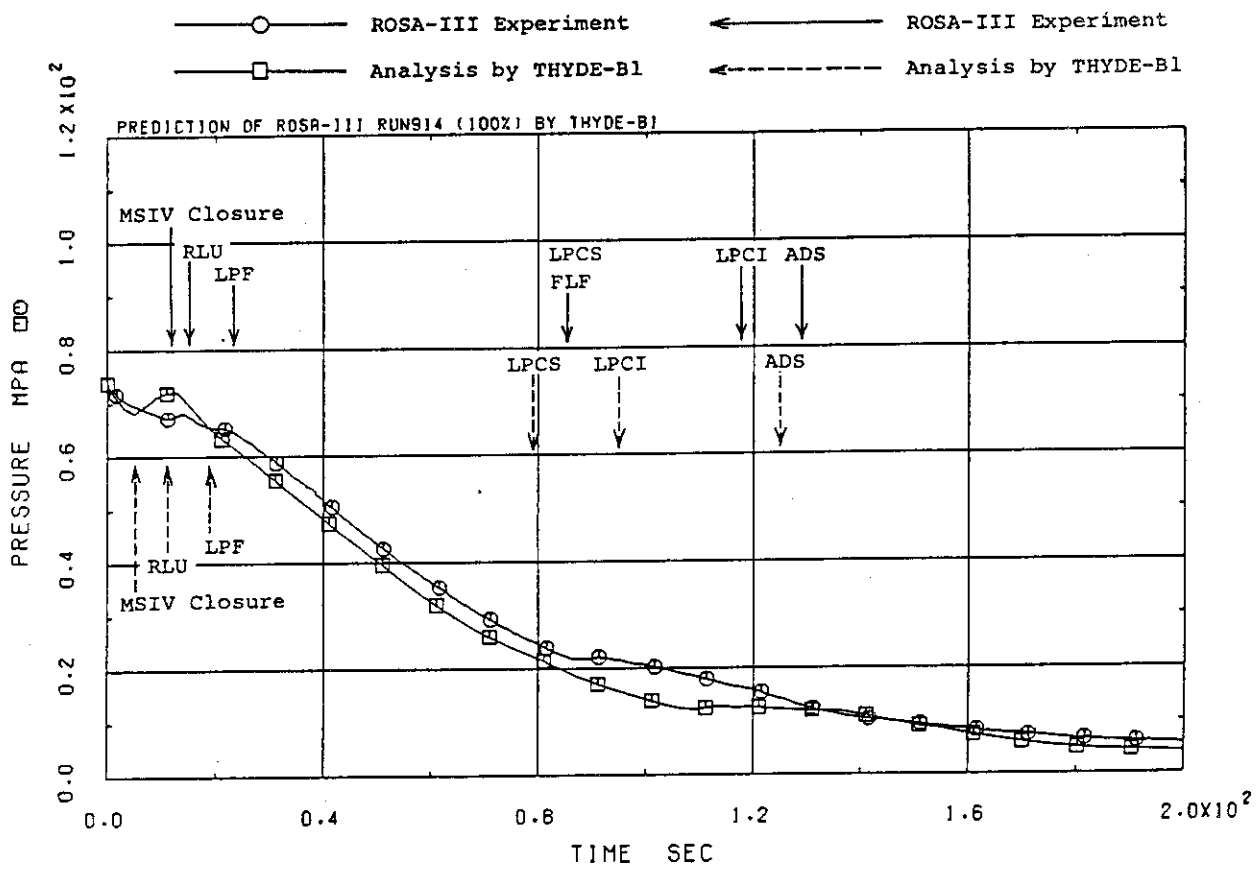

Fig. 4.11 Measured vs. calculated system pressures - 100 % break test

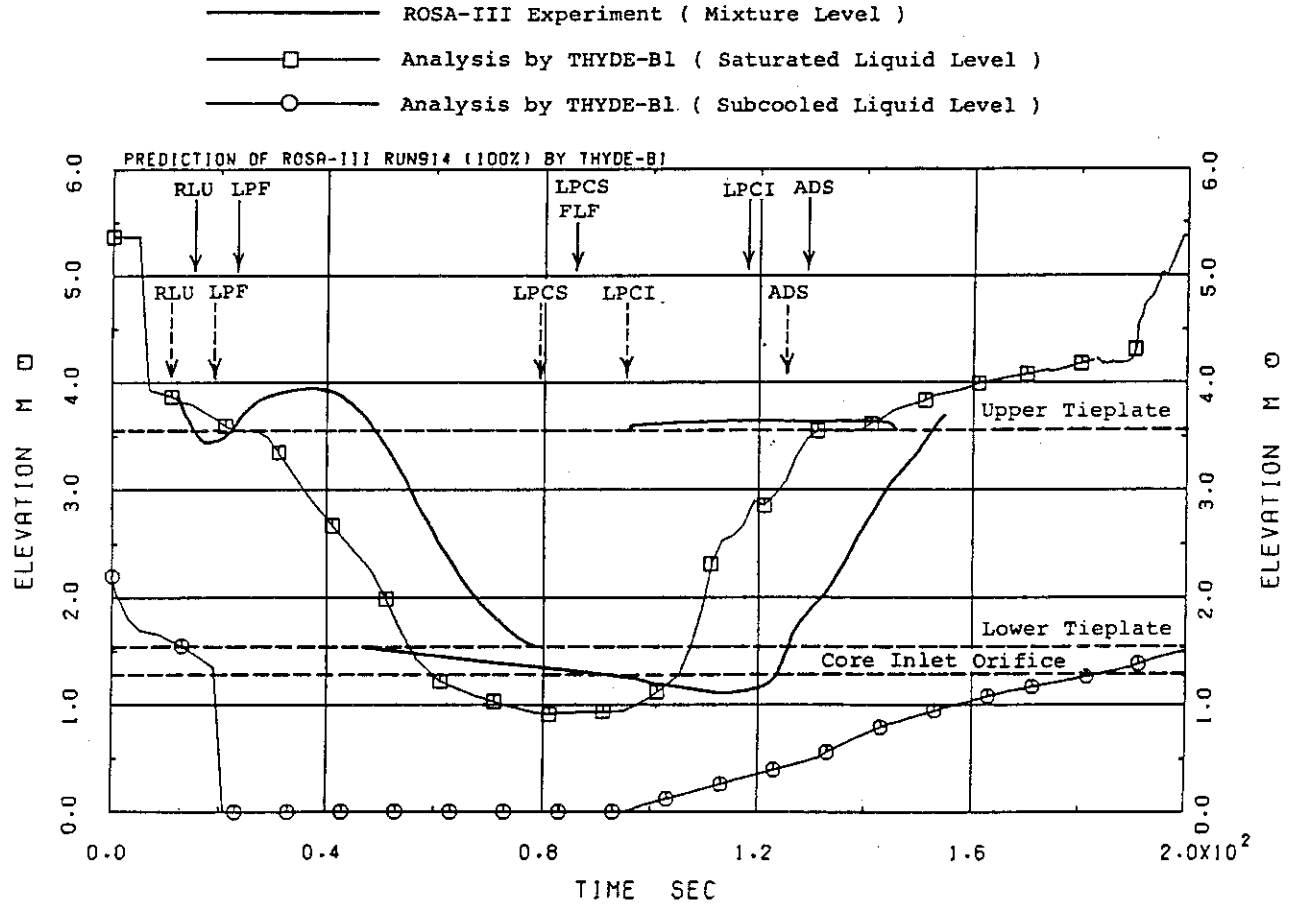

Fig. 4.12 Measured vs. calculated core mixture levels - 100 % break test

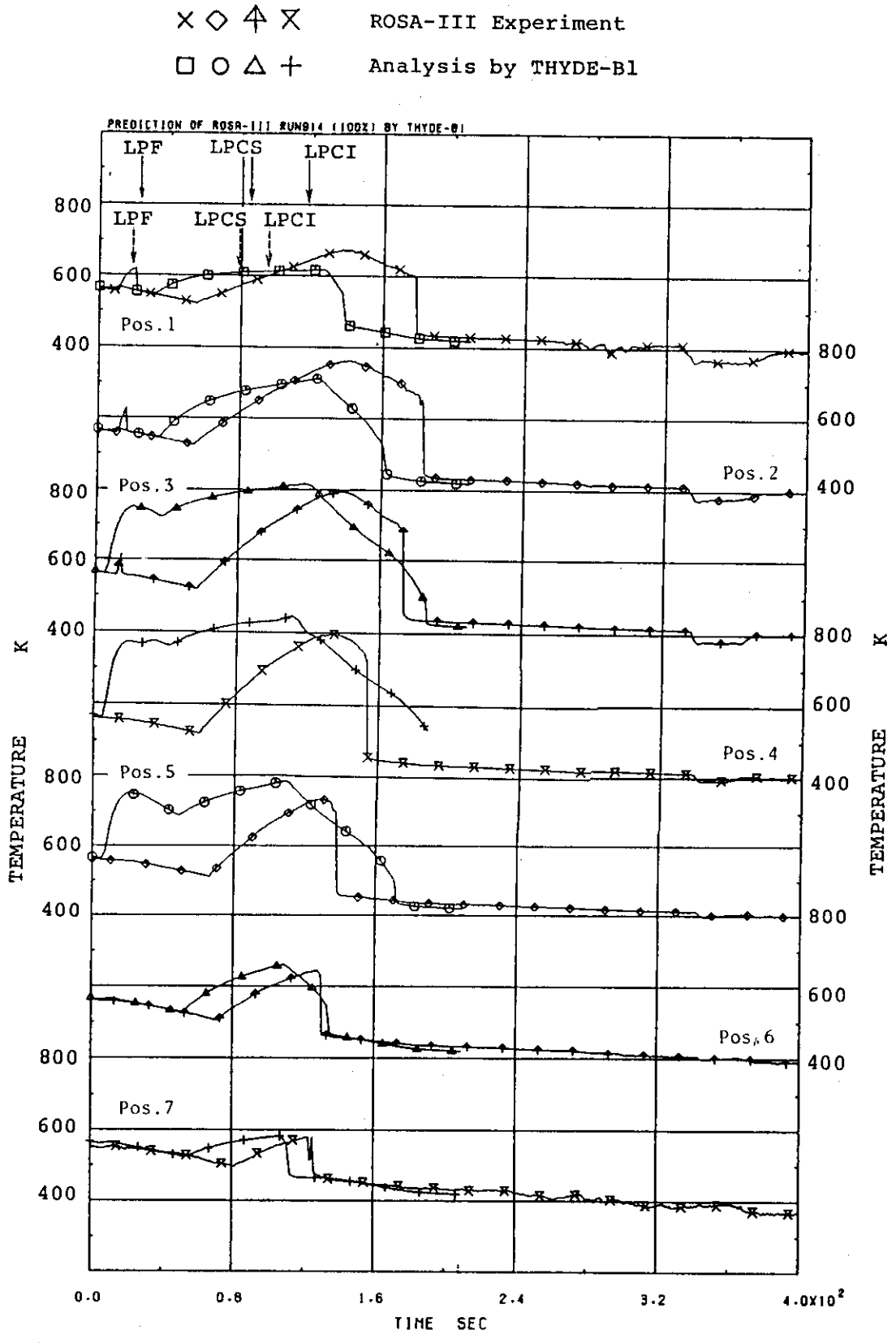

Fig. 4.13 Measured vs. calculated peak-power rod temperatures - 100 % break test

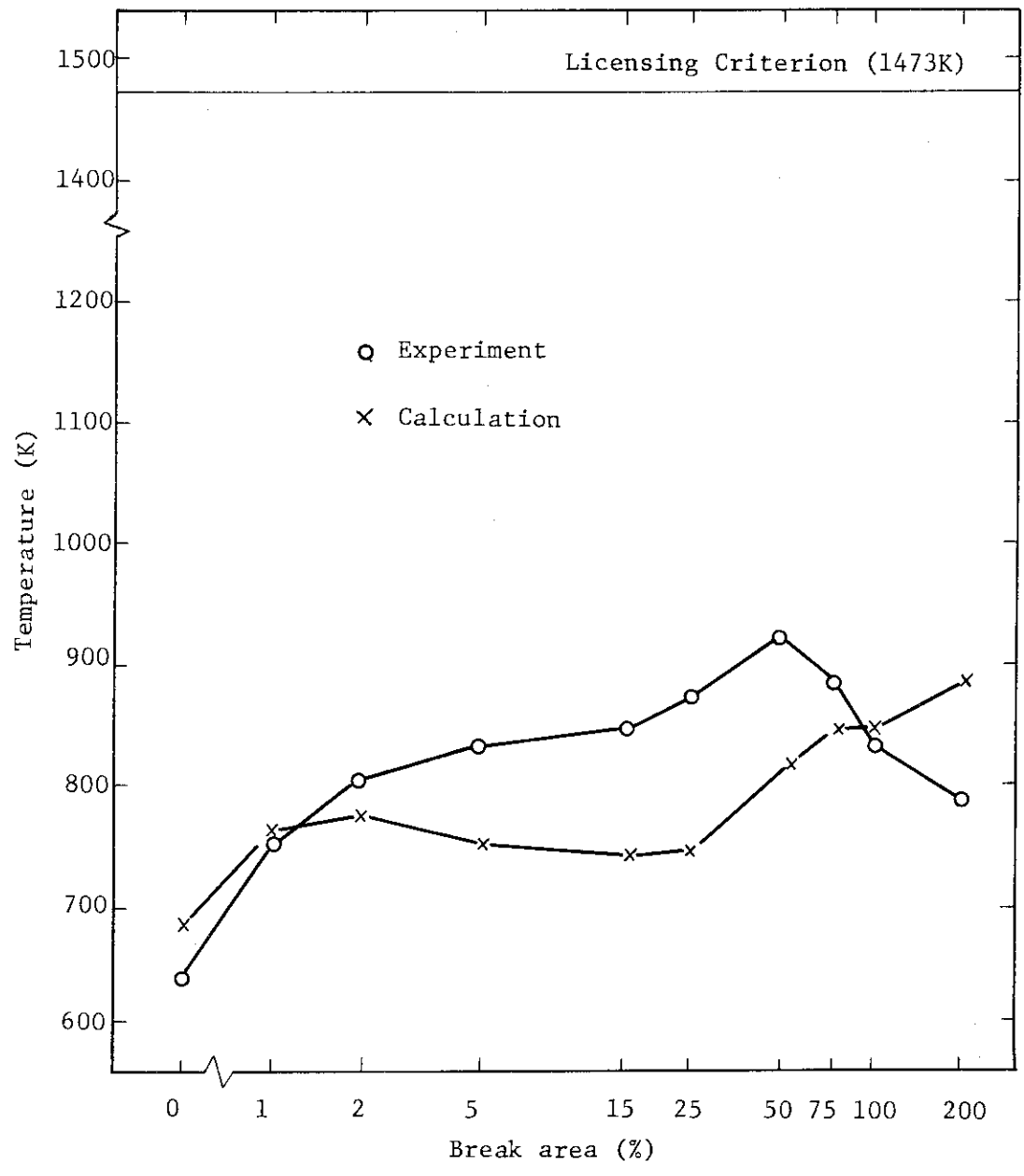

Fig. 4.14 Measured vs. calculated peak cladding temperatures for all tests

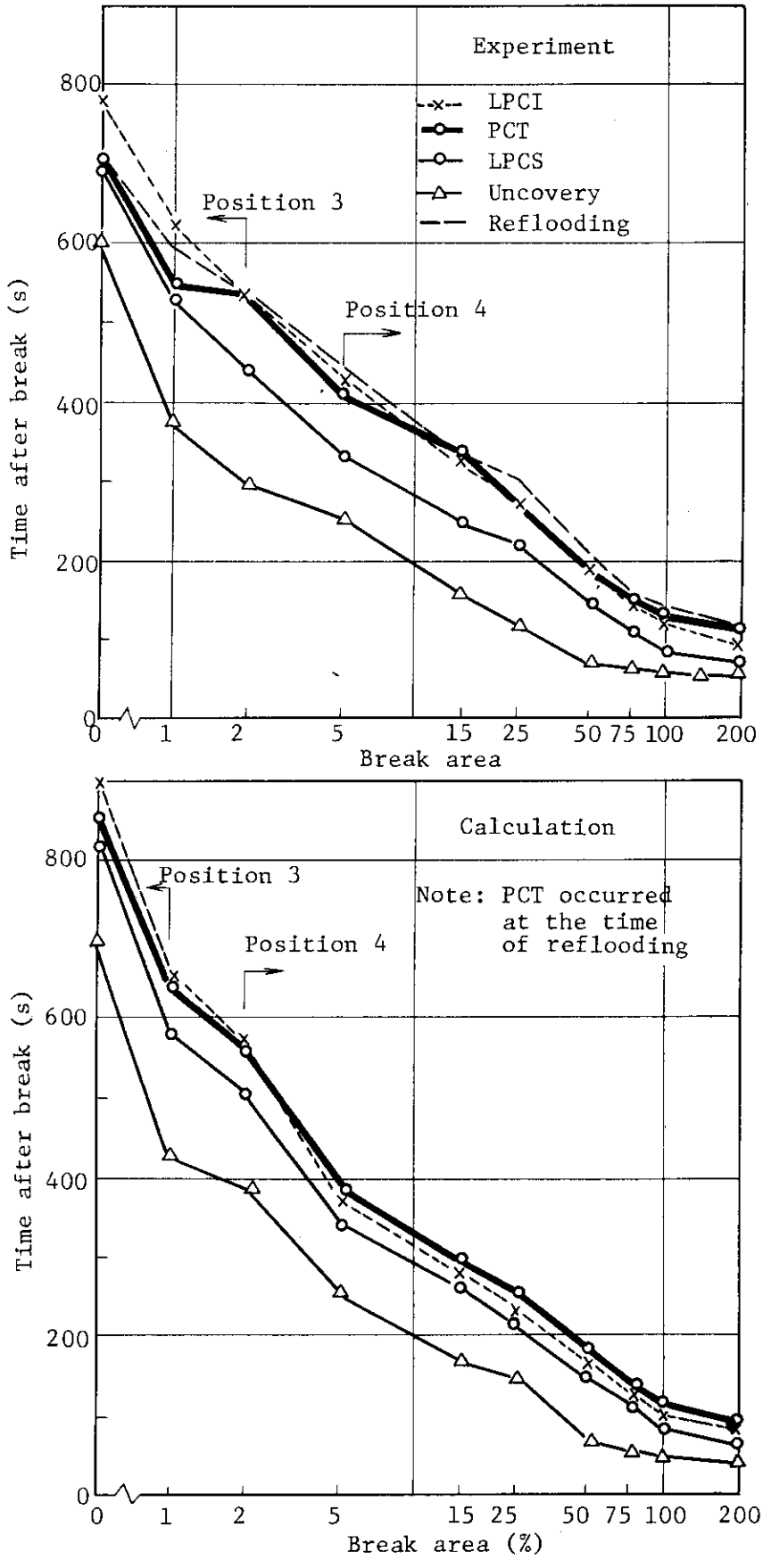

Fig 4.15 Measured vs. calculated timings of PCT and initiation of ECC flows.

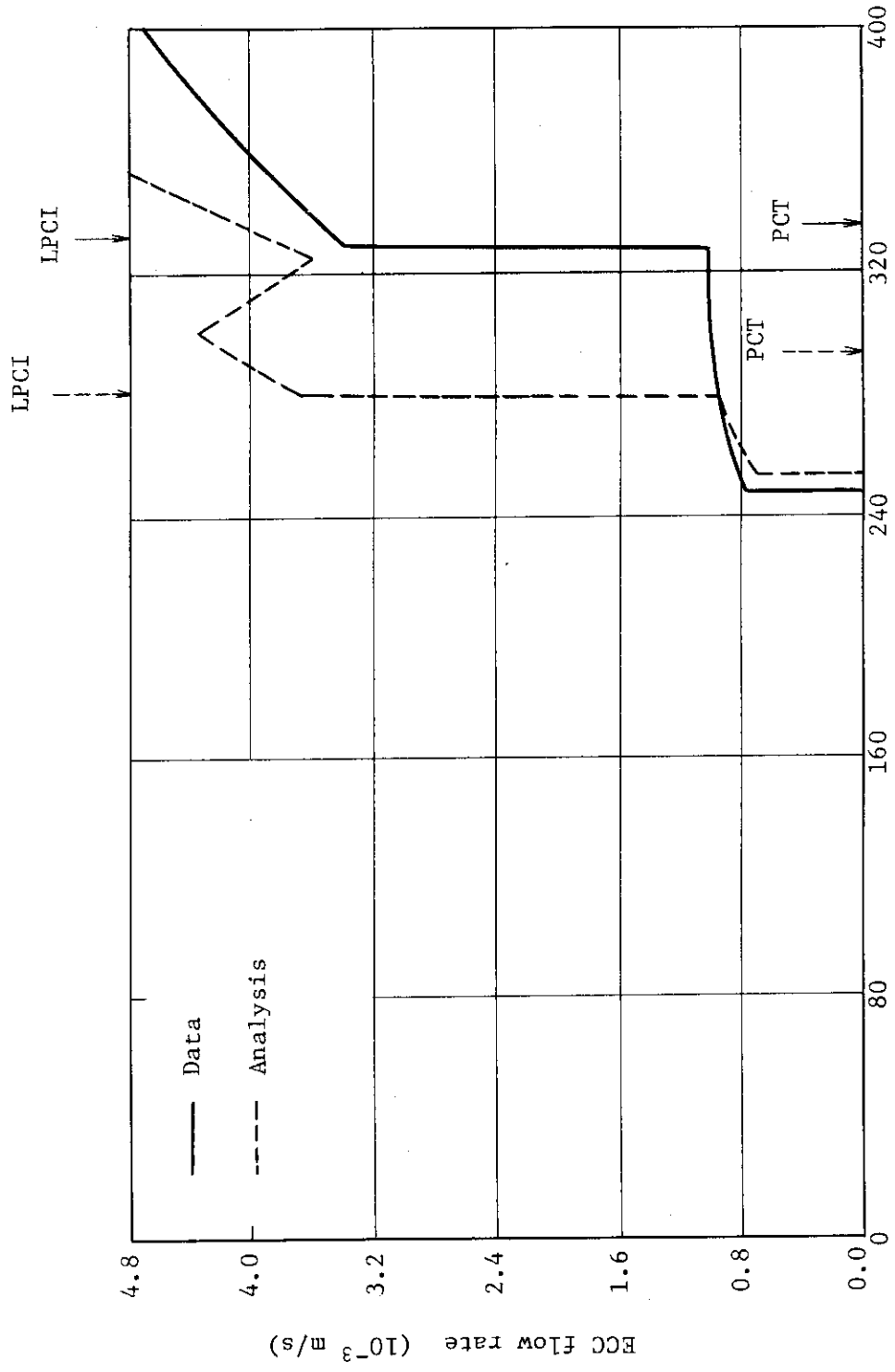

Fig. 4.16 Measured vs. calculated ECC flow rates - 15 % break test

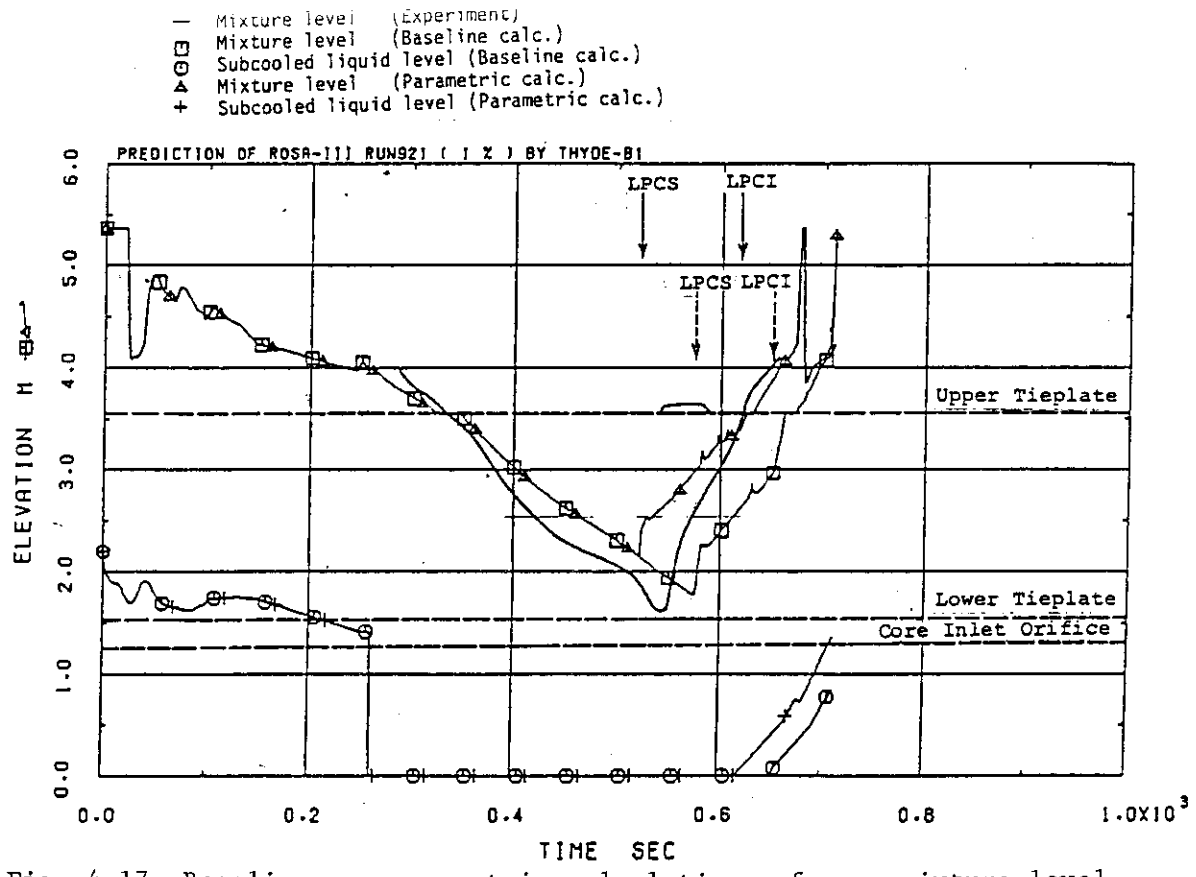

Fig. 4.17 Baseline vs. parametric calculations of core mixture level - 1 % break test

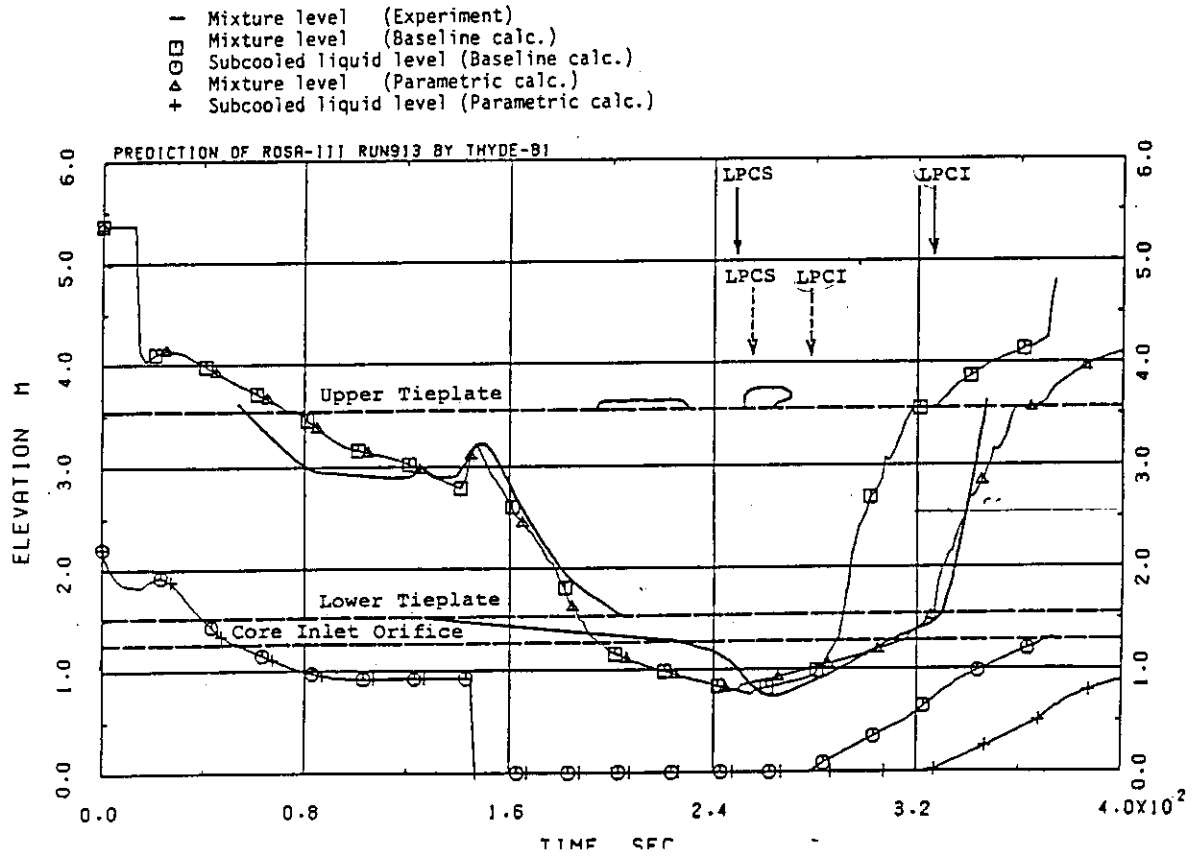

Fig. 4.18 Baseline vs. parametric calculations of core mixture level - 15 % break test

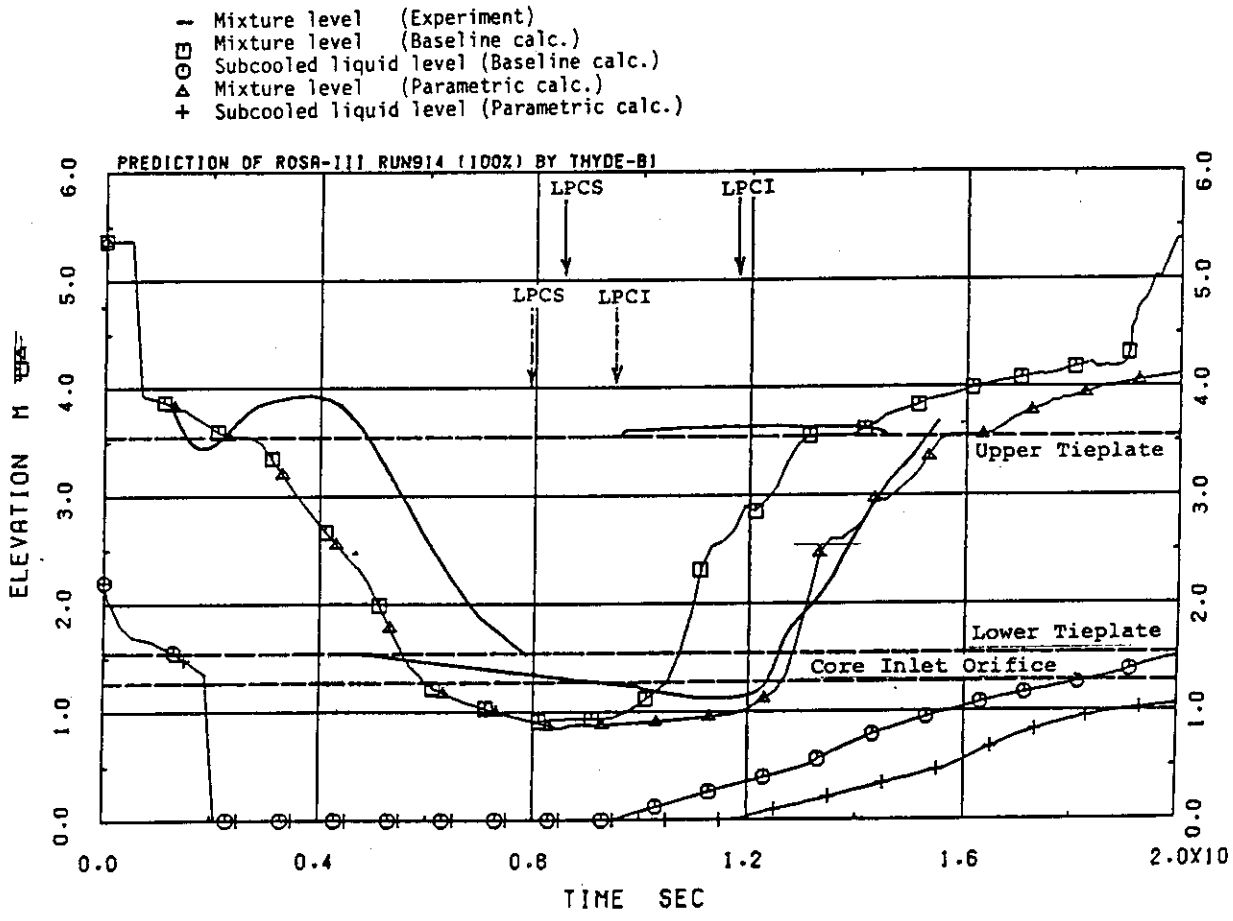

Fig. 4.19 Baseline vs. parametric calculations of core mixture level - 100 % break test

5. Conclusions

The calculational capability of the THYDE-B1/Mod 0 code was assessed against data from ten runs of ROSA-Ⅲ recirculation line break LOCA tests. In these tests the size of break was changed parametrically from 0 to 200%, and the failure of the high pressure core spray system (HPCS) was simulated.

The THYDE-B1 code is a fast-running best-estimate code developed for prediction of BWR small- and intermediate-break LOCAs. The code's fast-running capability is obtained at the cost of modeling the potential, complicated thermal-hydraulic phenomena during a LOCA, e.g., nonuniform void distribution in the two-phase mixture, thermal nonequilibrium in the steam phase, and the counter-current flow limiting (CCFL) phenomenon at the core inlet and outlet. Thus, dicrepancy was observed between the experimental and analytical results for the detailed system responses as follows:

(1) The rate of the initial downcomer liquid level fall was underpredicted for the small break tests with break areas <5%. Since the downcomer level signal was used to trip on the automatic depressurization system (ADS), both in the experiment and calculation, the slower level decrease led to delayed operation of ADS, and hence delayed core uncovery in the calculation.

(2) The break flow quality was underpredicted for the intermediate break tests with break areas between 5 and 50%, after the uncovery of the broken recirculation line inlet in the downcomer. This resulted in predicting slower system depressurization than the tests.

(3) The in-vessel steam generation due to evaporation of the low pressure core spray (LPCS) water was generally underpredicted. This resulted in overpredicting the system depressurization rate after the initiation of the LPCS flow, predicting earlier initiation of the low pressure injection system (LPCI) flow, and hence predicting earlier reflooding than the experiment.

(4) The height of core mixture level swell following the flashing in the lower plenum was generally underpredicted. This also resulted in underpredicting the in-vessel steam generation.

(5) The CCFL phenomenon at the core inlet influenced the core fluid drainage for the large break tests. Without consideration of this phenomenon, the code predicted earlier core emptying than the experiment.

(6) The top-down quench, occured in the tests at the core upper portion under the influence of the LPCS injection into the upper plenum, was not calculated because the code does not account for the direct contact between the falling ECCS water and the heater rods.
(7) Core temperature excursion occurred in the tests only after the dryout of the heater rod surface had occurred. However, the code predicted early DNB for the large breaks (larger than 50% in area). This resulted from underprediction of the core flow.
(8) The rod surface heat transter after the dryout was generally overpredicted, since the code assumes that steam is always at the saturation temperature.

Despite the above-mentioned discrepancies between the experimental and analytical results for the detailed system response, the comparisons showed that the THYDE-B1 code has capability to reproduce major system response for a wide range of break size. The time-dependent behavior of the system pressure, core mixture level, and rod surface temperature were reproduced by the code qualitatively. The peak cladding temperature (PCT) was well calculated for the small break tests, whereas considerably lower PCTs than the measurements were predicted for the intermediate break tests.

Good understanding has been obtained of the capability of the THYDE-B1 code through the assessment made in this report. This provides a basis for the study of applicability of the ROSA-Ⅲ test results to an actual BWR, to be made using the THYDE-B1/Mod 0 or later versions to predict the response of a BWR during a LOCA. The present results also provides basis for the future improvement of the code. It is recommended that updates be made particulary for the models for steam cooling, core flow, and in-vessel evaporation of ECC water and flashing.

Acknowledgment

The authors are grateful to K. Muramatsu for his valuable advices in conducting THYDE-B1 calculations.

Reference

(1) Yonomoto, T. et al., "Examination of Similarity between ROSA-Ⅲ and BWR/6 during a Large Break LOCA", JAERI-M 83-046 (February 1983)

(2) Yonomoto, T. et al., "Study on Similarity between ROSA-Ⅲ and BWR/6 during a Small Break LOCA", JAERI-M 84-030 (January 1984)

(3) Muramatsu, K., "Computer Programs, THYDE-B1 for Analysis of Small Break LOCA of a BWR and THYDE-B-REFLOOD for Analysis of Reflood Phase", JAERI-M 8119 (January 1979)

(4) Muramatsu, K. et al., "Analysis of ROSA-Ⅲ Small-Break LOCA Experiment RUN 804 by THYDE-B1 Computer Code", JAERI-M 9413 (February 1981)

(5) Anoda, Y. et al., "ROSA-Ⅲ System Description for Fuel Assembly No.4", JAERI-M 9363 (February 1981)

(6) GE Co., "General Electric Standard Safety Analysis Report, BWR/6, "DOCKET-STN-50477, General Electric Co. (1975)

(7) Tasaka, K. et al., "The LOCA/ECC System Effects Tests at ROSA-Ⅲ Changing the Break Area as Test Parameter, "Proc. Intl. Mtg. Thermal Nuclear Reactor Satety, Aug. 29 - Sep. 2, 1982, Chicago, NUREG/CP-0027 (1982)

(8) Special Committee on Safety Standards of Reactors, Nuclear Safety Commission of Japan, "Acceptance Criteria for Performance of ECCS for Light Water Cooled Nuclear Power Reactors." (1981)

(9) Moore K.V. et al., "RELAP4 - a Computer Program for Transient Thermal-Hydraulic Analysis", ANCR-1127 (1973)

Acknowledgment

The authors are grateful to K. Muramatsu for his valuable advices in conducting THYDE-B1 calculations.

Reference

(1) Yonomoto, T. et al., "Examination of Similarity between ROSA-Ⅲ and BWR/6 during a Large Break LOCA", JAERI-M 83-046 (February 1983)

(2) Yonomoto, T. et al., "Study on Similarity between ROSA-Ⅲ and BWR/6 during a Small Break LOCA", JAERI-M 84-030 (January 1984)

(3) Muramatsu, K., "Computer Programs, THYDE-B1 for Analysis of Small Break LOCA of a BWR and THYDE-B-REFLOOD for Analysis of Reflood Phase", JAERI-M 8119 (January 1979)

(4) Muramatsu, K. et al., "Analysis of ROSA-Ⅲ Small-Break LOCA Experiment RUN 804 by THYDE-B1 Computer Code", JAERI-M 9413 (February 1981)

(5) Anoda, Y. et al., "ROSA-Ⅲ System Description for Fuel Assembly No.4", JAERI-M 9363 (February 1981)

(6) GE Co., "General Electric Standard Safety Analysis Report, BWR/6, "DOCKET-STN-50477, General Electric Co. (1975)

(7) Tasaka, K. et al., "The LOCA/ECC System Effects Tests at ROSA-Ⅲ Changing the Break Area as Test Parameter, "Proc. Intl. Mtg. Thermal Nuclear Reactor Satety, Aug. 29 - Sep. 2, 1982, Chicago, NUREG/CP-0027 (1982)

(8) Special Committee on Safety Standards of Reactors, Nuclear Safety Commission of Japan, "Acceptance Criteria for Performance of ECCS for Light Water Cooled Nuclear Power Reactors." (1981)

(9) Moore K.V. et al., "RELAP4 - a Computer Program for Transient Thermal-Hydraulic Analysis", ANCR-1127 (1973)

APPENDIX

Appendix A THYDE-B1 Input Data for the 15% Break Test

```
----*----1----*----2----*----3----*----4----*----5----*----6----*----7-R--*----8

NO.1     MODULE NAME RUN913H              BLOCKS     14

                     LEVEL      1         DATE       83.07.19  TIME       09.59.46

                ***** APPOINTED MODULE INFORMATION *****

                     LEVEL      1         DATE       83.07.19  TIME       09.59.46


PREDICTION OF ROSA-III RUN913 BY THYDE-B1                                        00000100
/*****************************************************************           00000200
/**         BEST ESTIMATE CALCULATION                                **          00000300
/**              1983.07.08     BY IRIKO                            **          00000400
/**                 UPDATED  1983.07.14                             **          00000500
/**                                                                 **          00000600
/**        + CONSIDERATION OF CHANNEL BOXES HEAT CAPACITY           **          00000700
/**        + CONSIDERATION OF FILLER BLOCK  HEAT CAPACITY           **          00000800
/**        + CONSIDERATION OF CONTROL ROD   HEAT CAPACITY           **          00000900
/**        + RNJUNC = 9.6E+5  ( JP-THROAT )                         **          00001000
/*****************************************************************           00001100
000   /*      PLOT , RESTART CONTROL OPTION                                    00001200
/*     NREST   IDUMP    IDPLOT     ISPL                                       00001300
         0       1         1         1                                       00001400
001   /PROBLEM DIMENSION                                                      00001500
/*    NVOL NJUN NPMP NJG   NJP   NST   NLK   NFIL NHPI NLPI NCS   NTRP   NSEP 00001600
      6    19   2    2     1     0     4     1    0    1    2     14     1    00001700
/*    NTMAX                                                                  00001800
    6                                                                        00001900
003   / TIME STEP CONTROL DATA                                                00002000
/*    NRST       NPRINT     NPLOT      DELT       TMAX                       00002100
      5000            1          1     0.001      0.004                      00002200
      5000          200         20     0.001      0.2                        00002300
      5000          500        100     0.002      1.0                        00002400
      10000         10000     1000     0.002    180.                         00002500
      50000        50000       500     0.003    500.                         00002600
      5000         10000       500     0.003    510.                         00002700
/*                                                                           00002800
004   / VOLUME DATA  (6 VOLUMES )                                            00002900
/* CARD1  IHOMO                                                            00003000
/* CARD2  PRES       ZMAX       ZELEV      ZPRES      VMAX                  00003100
/* CARD3  X          AREA ( FOR HOMOGENEOUS NODE ONLY)                     00003200
/* CARD4  ENTN(1)    ALPHA                                                 00003300
/* CARD5  ZLEV(1)    ZLEV(2)                                               00003400
/* CARD6  CAS        CLM                                                   00003500
/*        HP1        HP2                                                   00003600
/* CARD8  NTV                                                              00003700
/* CARD9  Z-VOL TABLE                                                      00003800
/* CARD10 NTA                                                              00003900
/* CARD11 Z-A   TABLE                                                      00004000
/* CARD12 NTD                                                              00004100
/* CARD13 Z-DH  TABLE                                                      00004200
/*                                                                         00004300
/* NODE1  ( SHROUD INSIDE )                                                00004400
          2                                                  /CARD1         00004500
          742677.   5.365     0.         0.         0.5344   /CARD2         00004600
```

```
----*----1----*----2----*----3----*----4----*----5----*----6----*----7-R--*----8
          293.6      0.46                                          /CARD4        00004700
          2.2        5.365                                           /CARD5      00004800
          0.         1.0        0.0        5.365                   /CARD6      00004900
/*  CARD 8   NOMBER OF POINTS IN ELEV-VOL  TABLE                                 00005000
    10                        /                                                 00005100
/* CARD 9    ELEVATION - VOLUME TABLE                                           00005200
       0.           0.                                                         00005300
       0.497        0.1168                                                     00005400
       1.354        0.2235                                                     00005500
       3.589        0.3795                                                     00005600
       3.744        0.4050                                                     00005700
       4.243        0.5031                                                     00005800
       4.578        0.5095                                                     00005900
       4.654        0.5109                                                     00006000
       5.099        0.5291                                                     00006100
       5.365        0.5344      /                                              00006200
/*                                                                            00006300
/*                                                                            00006400
/*  CARD 10 NUMBER OF POINTS IN ELEVATION AREA TABLE                          00006500
    2                                                                         00006600
/*  CARD 11 ELEVATION - AREA TABLE                                            00006700
    0.   0.04    5.365   0.04        /                                        00006800
/*  CARD  12    NUMBER OF POINTS IN ELEV-DH TABLE                             00006900
    8     /                                                                   00007000
/*  CARD  13    ELEVATION - HYDRUALIC DIAMETER  TABLE                         00007100
        0.          0.032         1.284  0.032                               00007200
        1.294       0.0132        3.551  0.0132                              00007300
        3.561       0.499         4.254  0.499                               00007400
        4.264       0.1688        5.365  0.1688     /                        00007500
/* NODE2              (SHROUD OUTSIDE)                                       00007600
          2                                                      /CARD1       00007700
          737590.    5.5        0.494      0.          0.7111   /CARD2       00007800
          293.6      0.001                                       /CARD4       00007900
          3.83       4.506                                       /CARD5       00008000
          -10.       0.0        3.406      5.5                  /CARD6       00008100
/*  CARD 7  ELEVATION-VOLUME TABLE  POINT NUMBER                              00008200
    13 /                                                                      00008300
/*  CARD 8  ELEVATION-VOLUME TABLE                                            00008400
     0.             0.                                                       00008500
     0.89           0.0200                                                   00008600
     1.025          0.02897                                                  00008700
     2.861          0.0707                                                   00008800
     3.756          0.1424                                                   00008900
     3.919          0.1822                                                   00009000
     4.084          0.2253                                                   00009100
     4.16           0.2442                                                   00009200
     4.321          0.2826                                                   00009300
     4.421          0.3111                                                   00009400
     4.649          0.3886                                                   00009500
     4.871          0.4684                                                   00009600
     5.5            0.7111                                                   00009700
/*                                                                            00009800
/*                                                                            00009900
          10                                                     /CARD9       00010000
          0.          .0235      2.861      .0235      2.862    .0783        00010100
          3.754       .0783      3.755      .2288      3.918    .2288        00010200
          3.919       .3225      5.153      .3225      5.154    .3505        00010300
```

```
----*----1----*----2----*----3----*----4----*----5----*----6----*----7-R--*----8
          5.5        .3505                                    /CARD10      00010400
          10                                                                00010500
          0.         .0283      2.861      .0283      2.862    .0920        00010600
          3.754      .0920      3.755      .4220      3.918    .4220        00010700
          3.919      .6437      5.153      .6437      5.154    .6727        00010800
          5.5        .6727                            /CARD11               00010900
/* NODE3  ( BROKEN PIPE )                                                   00011000
          1                                                    /CARD1       00011100
          737525.    1.489      -0.526     0.         .01303   /CARD2       00011200
           293.6     2.1E-3                                    /CARD3       00011300
/*NODE4   ( PIPE FROM PUMP OUTLET TO JETPUMPS(BROKEN SIDE))                  00011400
          1                                                    /CARD1       00011500
          793967.   5.852      -2.526     0.        0.04050  /CARD2       00011600
           293.6    1.98E-3                                                 00011700
/* NODE5  (PIPE FROM VESSEL TO PUMP  (INTACT SIDE)                          00011800
      1                                                        /CARD1       00011900
      738765.        3.197      -2.235     0.        0.01057  /CARD2       00012000
       293.6       . 2.18E-3                                               00012100
/* NODE6  (PIPE FROM PUMP TO JET PUMP (INTACT SIDE)                         00012200
      1                                                        /CARD1       00012300
      791644.        5.851      -2.526     0.        0.03006  /CARD2       00012400
       293.6         2.03E-3                                  /CARD3       00012500
/*                                                                         00012600
005   / JUNCTION DATA                                                      00012700
/* CARD1  NIN        NOUT       IPUMP      IVALVE     WIJ       ZIN        00012800
/*        ZOUT       AJUNC      INERTA     RJUNC      RNJUNC               00012900
/*                                                                         00013000
/* J1     (STEAM SEPARATOR)                                                00013100
          1          2          -1         0          17.2      5.365      00013200
          4.871      1.496E-2   426.       0.         0.                 /  00013300
/*        4.871      1.496E-2   213.       0.         0.                 /  00013400
/* J2     (DOWNCOMER - BROKEN PIPE)                                        00013500
          2          3          0          0          3.4       0.444      00013600
          1.464      1.923E-3   3108.      0.         0.                 /  00013700
/*        1.464      1.923E-3   1554.      0.         0.                 /  00013800
/* J3     (BROKEN PIPE - PUMP)                                             00013900
          3          4          1          0          3.4       0.025      00014000
/*        2.025      1.923E-3   6673.      0.         0.                 /  00014100
          2.025      1.923E-3   13346.     0.         0.                 /  00014200
/* J4     (JET PUMP DRIVE FLOW  (BROKEN SIDE))                             00014300
          4          0          0          0          3.4       5.267      00014400
          0.         1.110E-4   6968.      0.         0.                 /  00014500
/*        0.         1.110E-4   3484.      0.         0.                 /  00014600
/* J5     (JET PUMP THROAT FLOW (BROKEN SIDE))                             00014700
          0          1          0          0          8.6       0.         00014800
          0.4        1.785E-3   2830.      0.         9.6E+5             /  00014900
/*        0.4        1.785E-3   1415.      0.         0.                 /  00015000
/* J6     (JET PUMP SUCTION FLOW (BROKEN SIDE))                            00015100
          2          0          0          0          5.2       2.247      00015200
          0.         1.674E-3   1776.      0.         0.                 /  00015300
/*        0.         1.674E-3   888.       0.         0.                 /  00015400
/* J7     (DOWNCOMER - PIPE (INTACT SIDE)                                  00015500
          2          5          0          0          3.4       0.444      00015600
          3.173      1.923E-3   3312.      0.         0.                 /  00015700
/*        3.173      1.923E-3   1656.      0.         0.                 /  00015800
/* J8     ( PUMP SUCTION    (INTACT SIDE))                                 00015900
          5          6          2          0          3.4       0.         00016000
```

```
----*----1----*----2----*----3----*----4----*----5----*----6----*----7-R--*----8
          0.291     1.923E-3  9000.     0.        0.                    /  00016100
/* J9     (JET PUMP DRIVE FLOW (INTACT SIDE))                               00016200
          6         0         0         0         3.4       5.267       00016300
          0.        1.110E-4  15072.    0.        0.                    /  00016400
/*        0.        1.110E-4  7536.     0.        0.                    /  00016500
/* J10    (JET PUMP THROAT (INTACT SIDE)                                    00016600
          0         1         0         0         8.6       0.          00016700
          0.4       1.785E-3  2828.     0.        9.6E+5                /  00016800
/*        0.4       1.785E-3  1414.     0.        0.                    /  00016900
/* J11    (JET PUMP SUCTION (INTACT SIDE))                                  00017000
          2         0         0         0         5.2       2.247       00017100
          0.        1.674E-3  1772.     0.        0.                    /  00017200
/*        0.        1.674E-3  886.      0.        0.                    /  00017300
/* J12    (HPCS (CS NO.1))                                                  00017400
          -4        1         1         0         0.        0.          00017500
          4.099     0.        0.        0.        0.                    /  00017600
/* J13    (LPCS (CS NO.2))                                                  00017700
          -4        1         2         -2        0.        0.          00017800
          4.099     0.        0.        0.        0.                    /  00017900
/* J14    (LPCI (LPCI NO.1))                                                00018000
          -3        1         1         -3        0.        0.          00018100
          0.1       0.        0.        0.        0.                    /  00018200
/* J15    (ADS  (LEAK NO.1))                                                00018300
          2         -1        1         0         0.        5.50        00018400
          0.        1.885E-4  0.        0.        0.                    00018500
/* J16    (BREAK (LEAK NO.2))                                               00018600
          3         -1        2         0         0.        0.025       00018700
          0.        8.012E-5  0.        0.        0.                    /  00018800
/* J17    (SRV  (LEAK NO.3))                                                00018900
          2         -1        3         0         0.        5.5         00019000
          0.        5.16E-4   0.        0.        0.                    /  00019100
/* J18    (FW   (FILL NO.1))                                                00019200
          -1        2         1         0         2.04      0.          00019300
          3.839     0.        0.        0.        0.                    /  00019400
/* J19    (MSL  (LEAK NO.4))                                                00019500
          2         -1        4         1         2.04      5.5         00019600
          0.      3.1416E-4   0.        0.        0.                    /  00019700
/*                                                                         00019800
/*                                                                         00019900
006   / JET PUMP JUNCTION GROUP                                           00020000
/* CARD1  JMOPT     IJPUMP    JETGRP(1) (2)       (3)       PIN         /00020100
                                                                          00020200
/* GROUP1 (BROKEN SIDE)                                                   /00020300
          2         1         6         4         5         721219.     00020400
/* GROUP2 (INTACT SIDE)                                                   /00020500
          2         1         11        9         10        721475.     00020600
/*                                                                         00020700
007   / JET PUMP GEOMETRY DATA CARD                                       00020800
/* CARD1  AS        AD        AJ        ADIF      DL1       DL2         00020900
/*        DL3       AJS       AJD       AJJ                             00021000
          4.743E-4  1.108E-4   5.851E-4  1.         0.1       0.285      /00021100
          1.956     1.         1.        1.                              00021200
/*                                                                         00021300
008 / RECIRCULATION PUMP DATA                                             00021400
/* CARD1 TPCON      HO        QO        XNO       FX  XKSP              00021500
/*      INTACT SIDE                                                       00021600
          4.718     57670.    3.4       197.      0.  0.      /           00021700
/* PUMP CHARACTERISTIC CURVE
```

```
----*----1----*----2----*----3----*----4----*----5----*----6----*----7-R--*----8
/*                                                                      00021800
     2                                                    /CARD2        00021900
     9  0.                                                              00022000
 0.0          0.92         0.222        0.94         0.443        0.97   00022100
 0.665        1.0          1.109        1.0          1.583        1.019  00022200
 2.772        0.75         4.434        0.           10.E20       0.     00022300
   2   0.025                                                            00022400
 0.0          0.0          1.E20        0.0           /                 00022500
/* CARD1 TPCON      HO          QO          XNO       FX  XKSP          00022600
         4.718      58609.     3.4         202.      0.    0.     /     00022700
/* PUMP CHARACTERISTIC CURVE                                            00022800
/*                                                                      00022900
     2                                                    /CARD2        00023000
     9  0.                                                              00023100
 0.0          0.92         0.222        0.94         0.443        0.97   00023200
 0.665        1.0          1.109        1.0          1.583        1.019  00023300
 2.772        0.75         4.434        0.           10.E20       0.     00023400
   2   0.025                                                            00023500
 0.0          0.0          1.E20        0.0           /                 00023600
/*                                                                      00023700
/*    PUMP 2                                                            00023800
010   / LEAK DATA                                                       00023900
/* CARD1  ICHOKE    SINK PR.  CONCO      ZLEAK      HLEAK               00024000
/*        ICHOKE=-3 TIME-FLOW TABLE                                     00024100
/*        ICHOKE=-2                                                     00024200
/*        ICHOKE=-1 PRESSURE FLOW TABLE                                 00024300
/*                                                                      00024400
/*                                                                      00024500
/*                                                                      00024600
/* CARD1(PS)   CONC1  TRNQL    (THIS CARD IS USED ONLY WHEN ICHOKE=2)    00024700
/* CARD2  NFAT                                                          00024800
/* CARD3  TABA(1) ---TABA(2*NFAT)                                       00024900
/*                                                                      00025000
/* LEAK 1 (ADS  JUNC.15)                                                00025100
/*        CHOKED FLOW LEAK DATA FOR BASE CASE                           00025200
          1          1.E4       0.6         5.4        0.1          / 00025300
          3                                                         /  00025400
          0.         0.         .1          1.         2000.      1.  /  00025500
/*                                                                      00025600
/* LEAK 2 (BREAK  JUNC.16)                                              00025700
          2          1.E4       0.6         0.025      0.           /  00025800
          0.61       0.02                               /               00025900
          3                                                         /  00026000
          0.         0.         0.1         1.         2000.      1.  /  00026100
/* LEAK 3 (SRV    JUNC.17)                                              00026200
          -1         1.E4       1.          5.4        0.1    /        00026300
          4                                                         /  00026400
          0.        0.        810000.     0.       820000.    2.        00026500
          1406142.     6.     /                                        00026600
/*        0.         0.         828218.     0.         828921.    2.128  00026700
/*        843123.    2.128      843137.     4.867      857044.    4.867  00026800
/*        857184.    6.044      1406142.    6.044                    /  00026900
/* LEAK 4 (MSL  JUNC.19)                                                00027000
/*                                                                      00027100
          1          1.E4       0.6         5.4        0.1          /  00027200
          3                                                         /  00027300
          0.         1.         0.1         1.         2000.      1.  /  00027400
```

```
----*----1----*----2----*----3----*----4----*----5----*----6----*----7-R--*----8
/*                                                                      00027500
011  / FILL                                                             00027600
/* CARD1  CGL        CML        FEG        FEM                         00027700
/* CARD2  NT                                                           00027800
/* CARD3  T OR H TABLE                                                 00027900
/* CARD4  NW                                                           00028000
/* CARD5  W      TABLE                                                 00028100
/* FILL 1 (FEED WATER  JUNC.18)                                        00028200
          0.1        0.         1.         1.        / COMPLETE MIXING  /  00028300
/*        0.1        1.         0.         0.        /COMPLETE NO-MIXING   00028400
/*        0.1        0.         0.         1.  /MIXING IN MIXTURE          00028500
/*                                             NOMIXING IN VAPOR SUB NODE  00028600
          0                                                          /      00028700
          221.4                                                      /      00028800
/*        TIME-FLOW TABLE FOR BASE CASE                                     00028900
          -4                                                                00029000
          0.         2.04       2.0        2.04       4.0        0.0       00029100
          2000.0     0.0          /                                        00029200
/*                                                                          00029300
/* LPCI   (JUNC.14)                                                        00029400
013 / LPCI                                                                  00029500
          1.         0.2        0.         1.                        /     00029600
          0                                                          /      00029700
          40.                                                        /      00029800
/*                                                                          00029900
/*        PRESSURE DEPENDENT FLOW TABLE                                     00030000
          7                                                                 00030100
          0.         4.3        5.E4       4.2        10.E4      4.        00030200
          15.E4      3.2        20.E4      1.4        22.E4      0.        00030300
          100.E4     0.  /                                                 00030400
/*        P-W TABLE END                                                     00030500
/*                                                                          00030600
014/ CORE SPRAY                                                             00030700
/* CS 1   (HPCS      JUNC.12)                                              00030800
          0.1        0.         1.         1.                        /     00030900
          0                                                          /      00031000
          40.                                                        /      00031100
/*                                                                          00031200
/*        P-W TABLE FOR BASE CASE                                           00031300
          5                                                          /      00031400
          0.         0.82       45.E4      0.78       88.E4      0.25      00031500
          89.E4      0.        100.E4       0.  /                          00031600
/*        P-W TABLE END                                                     00031700
/*                                                                          00031800
/* CS 2   (LPCS      JUNC.13)                                              00031900
          0.1        0.         1.         1.                        /     00032000
          0                                                          /      00032100
          40.  /                                                             00032200
          8                                                          /      00032300
          0.         1.         5.E4       0.98       15.E4      0.84      00032400
          20.E4      0.74       30.E4      0.4        32.E4      0.3       00032500
          33.E4      0.         1.E7      0.   /                           00032600
/*                                                                          00032700
015   / STEAM SEPARATOR EFFICIENCY                                          00032800
/* CARD1  NTAB                                                            00032900
/* CARD2  TABLE                                                           00033000
          2                                                          /      00033100
```

```
----*----1----*----2----*----3----*----4----*----5----*----6----*----7-R--*----8
          0.        1.        10.       1.                              /  00033200
/*                                                                          00033300
016   / TRIP CONTROL                                                        00033400
/*CARD1   IDACT     KSIG      IV        IPV       SETP      DELAY          00033500
/*                                                                        00033600
/*                                                                        00033700
          22        1         0         0         0.        0.    /BREAK 00033800
          81        -3        2         0         4.264     1.E6   /HPCS 00033900
          82        -3        2         0         3.756     40.   /LPCS  00034000
          71        -3        2         0         3.756     40.   /LPCI  00034100
          21        -3        2         0         3.756     120.  /ADS   00034200
          31        1         0         0         0.        0.    /PUMP1 00034300
          32        1         0         0         0.        0.    /PUMP2 00034400
          -101      -3        2         0         4.264     3.    /MSIV  00034500
          23         1        0         0         0.        0.    /SRV   00034600
          102       -2        2         0         220000.   0.    /LPCS  00034700
          103       -2        2         0         160000.   0.    /LPCI  00034800
/* DUMMY                                                                   00034900
          -101       1        0         0          10000.  0.              00035000
          -101       1        0         0          10000.  0.              00035100
          -101       1        0         0          10000.  0.              00035200
/*                                                                        00035300
/*                                                                        00035400
017   /***  DIMENSION CARD FOR SLABS  ***                                  00035500
/* NSLAB   NGEOM  NMATG    NTVSNP   NTALP                                 00035600
/*     NOCOR   NMAT   MAXREG    NTROD   NTFUT                            00035700
    22  16   9  8   0   4    45   0   0   0                               00035800
/*                                                                        00035900
018   /***  HEAT SLAB DATA CARDS  ***                                      00036000
/* NVSL   NVSR   IGEOM       ZSLB      HLSLB     VOLS                    00036100
/*                           AHTR      HMDR      DHER                    00036200
    1        0       1        1.586     0.2350    2.894E-5                00036300
                              0.009236  0.01438   0.01438   /SLAB1 CORE100036400
    1        0       1        1.821     0.2350    2.854E-5                00036500
                              0.009236  0.01438   0.01438   /SLAB2 CORE200036600
    1        0       1        2.056     0.2350    2.854E-5                00036700
                              0.009236  0.01438   0.01438   /SLAB3 CORE300036800
    1        0       1        2.291     0.4700    5.782E-5                00036900
                              0.01847   0.01438   0.01438   /SLAB4 CORE400037000
    1        0       1        2.761     0.2350    2.894E-5                00037100
                              0.009236  0.01438   0.01438   /SLAB5 CORE500037200
    1        0       1        2.996     0.2350    2.894E-5                00037300
                              0.009236  0.01438   0.01438   /SLAB6 CORE600037400
    1        0       1        3.231     0.2350    2.894E-5                00037500
                              0.009236  0.01438   0.01438   /SLAB7 CORE700037600
    1        0       2        0.        1.110     7.06E-5                 00037700
                              0.0314    0.02      0.02 /SLAB8 CABLE 1     00037800
    2        0       3        0.494     5.500     0.2920                  00037900
                              6.547     0.4025    0.4025    /SLAB9        00038000
    1        0       4        0.        0.517     0.3594                  00038100
                              1.5218    0.7000    0.7000    /SLB10        00038200
    1        0       1        1.586     0.2350    2.894E-5                00038300
                              0.009256  0.01438   0.01438   /SLB11 CORE800038400
    1        0       1        1.821     0.2350    2.894E-5                00038500
                              0.009236  0.01438   0.01438   /SLB12 CORE900038600
    1        0       1        2.056     0.2350    2.894E-5                00038700
                              0.009236  0.01438   0.01438   /SLB13 COR1000038800
```

```
----*----1----*----2----*----3----*----4----*----5----*----6----*----7-R--*----8
    1       0       1          2.291     0.4700    5 .782E-5                00038900
                               0.01847   0.01438    0.01438   /SLB14 COR1100039000
    1       0       1          2.761     0.2350    2.894E-5                 00039100
                               0.009236  0.01438    0.01438   /SLB15 COR1200039200
    1       0       1          2.996     0.2350    2.894E-5                 00039300
                               0.009236  0.01438    0.01438   /SLB16 COR1300039400
    1       0       1          3.231     0.2350    2.894E-5                 00039500
                               0.009236  0.01438    0.01438   /SLB17 COR1400039600
    1       0       6          1.11      1.587     5.64E-5                  00039700
                               0.01839   0.02       0.02  /SLAB18 CABLE 2  00039800
    1       0       5          1.159     2.391     1.555E-2                 00039900
                               5.069     0.01227   0.01227 /SLAB19 C.B.     00040000
    1       2       7          1.519     1.836     0.08329                  00040100
                               2.9551    0.323     0.323                    00040200
                               2.6648    0.323     0.323    /SLAB20 F.B.    00040300
    1       0       8          0.0       0.2871    1.373E-2                 00040400
                               1.7585    0.02425   0.02425 /SLAB21 L.P.     00040500
    1       0       9          1.524     2.026     0.6697E-2                00040600
                               2.026     0.012     0.012    /SLAB22 C.R.    00040700
/*                                                                          00040800
/*                                                                          00040900
019   /***  CORE SECTION DATA CARDS  ***                                     00041000
/* ISLB    IXSN      PSLB      X         TFCT                              00041100
    1       186       0.0399    1.0       0.0399              /CORE #01     00041200
    2       186       0.0766    1.0       0.0766              /CORE #02     00041300
    3       186       0.1039    1.0       0.1039              /CORE #03     00041400
    4       186       0.2409    1.0       0.2409              /CORE #04     00041500
    5       186       0.1039    1.0       0.1039              /CORE #05     00041600
    6       186       0.0766    1.0       0.0766              /CORE #06     00041700
    7       186       0.0399    1.0       0.0399              /CORE #07     00041800
   11        62       0.0186    1.0       0.0186              /CORE #08     00041900
   12        62       0.0358    1.0       0.0358              /CORE #09     00042000
   13        62       0.0485    1.0       0.0485              /CORE #10     00042100
   14        62       0.1125    1.0       0.1125              /CORE #11     00042200
   15        62       0.0485    1.0       0.0485              /CORE #12     00042300
   16        62       0.0358    1.0       0.0358              /CORE #13     00042400
   17        62       0.0186    1.0       0.0186              /CORE #14     00042500
    8       248       0.        1.        0.        /CABLE 1                00042600
   18       248       0.        1.        0.        /CABLE 2                00042700
/*                                                                          00042800
020   /***  SLAB GEOMETRY DATA CARDS  ***                                    00042900
/* JGOM    JREG                                                            00043000
/* JGAP    (GAP INDEX)                                                     00043100
/* JMAT    (MTERIAL INDEX)                                                 00043200
/* JPNT    (NUMBER OF SPACE MESH)                                          00043300
/* WREG    (REGIO WIDTH)                                                   00043400
/* DREG    (MATERIAL DENSITY)                                              00043500
/* PREG    (POWER FRACTION)                                                00043600
/* TREG    (WEIGHTING FACTOR FOR AVE. TEMP. CALC.)                         00043700
/* SLAB GEOMETRY DATA SET NO. 1                                            00043800
    2       4                                                               00043900
    0               0               0               0                       00044000
    3               2               3               4                       00044100
    3               1               1               1                       00044200
    0.002825        0.0007          0.00131         0.0013                  00044300
    1850.           8410.           1850.           8430.                   00044400
    0.0             1.0             0.0             0.0                     00044500
```

```
----*----1----*----2----*----3----*----4----*----5----*----6----*----7-R--*----8
    0.0           1.0           0.0           0.0                          00044600
/* SLAB GEOMETRY DATA SET NO. 2                                            00044700
    2     3                                                                 00044800
    0             0             0                                           00044900
    7             6             4                                           00045000
    1             1             1                                           00045100
    0.0025        0.001         0.001                                       00045200
    8960.         2700.         8430.                                       00045300
    1.0           0.0           0.0                                         00045400
    1.0           0.0           0.0                                         00045500
/* SLAB GEOMETRY DATA SET NO. 3                                            00045600
    1     1                                                                 00045700
    0                                                                       00045800
    5                                                                       00045900
    4                                                                       00046000
    0.03962                                                                 00046100
    7910.                                                                   00046200
    0.0                                                                     00046300
    0.0                                                                     00046400
/* SLAB GEOMETRY DATA SET NO. 4                                            00046500
    1     1                                                                 00046600
    0                                                                       00046700
    5                                                                       00046800
    4                                                                       00046900
    0.155                                                                   00047000
    7910.                                                                   00047100
    0.0                                                                     00047200
    0.0                                                                     00047300
/* SLAB GEOMETRY DATA SET NO. 5 ( CHANNEL BOX )                            00047400
    1     1                                                                 00047500
    0                                                                       00047600
    5                                                                       00047700
    4                                                                       00047800
    0.003                                                                   00047900
    7910.                                                                   00048000
    0.0                                                                     00048100
    0.0                                                                     00048200
/* SLAB GEOMETRY DATA SET NO. 6                                            00048300
    2     3                                                                 00048400
    0             0             0                                           00048500
    8             6             4                                           00048600
    1             1             1                                           00048700
    0.0034        0.001435      0.0013                                      00048800
    8960.         2700.         8430.                                       00048900
    1.0           0.0           0.0                                         00049000
    1.0           0.0           0.0                                         00049100
/* SLAB GEOMETRY DATA SET NO. 7 ( FILLER BLOCK )                           00049200
    1     1                                                                 00049300
    0                                                                       00049400
    5                                                                       00049500
    4                                                                       00049600
    0.0488                                                                  00049700
    7910.                                                                   00049800
    0.0                                                                     00049900
    0.0                                                                     00050000
/* SLAB GEOMETRY DATA SET NO. 8 ( LOWER PLENUM STRUCTURE )                 00050100
    1     1                                                                 00050200
```

```
----*----1----*----2----*----3----*----4----*----5----*----6----*----7-R--*----8
    0                                                                   00050300
    5                                                                   00050400
    4                                                                   00050500
    0.012                                                               00050600
    7910.                                                               00050700
    0.0                                                                 00050800
    0.0                                                                 00050900
/* SLAB GEOMETRY DATA SET NO. 9 ( CONTROL ROD )                        00051000
    1     1                                                             00051100
    0                                                                   00051200
    5                                                                   00051300
    4                                                                   00051400
    0.006                                                               00051500
    7910.                                                               00051600
    0.0                                                                 00051700
    0.0                                                                 00051800
/*                                                                      00051900
021   /***  MATERIAL PROPERTY DATA CARDS  ***                           00052000
/* (1) THERMAL CONDUCTIVITY TABLE                                      00052100
/* NTPK                                                                00052200
/* TPK    (TEMP. COND. ---)                                            00052300
    7     / BORON-NITRIDE ( NOT USED )                                  00052400
      0.  7.213E-3      300.  6.903E-3      500.  6.696E-3              00052500
    700.  6.489E-3      900.  6.283E-3     1000.  6.407E-3              00052600
   2000.  7.647E-3                                                      00052700
    3     / NICHROME-5                                                  00052800
     20.  4.175E-3      100.  3.307E-3     2605.  2.778E-3              00052900
    5     / BORON-NITRIDE                                               00053000
    100.  1.500E-3      200.  1.639E-3      400.  1.833E-3              00053100
    600.  1.944E-4      800.  2.000E-3                                  00053200
   11     / INCONEL-600                                                 00053300
      0.0 3.486E-3       21.1 3.548E-3       93.3 3.754E-3             00053400
    204.4 4.168E-3      315.6 4.581E-3      426.7 4.994E-3              00053500
    537.8 5.442E-3      648.9 5.924E-3      760.0 6.407E-3              00053600
    871.1 6.889E-3     2000.0 1.194E-3                                  00053700
    2     / SUS                                                         00053800
      0.  3.889E-3      500.  5.000E-3                                  00053900
/* 12     / MGO                                                        00054000
/*    0.  9.259E-3      200.  6.365E-3      300.  4.919E-3              00054100
/*  400.  4.100E-3      500.  3.360E-3      600.  2.798E-3              00054200
/*  700.  2.401E-3      800.  2.100E-3     1000.  1.649E-3              00054300
/* 1200.  1.500E-3     1233.  1.600E-3     1600.  1.748E-3              00054400
    2     / MGO                                                         00054500
    200.  2.222E-4      800.  2.222E-4                                  00054600
    2   / CU                                                            00054700
    0.   9.22E-2    100.     8.75E-2                                    00054800
    2  / CU                                                             00054900
    0.   9.22E-2    100.     8.75E-2                                    00055000
/* (2) SPECIFIC HEAT CAPACITY TABLE                                    00055100
/* NTPC                                                                00055200
/* TPC    (TEMP. SPECIFIC HEAT ---)                                    00055300
/*  6     / BORON-NITRIDE                                               00055400
/*    0.    57.67       360.    84.59       510.    95.80              00055500
/*  683.   121.0       1260.   151.7       2000.   191.2               00055600
    4   /  BORON-NITRIDE   UPDATE 80.04.20                             00055700
    0.  497.   100.   497.   1000.   698.    3000.   1195.  /           00055800
    2     / NICHROME-5                                                  00055900
```

```
----*----1----*----2----*----3----*----4----*----5----*----6----*----7-R--*----8
      0.    0.104        2000.     0.104                                  00056000
/*  6      / BORON-NITRIDE                                                00056100
/*    0.     57.29         360.     84.59        510.     95.96           00056200
/*  850.    121.1         1260.    151.7        2000.    206.9            00056300
    3   /  BORON-NITRIDE   UPDATE 82.09.20                                00056400
    298.    0.1925        1000.    0.4418       2000.    0.5015           00056500
   10      / INCONEL-600                                                  00056600
      0.0  0.106          21.1    0.106         93.3    0.111            00056700
    204.4  0.116         315.6    0.121        426.7    0.126            00056800
    537.8  0.132         648.9    0.140        760.0    0.145            00056900
    871.1  0.149                                                          00057000
    2      / SUS                                                         00057100
      0.    0.120        2000.    0.120                                  00057200
    3      / MGO                                                         00057300
    177.     0.25         527.     0.30         847.    0.33             00057400
    3      / CU                                                          00057500
    20.    9.22E-2     100.     9.00E-2         300.    8.75E-2          00057600
    3   /CU                                                            00057700
    20.    9.22E-2     100.     9.00E-2         300.    8.75E-2          00057800
/*                                                                       00057900
022    /***  OTHER HEAT SLAB DATA CARDS  ***                             00058000
/* IVOLC  QINIT      BETABL                                             00058100
    1     946.8       0.0                                               00058200
/* PTABL  (TIME  NORMALIZED POWER ---)                                   00058300
/*  NEW P(T) CURVE   MAY BE USED IN THE FUTURE                           00058400
/*   0.0  1.0           11.4  1.0           20.0  0.597                  00058500
/*  30.0  0.362         40.0  0.304         50.0  0.254                  00058600
/*  70.0  0.195        100.0   0.172       200.0  0.108                  00058700
/* 400.0  0.0813       800.0   0.0659     2000.0  0.0555                 00058800
/*4000.0  0.0478                                                        00058900
/*  POWER CURVE NOW USED (UNTIL JUNE OF 1980)                           00059000
/*   0.0  1.0          11.208  1.          11.352  0.987                 00059100
/*  11.5  0.971        12.0   0.938        12.5   0.905                  00059200
/*  13.   0.874        14.    0.819        15.    0.766                  00059300
/*  16.   0.715        17.    0.664        18.    0.615                  00059400
/*  20.   0.523        25.    0.349        28.    0.261                  00059500
/*  30.   0.218        35.    0.134        36.    0.121                  00059600
/*  37.   0.119        50.    0.111        70.    0.104                  00059700
/* 100.   0.097       200.    0.085       300.    0.079                  00059800
/* 500.   0.071       700.    0.066      1000.    0.061                  00059900
/*2000.   0.051      3000.    0.046      4000.    0.042                  00060000
/*      POWER CURVE FOR RUN 901                                         00060100
    0.    1.          7.5     1.          8.0   0.951      9.    0.885   00060200
   10.    0.824      12.      0.707      14.    0.614      16.    0.545   00060300
   18.    0.496      20.      0.429      22.    0.386      24.    0.348   00060400
   26.    0.309      28.      0.274      30.    0.262      32.    0.253   00060500
   34.    0.244      36.      0.236      38.    0.227      40.    0.219   00060600
   42.    0.212      44.      0.205      46.    0.198      48.    0.191   00060700
   50.    0.184      60.      0.163      70.    0.151      80.    0.141   00060800
   90.    0.132     100.      0.125     110.    0.12      120.    0.115   00060900
  150.    0.102     180.      0.088     210.    0.077     240.    0.072   00061000
  270.    0.067     300.      0.062     360.    0.06      420.    0.058   00061100
  480.    0.056     540.      0.054     600.    0.053    1200.    0.042   00061200
 1800.    0.041   /                                                      00061300
/*                                                                       00061400
999                                                                     00061500
/* END OF DATA                                                          00061600
```

Appendix B Calculational Results for 0, 2, 5, 25, 50, 75, and 200% Break Tests

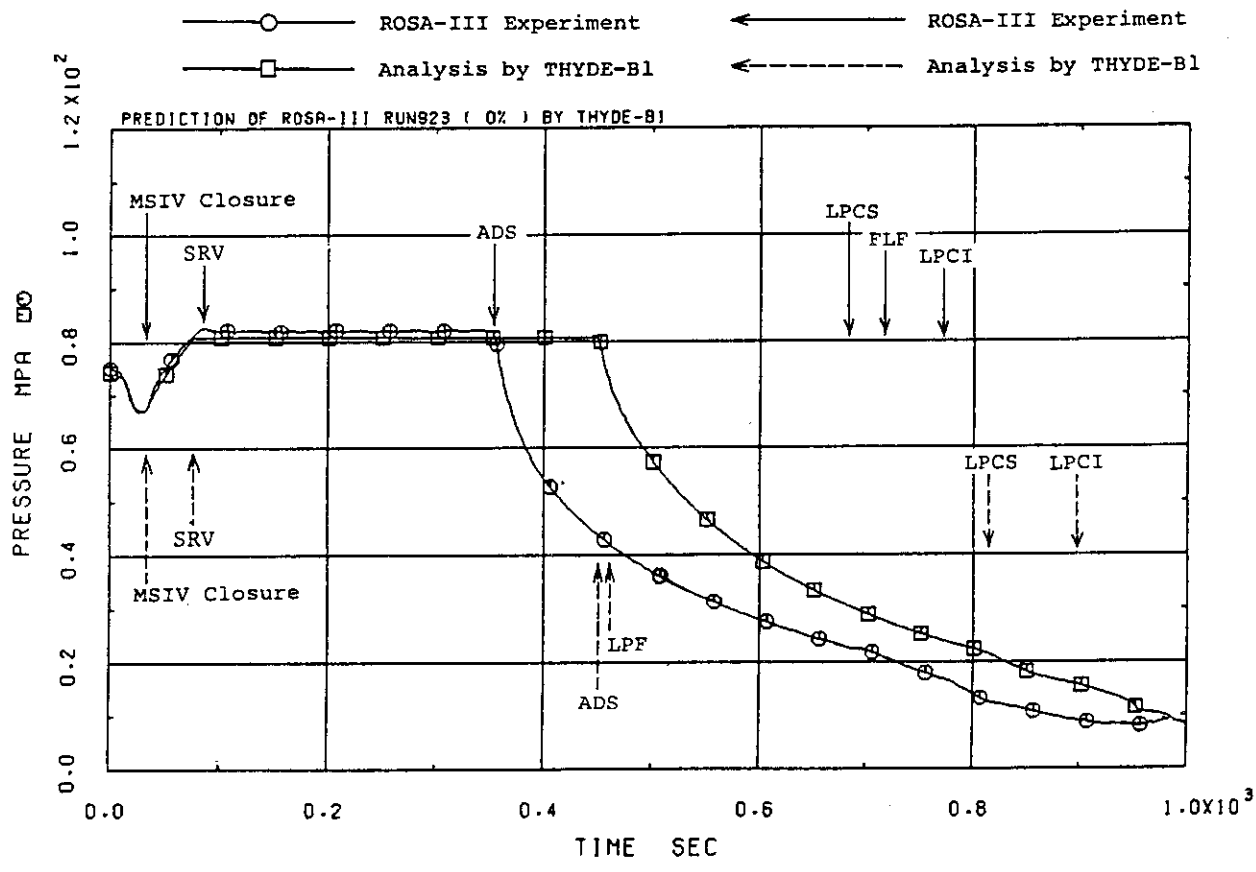

Fig. B.1 Measured vs. calculated system pressures - 0 % break test

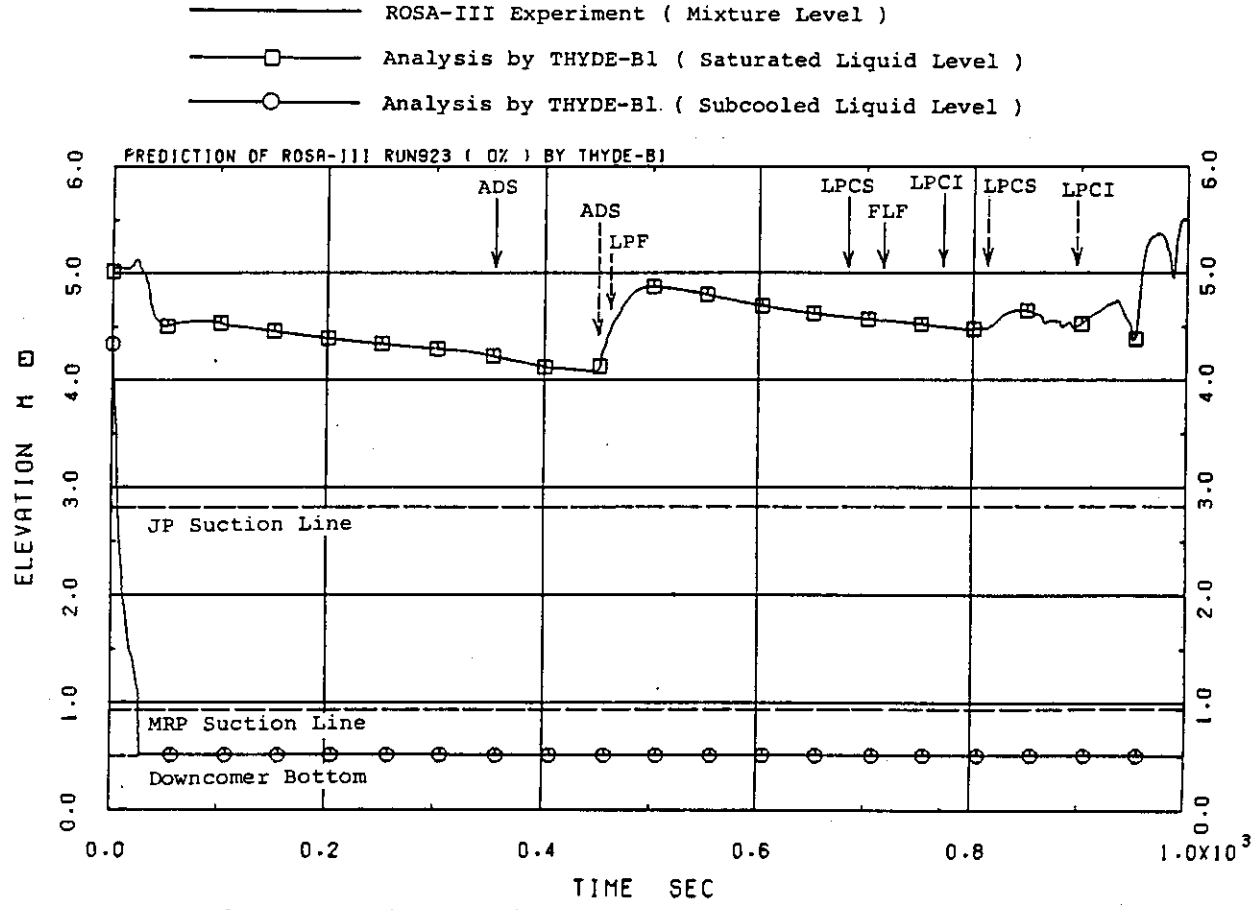

Fig. B.2 Measured vs. calculated downcomer mixture levels - 0 % break test

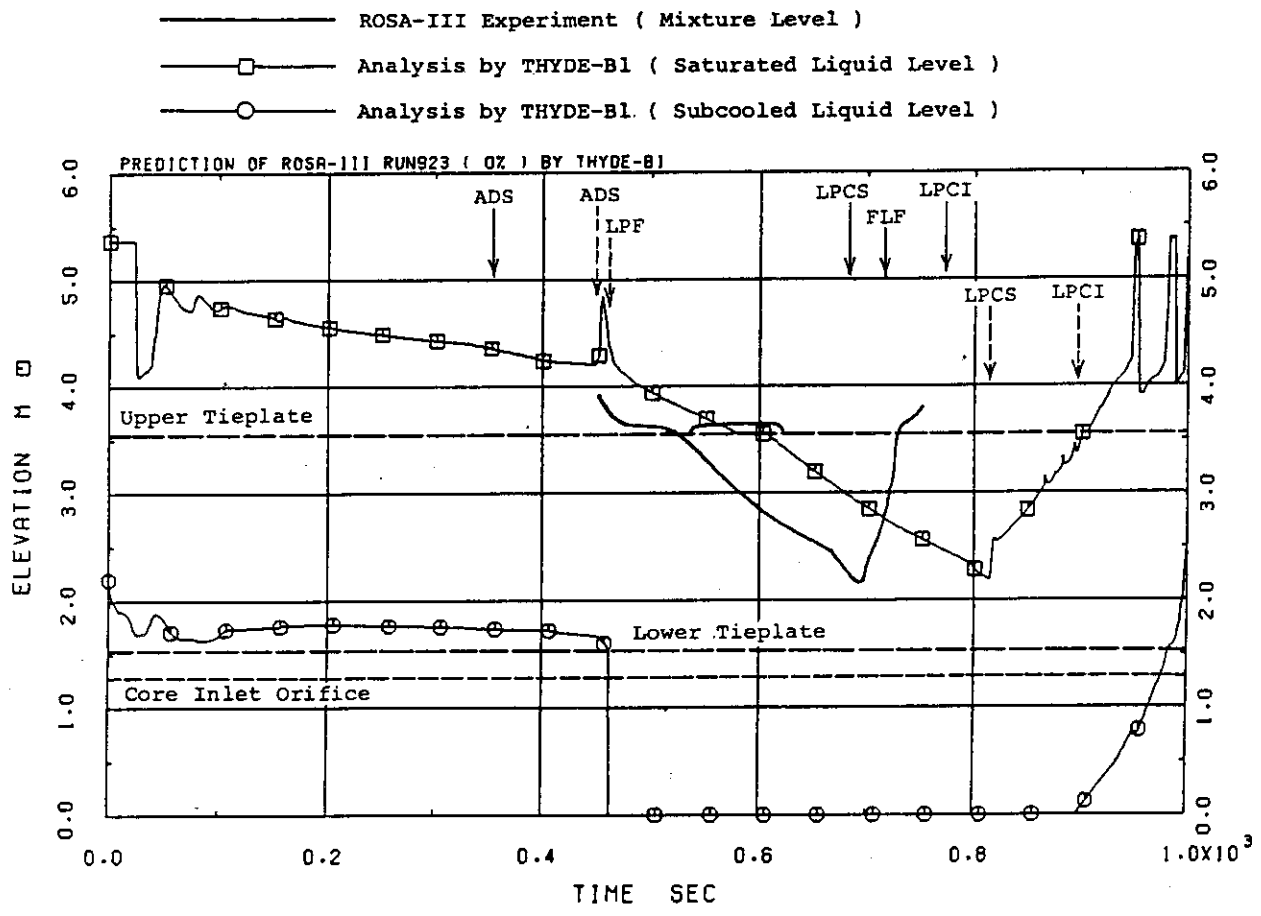

Fig. B.3 Measured vs. calculated core mixture levels - 0 % break test

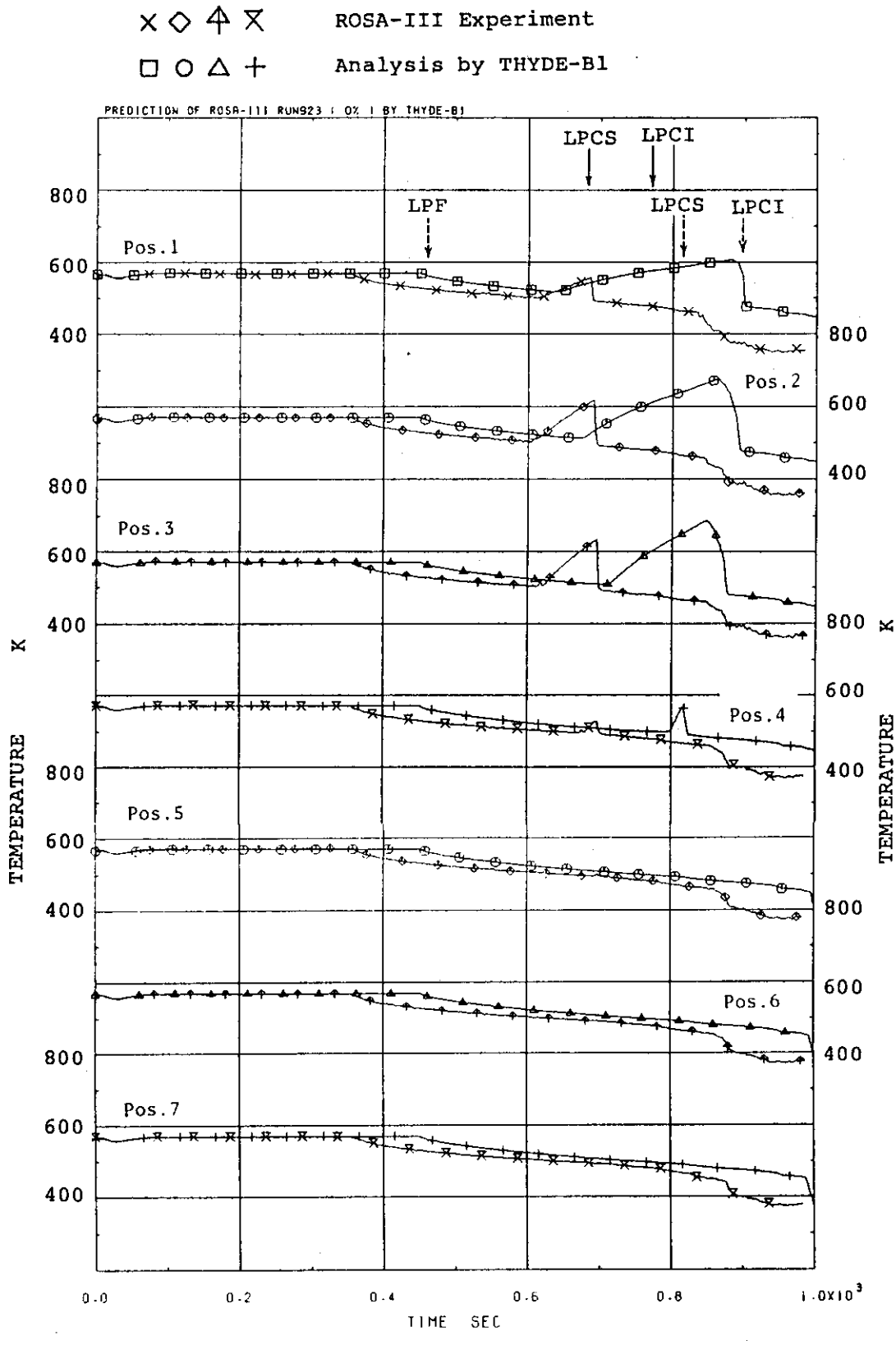

Fig. B.4 Measured vs. calculated peak-power rod temperatures - 0 % break

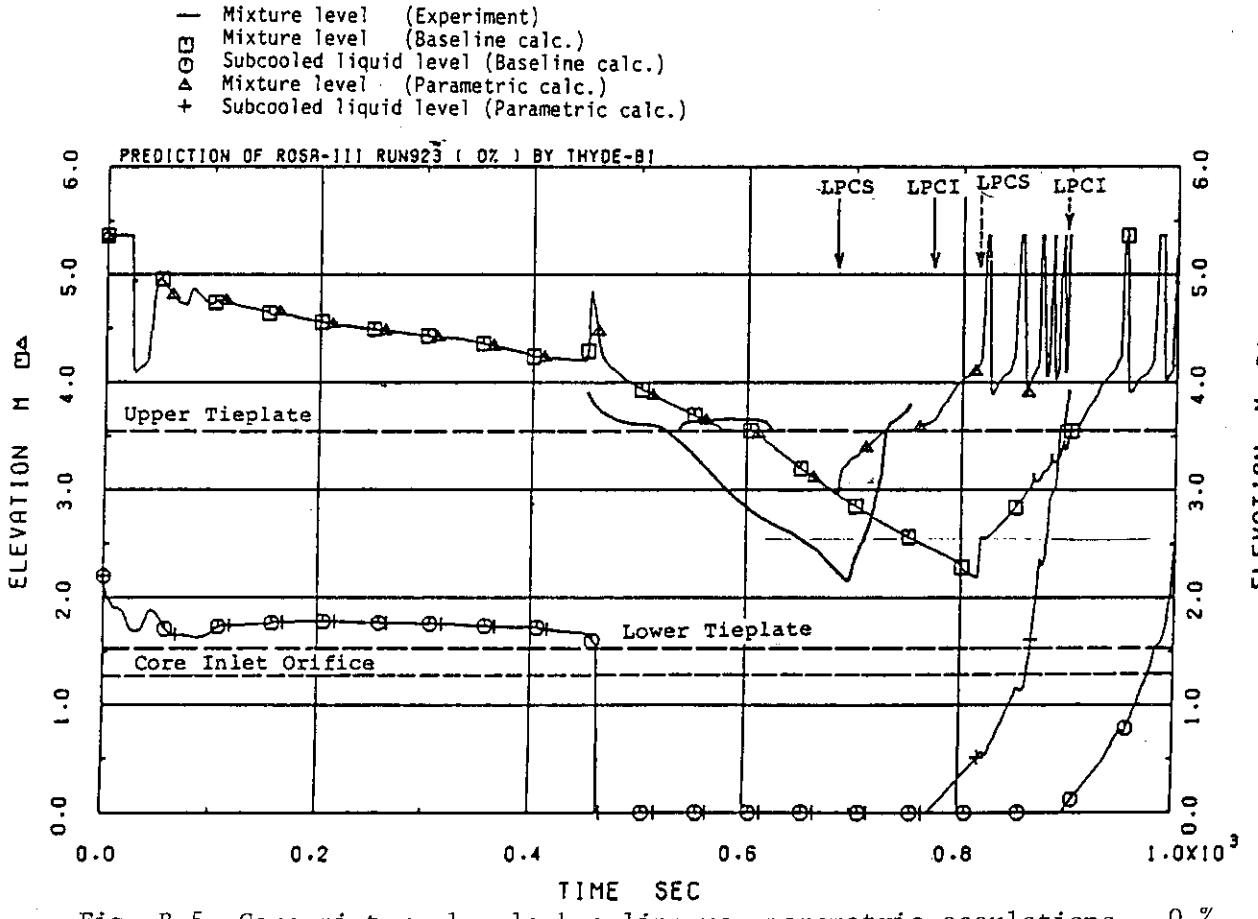

Fig. B.5 Core mixture level: baseline vs. parametric caculations - 0 % break test

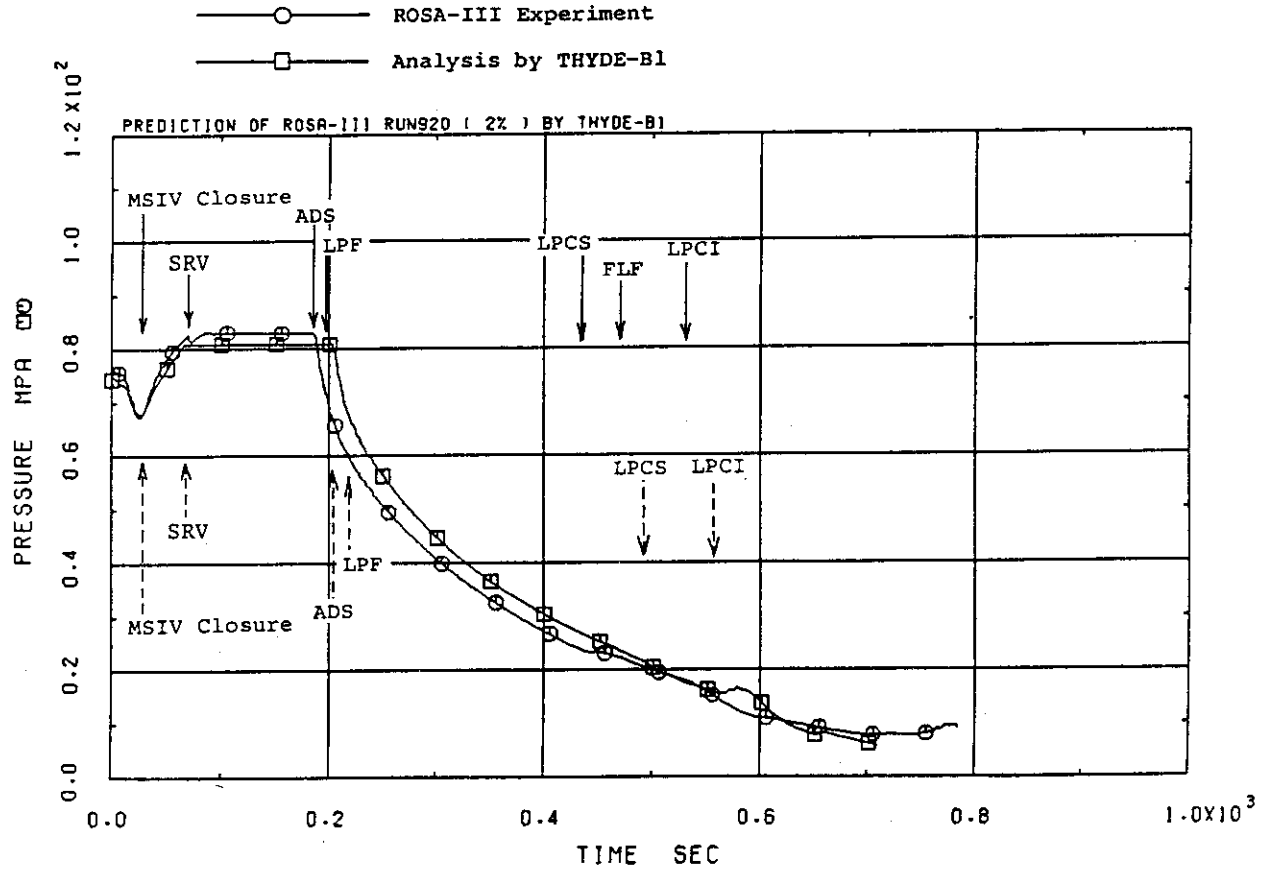

Fig. B.6 Measured vs. calculated system pressures - 2 % break test

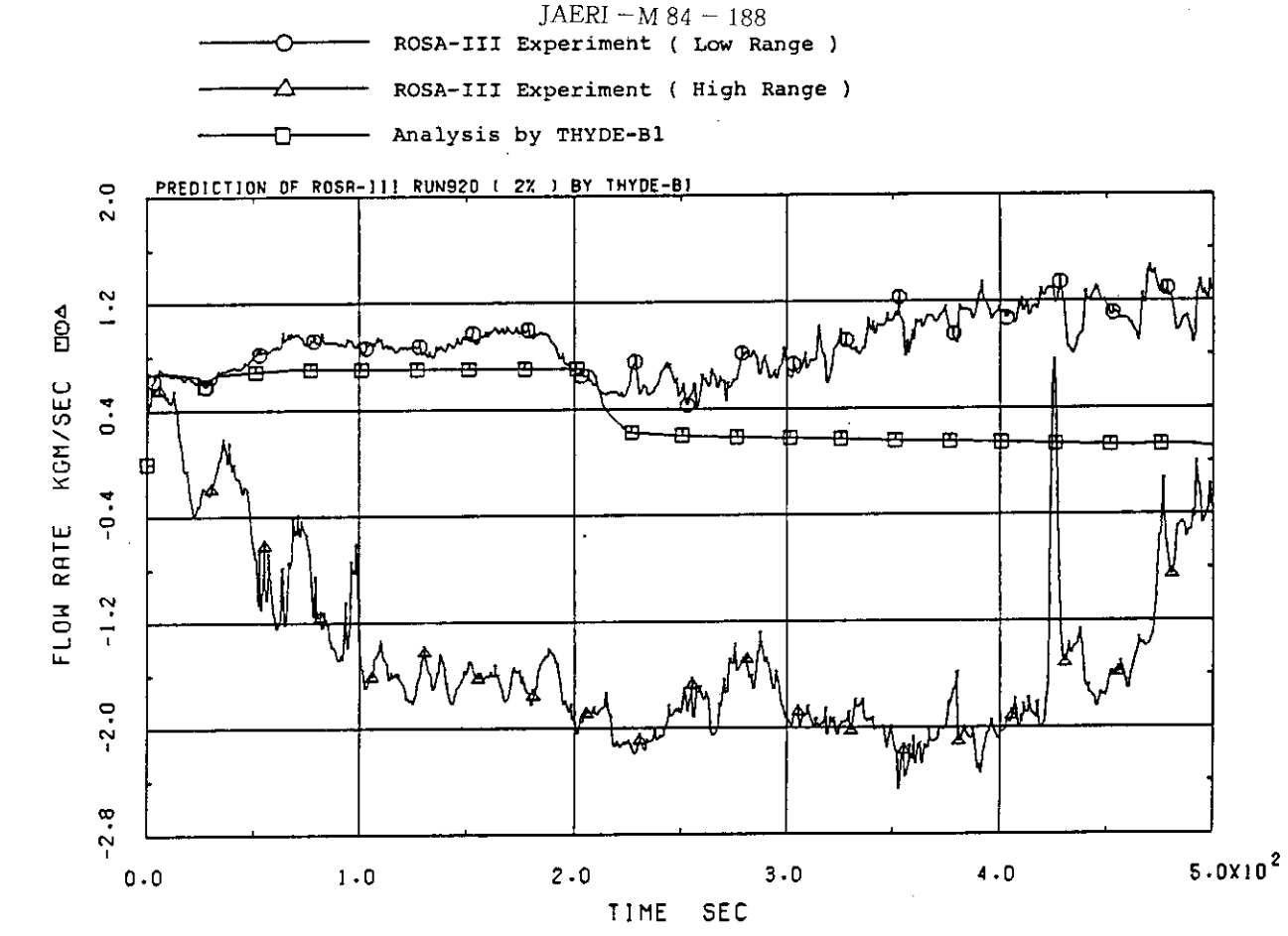

Fig. B.7 Measured vs. calculated break flow rates - 2 % break test

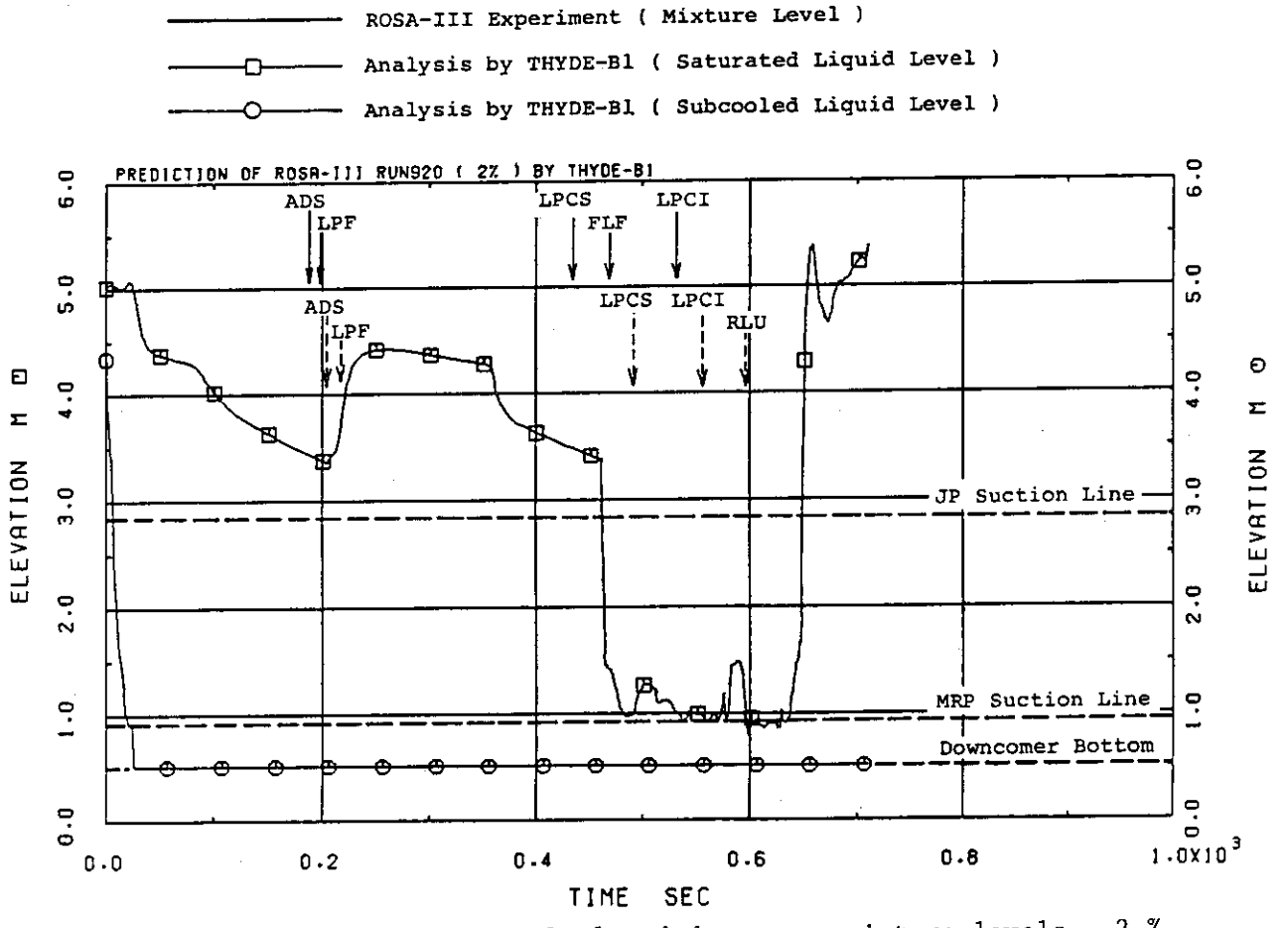

Fig. B.8 Measured vs. calculated downcomer mixture levels - 2 % break test

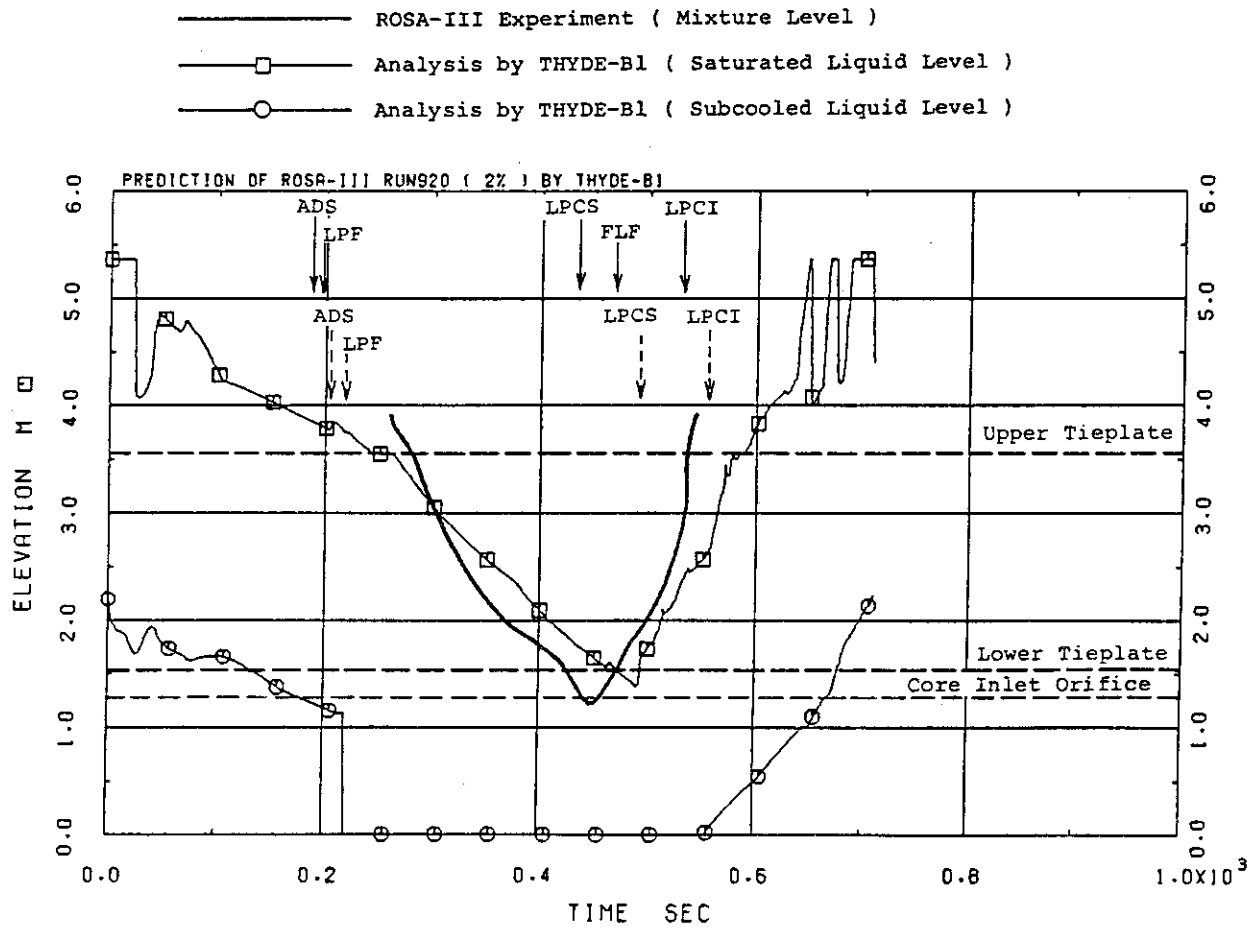

Fig. B.9 Measured vs. calculated core mixture levels - 2 % break test

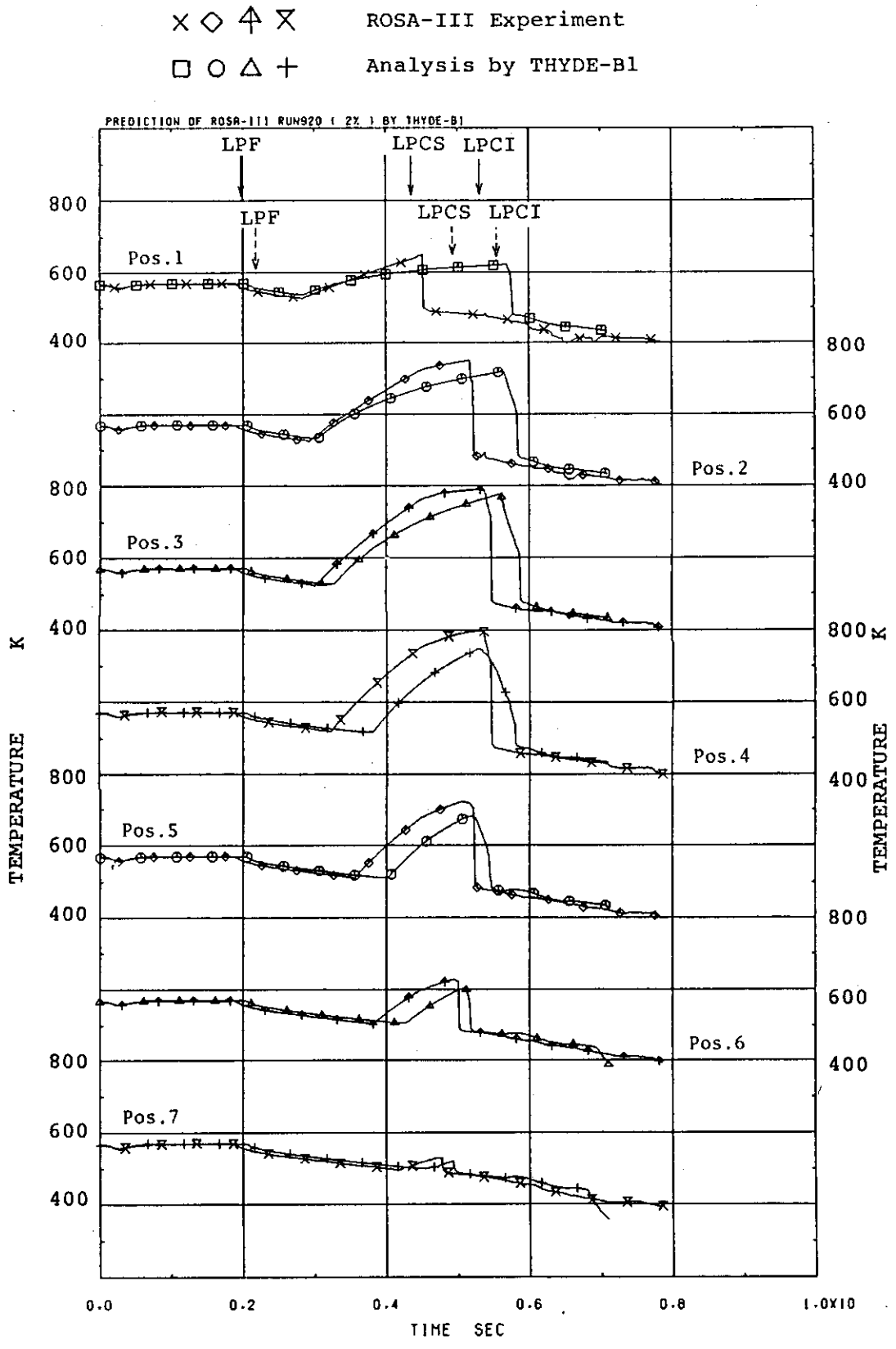

Fig. B.10 Measured vs. calculated peak-power rod temperatures - 2 % break test

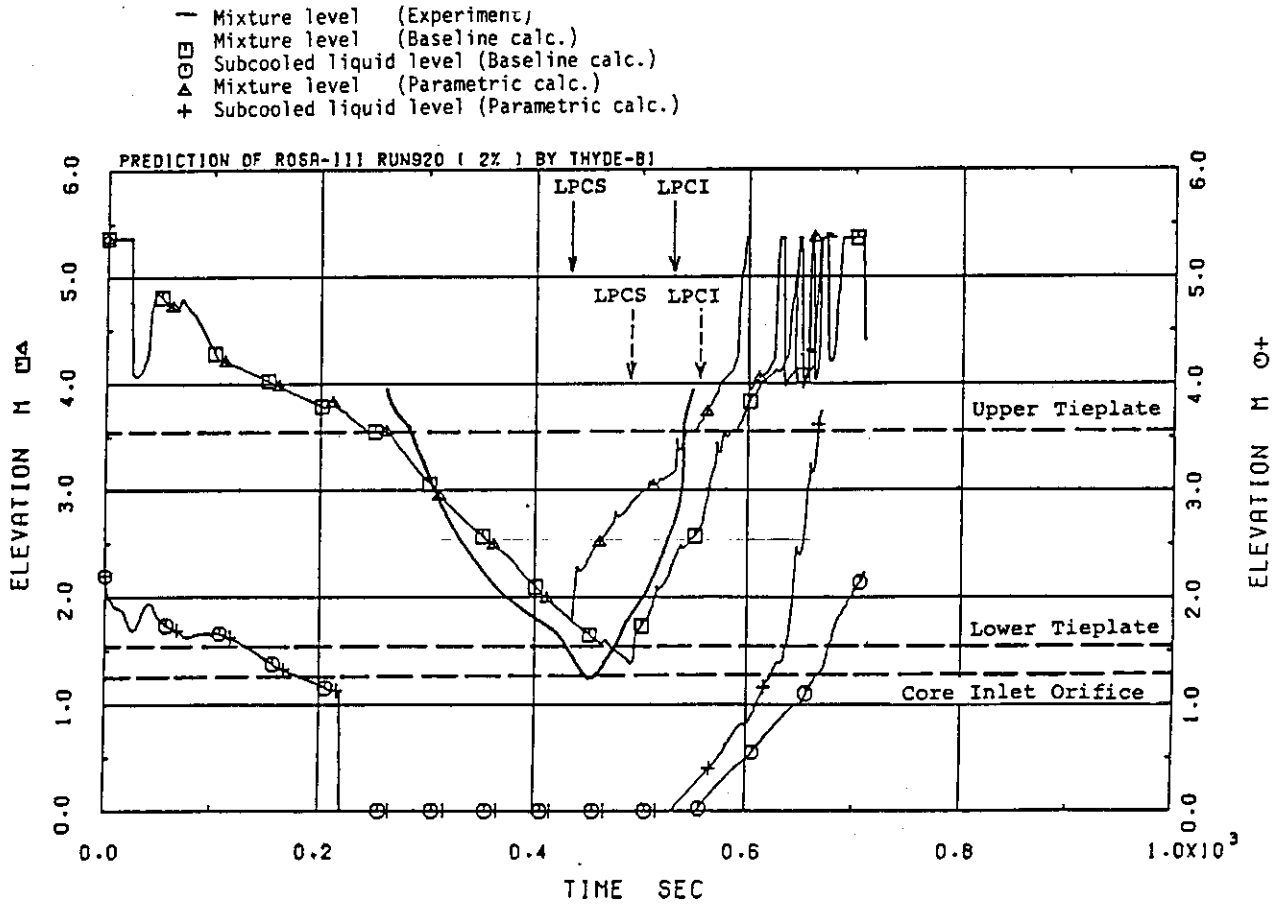

Fig. B.11 Core mixture level: baseline vs. parametric calculations - 2 % break test

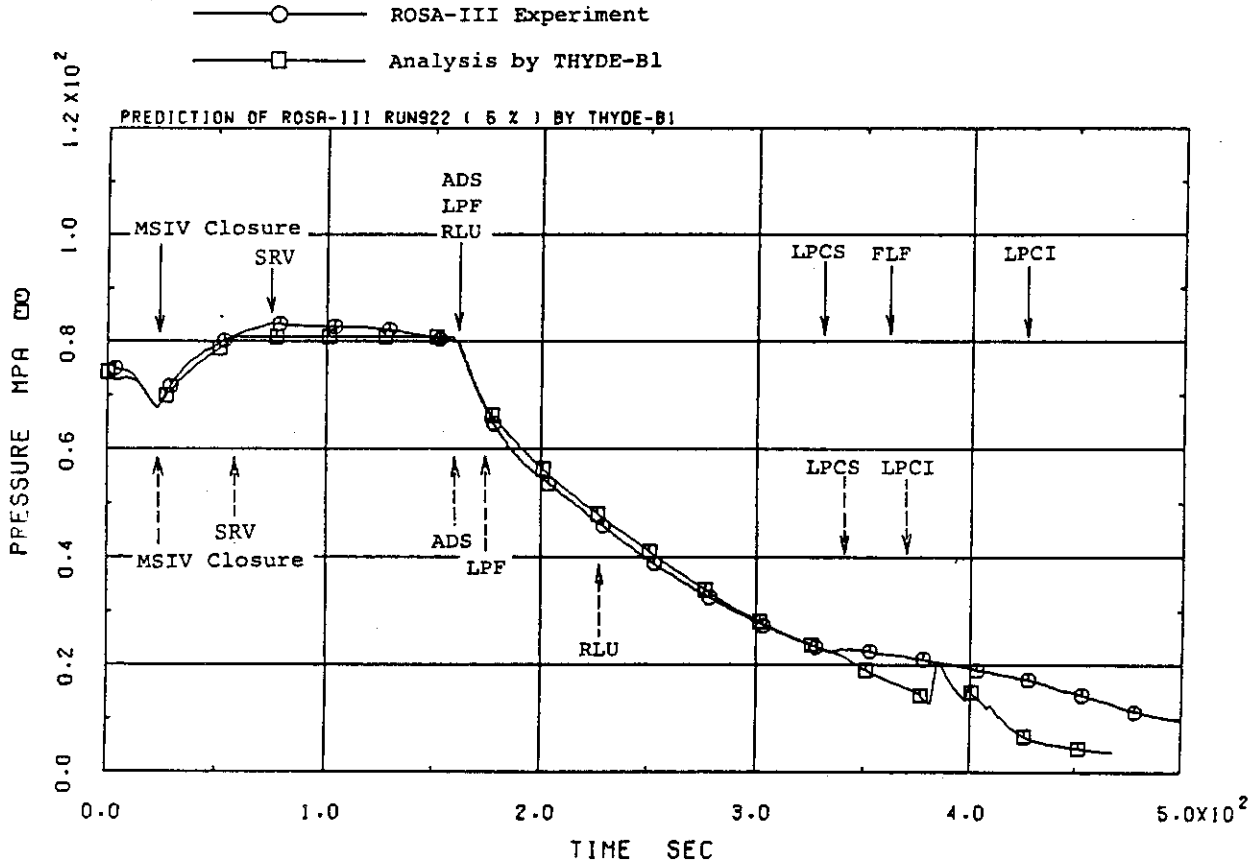

Fig. B.12 Measured vs. calculated system pressures - 5 % break test

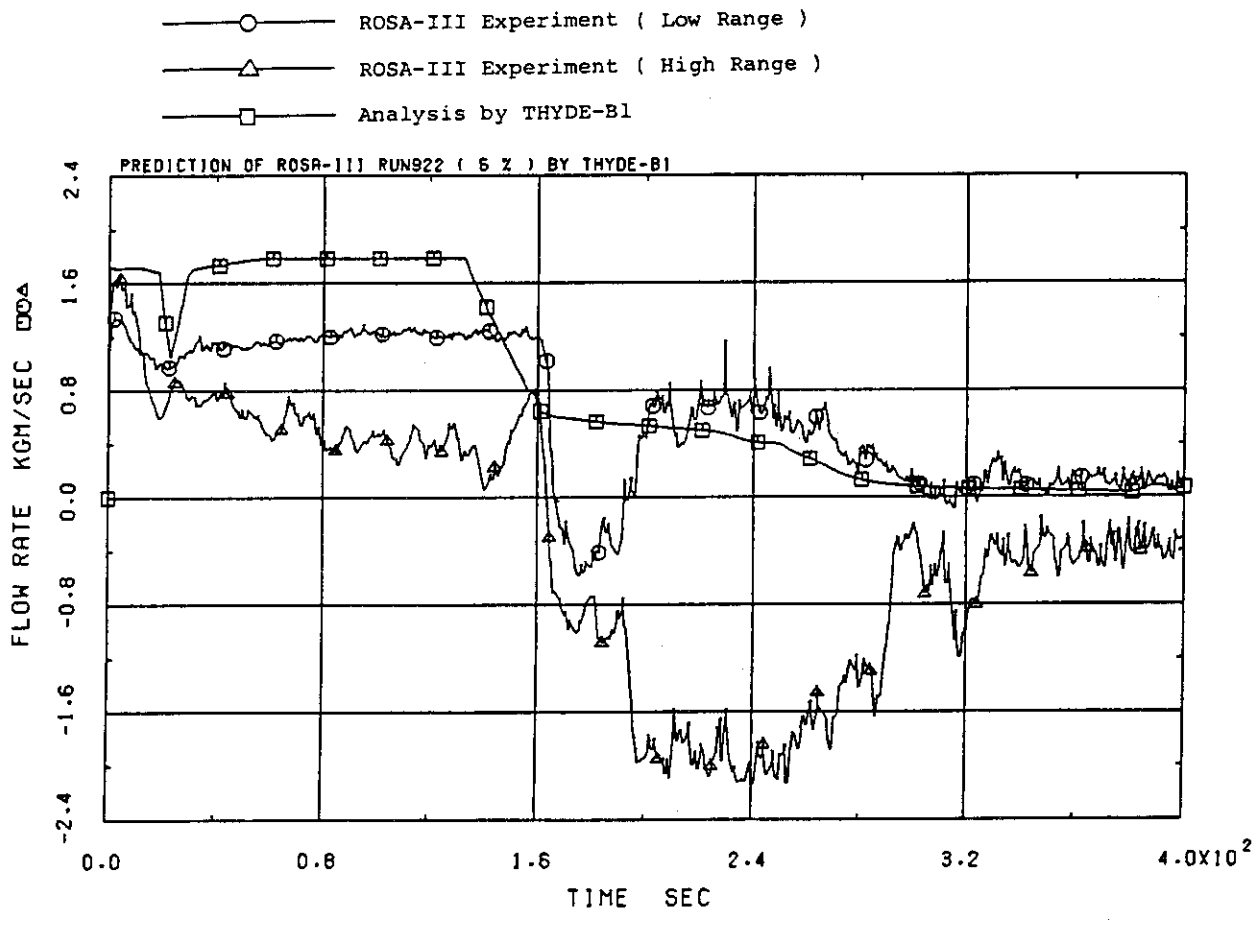

Fig. B.13 Measured vs. calculated break flow rates - 5 % break test

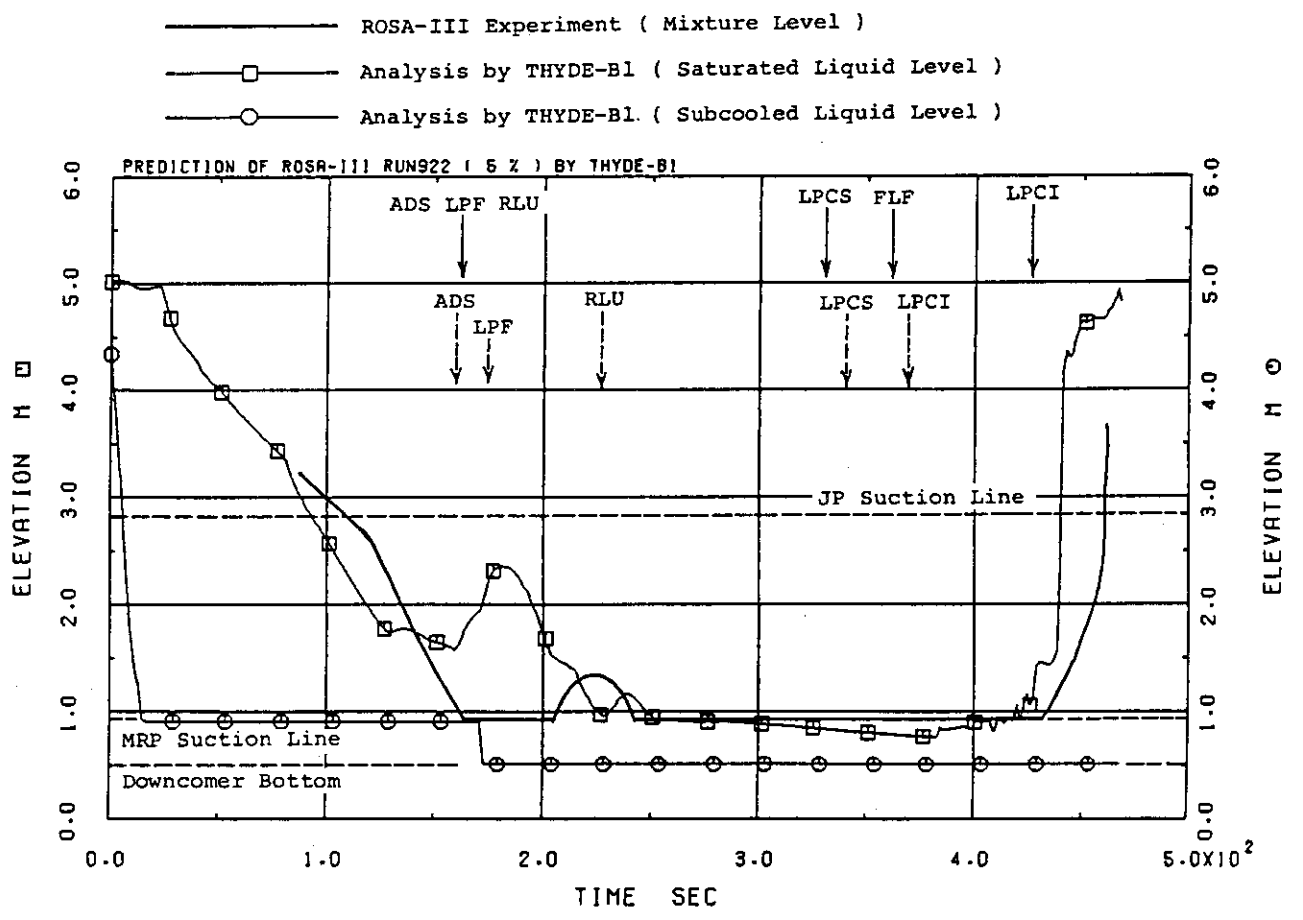

Fig. B.14 Measured vs. calculated downcomer mixture levels - 5 % break test

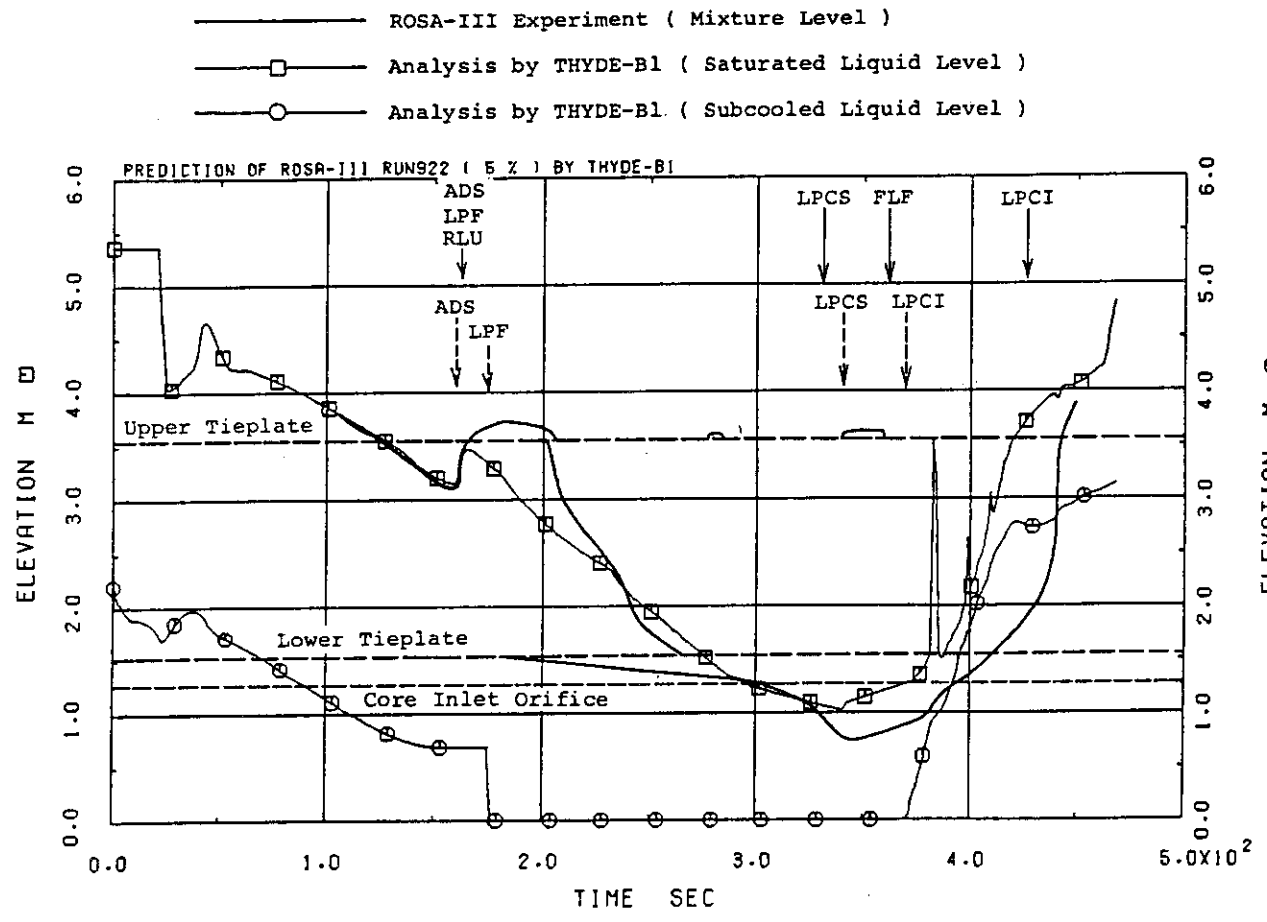

Fig. B.15 Measured vs. calculated core mixture levels - 5 % break test

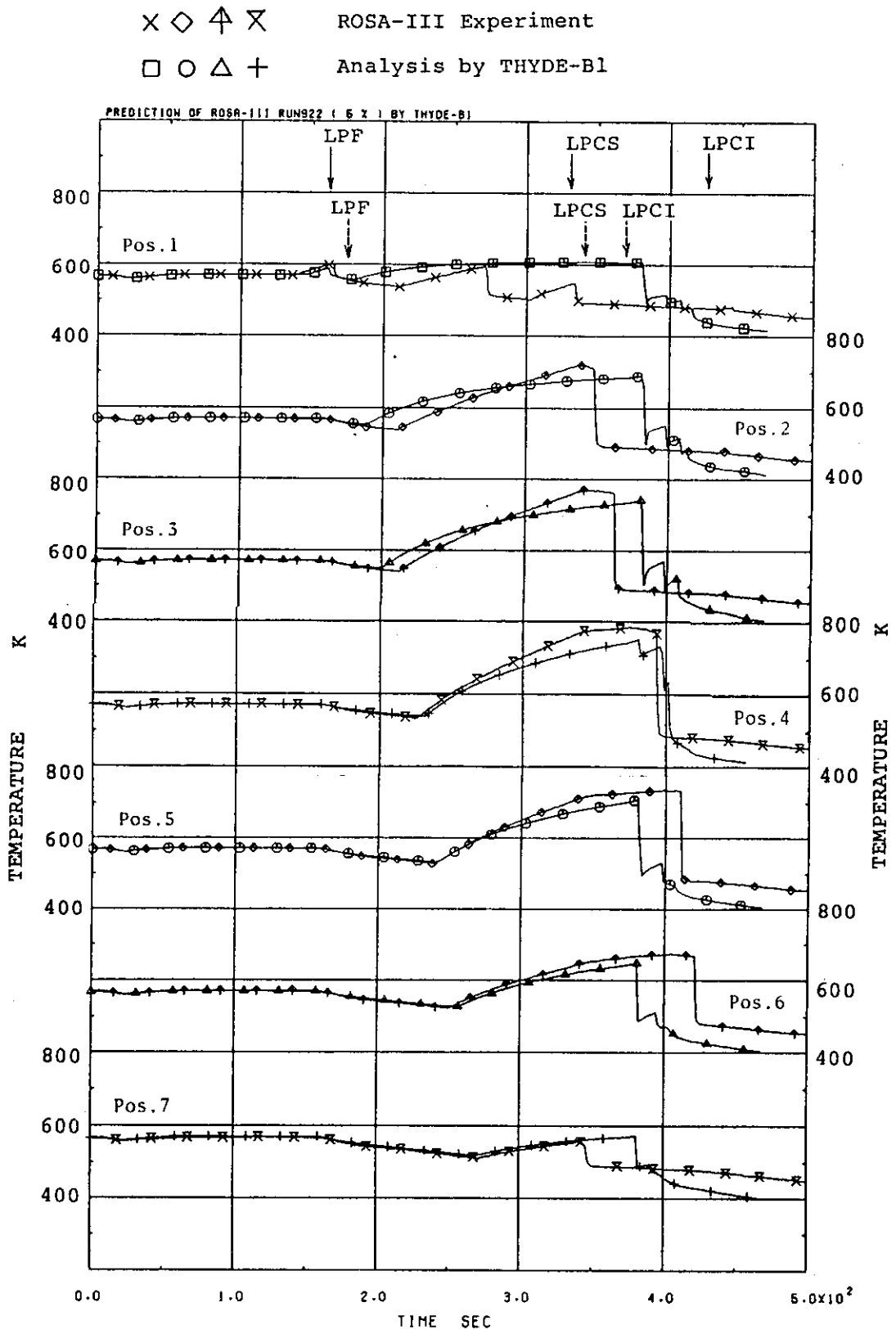

Fig. B.16 Measured vs. calculated peak-power rod temperatures - 5 % break test

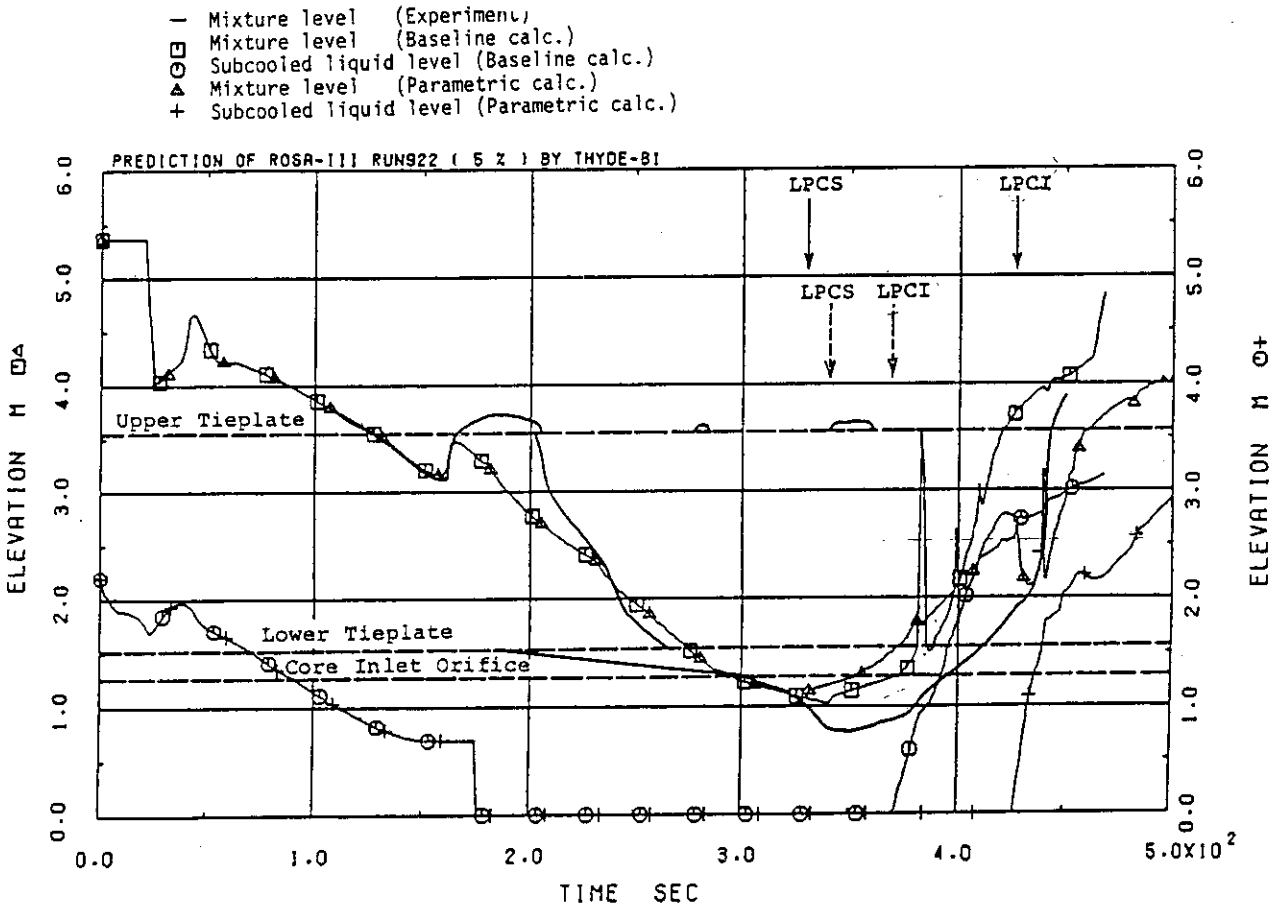

Fig. B.17 Core mixture level: baseline vs. parametric calculations - 5 % break test

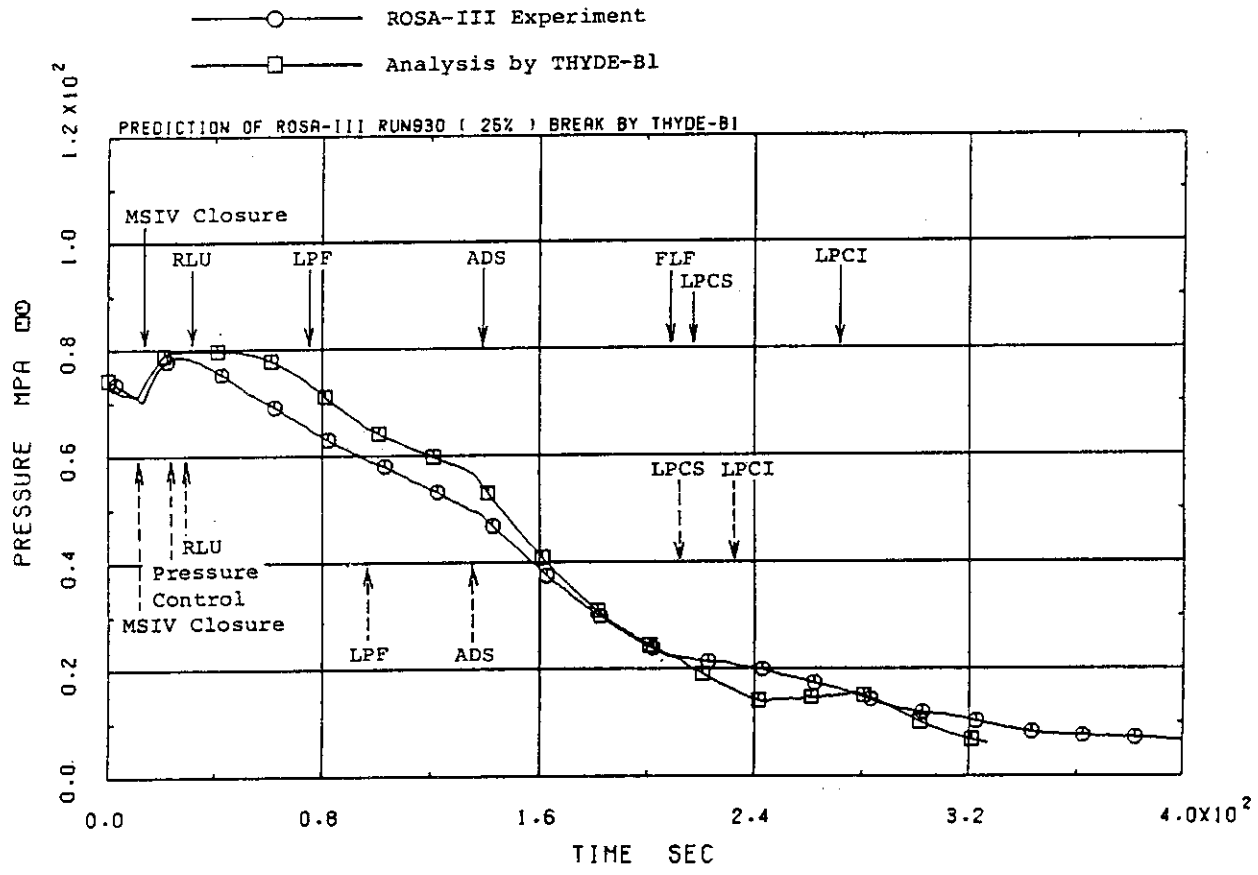

Fig. B.18 Measured vs. calculated system pressures - 25 % break test

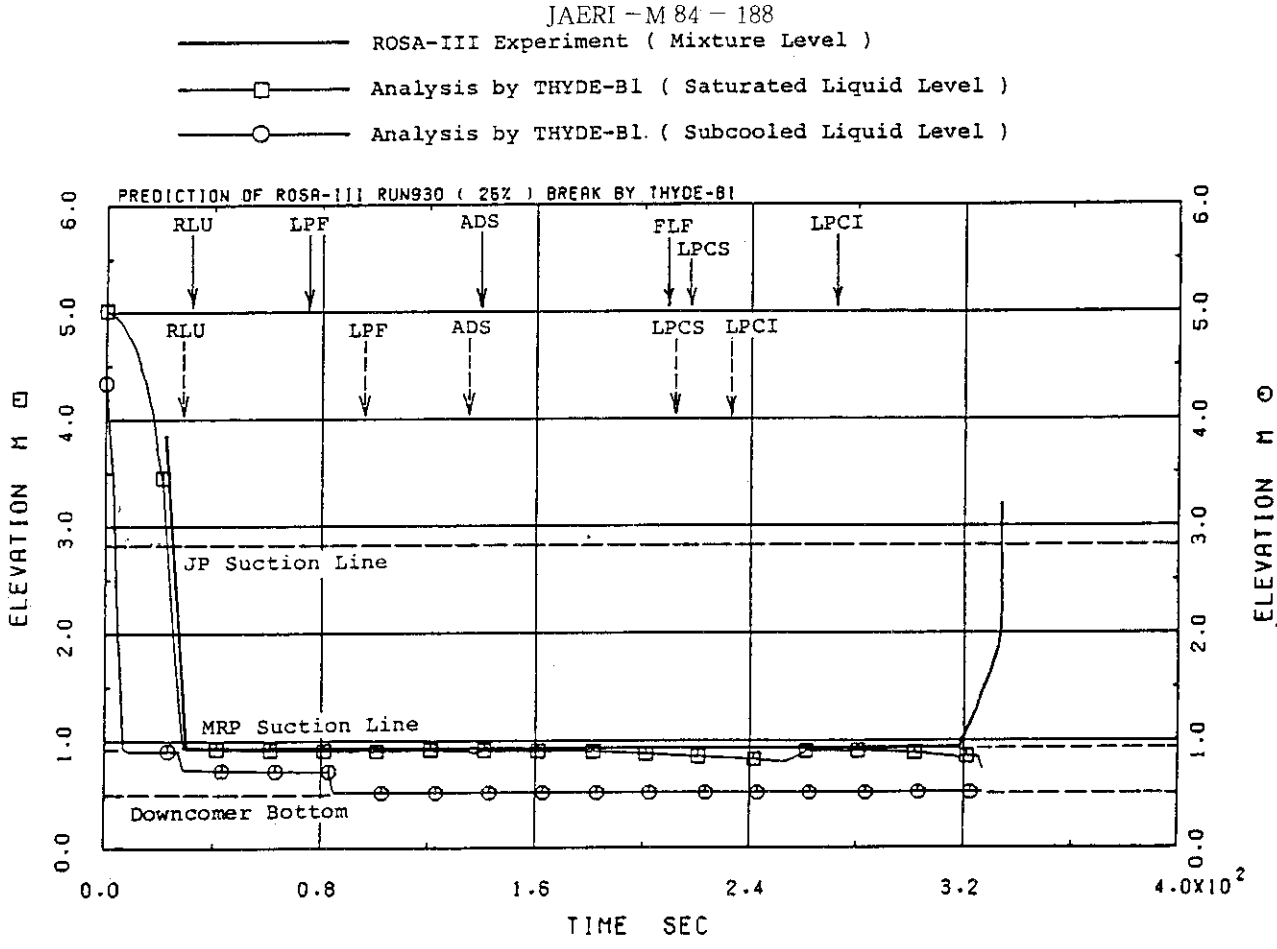

Fig. B.19 Measured vs. calculated downcomer mixture levels - 25 % break test

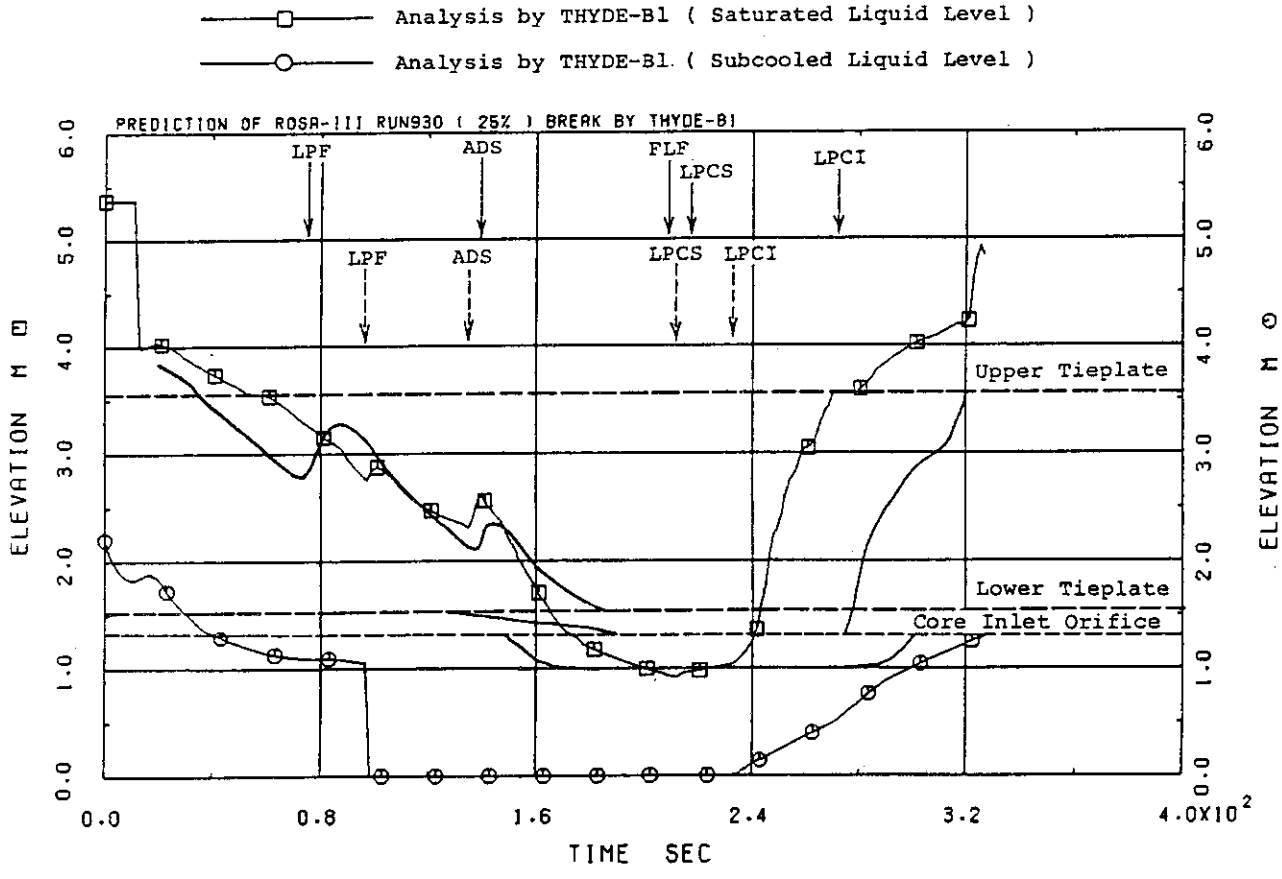

Fig. B.20 Measured vs. calculated core mixture levels - 25 % break test

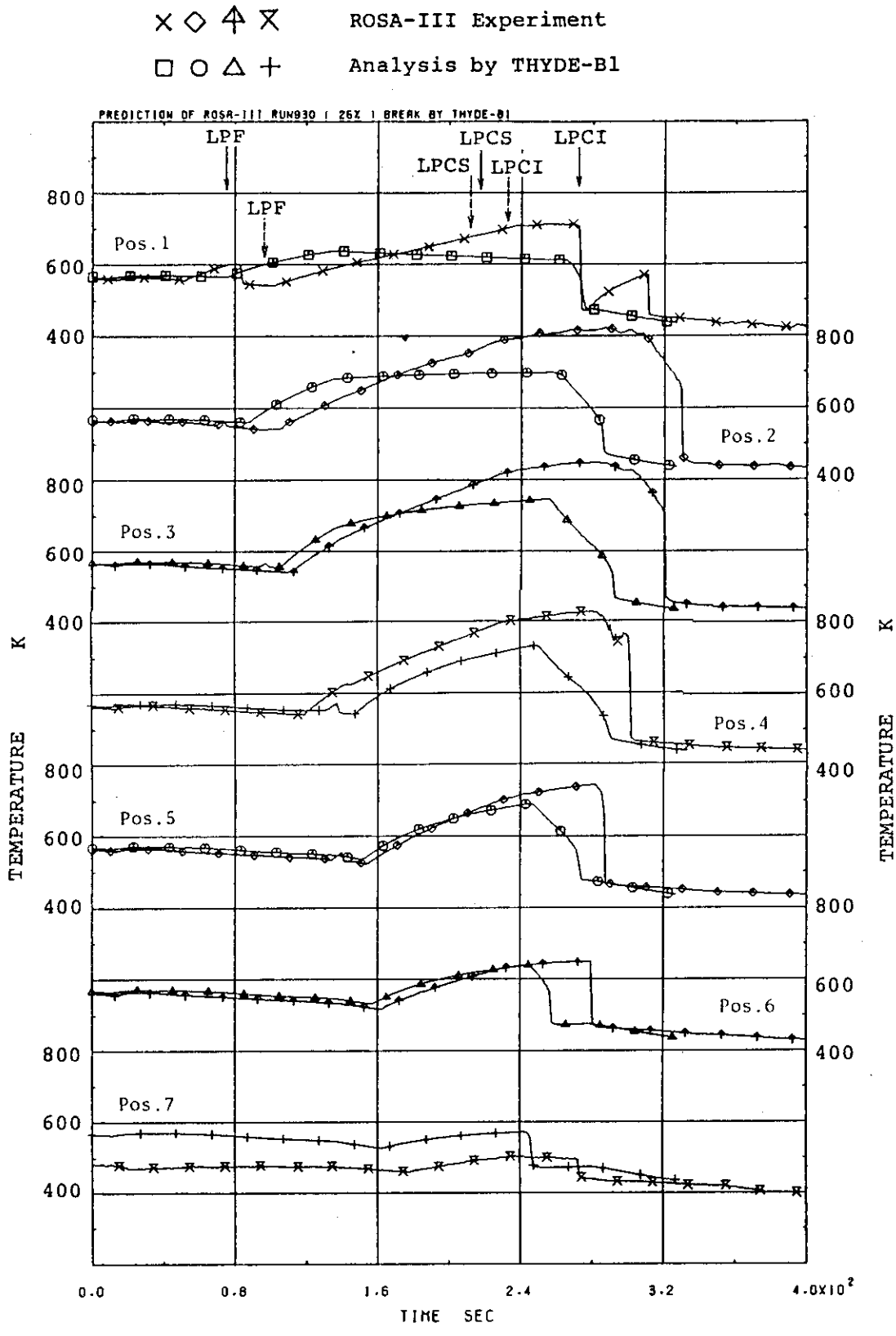

Fig. B.21 Measured vs. calculated peak-power rod temperature - 25 % break test

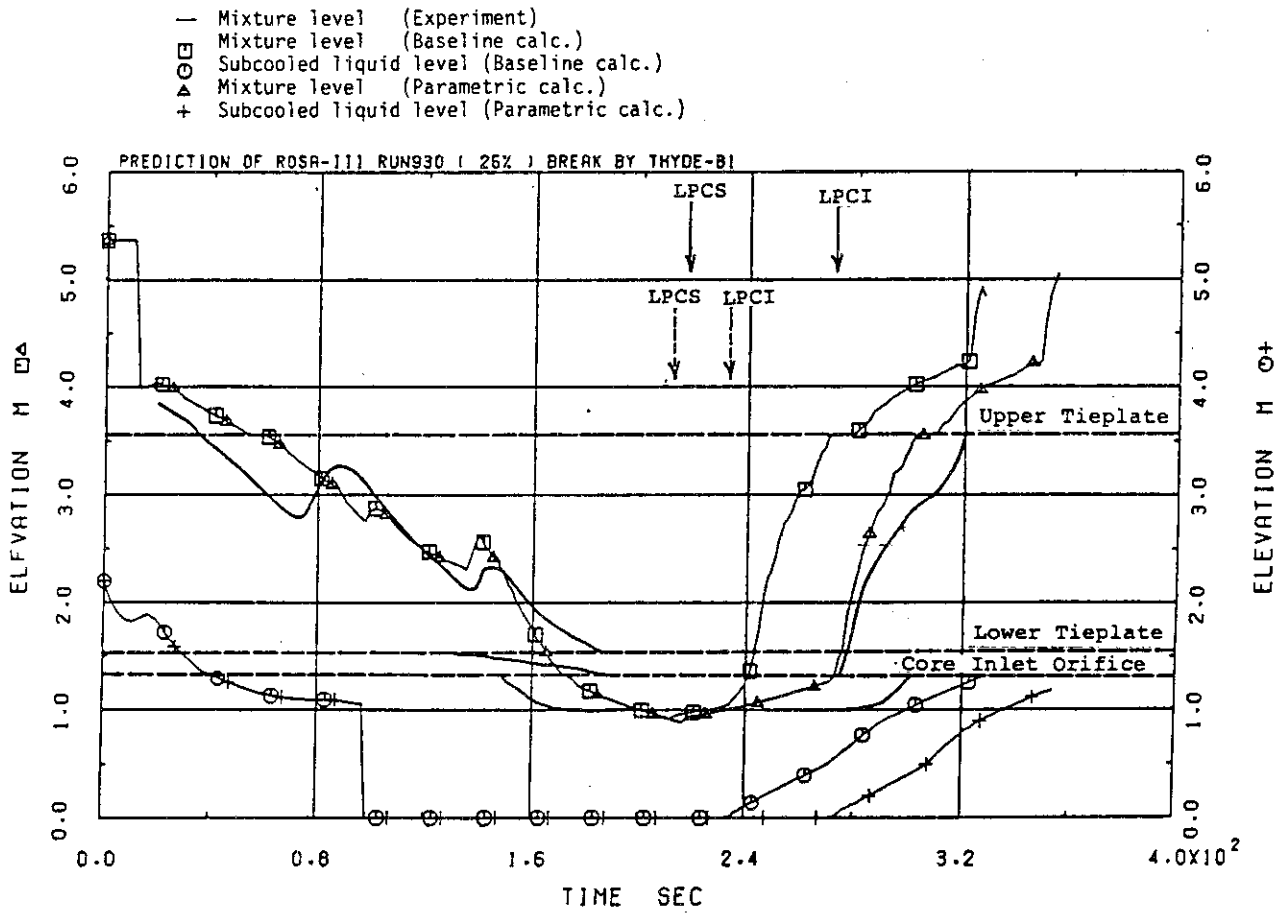

Fig. B.22 Core mixture level: baseline vs. parametric calculations – 25 % break test

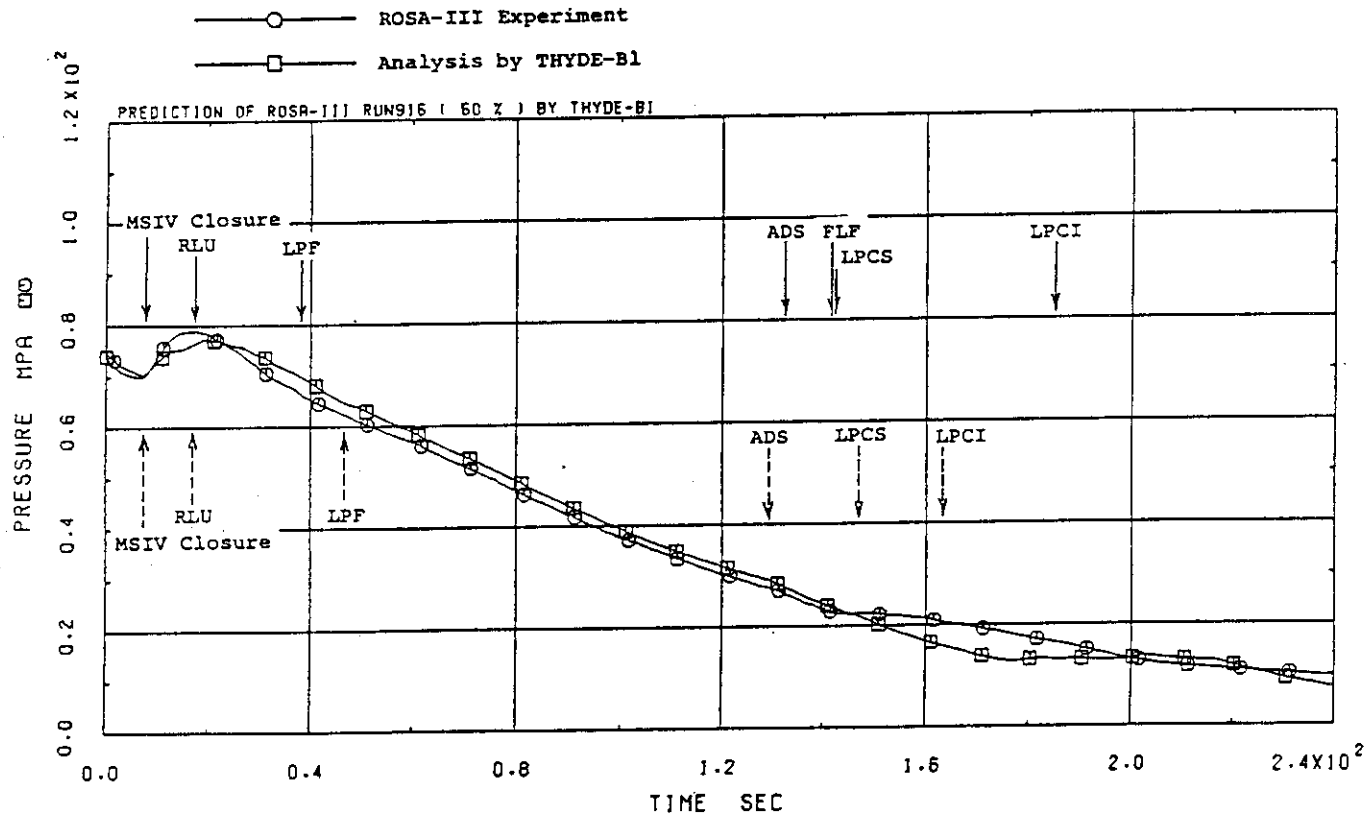

Fig. B.23 Measured vs. calculated system pressures - 50 % break test

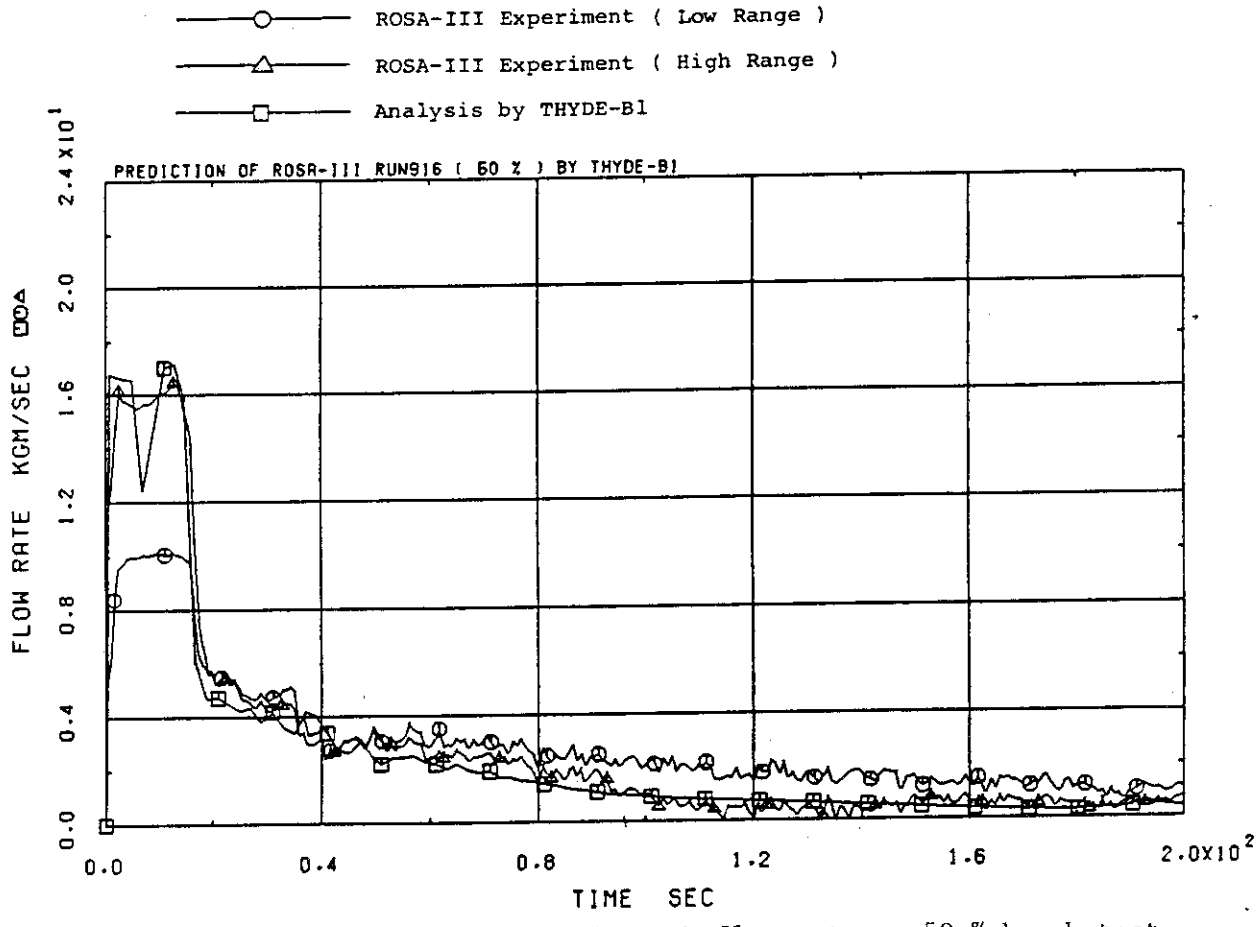

Fig. B.24 Measured vs. calculated break flow rates - 50 % break test

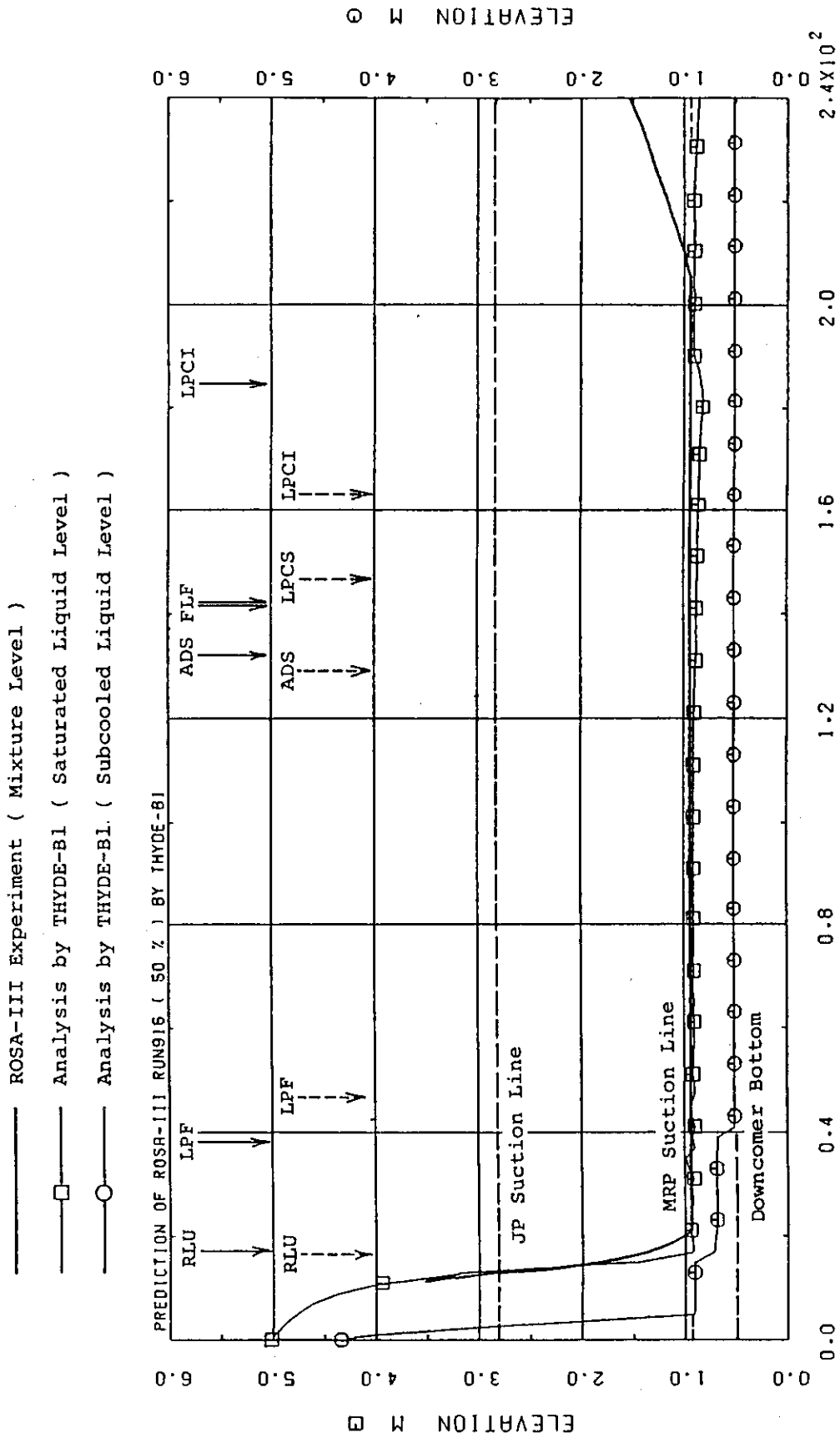

Fig. B.25 Measured vs. calculated downcomer mixture levels - 50 % break test

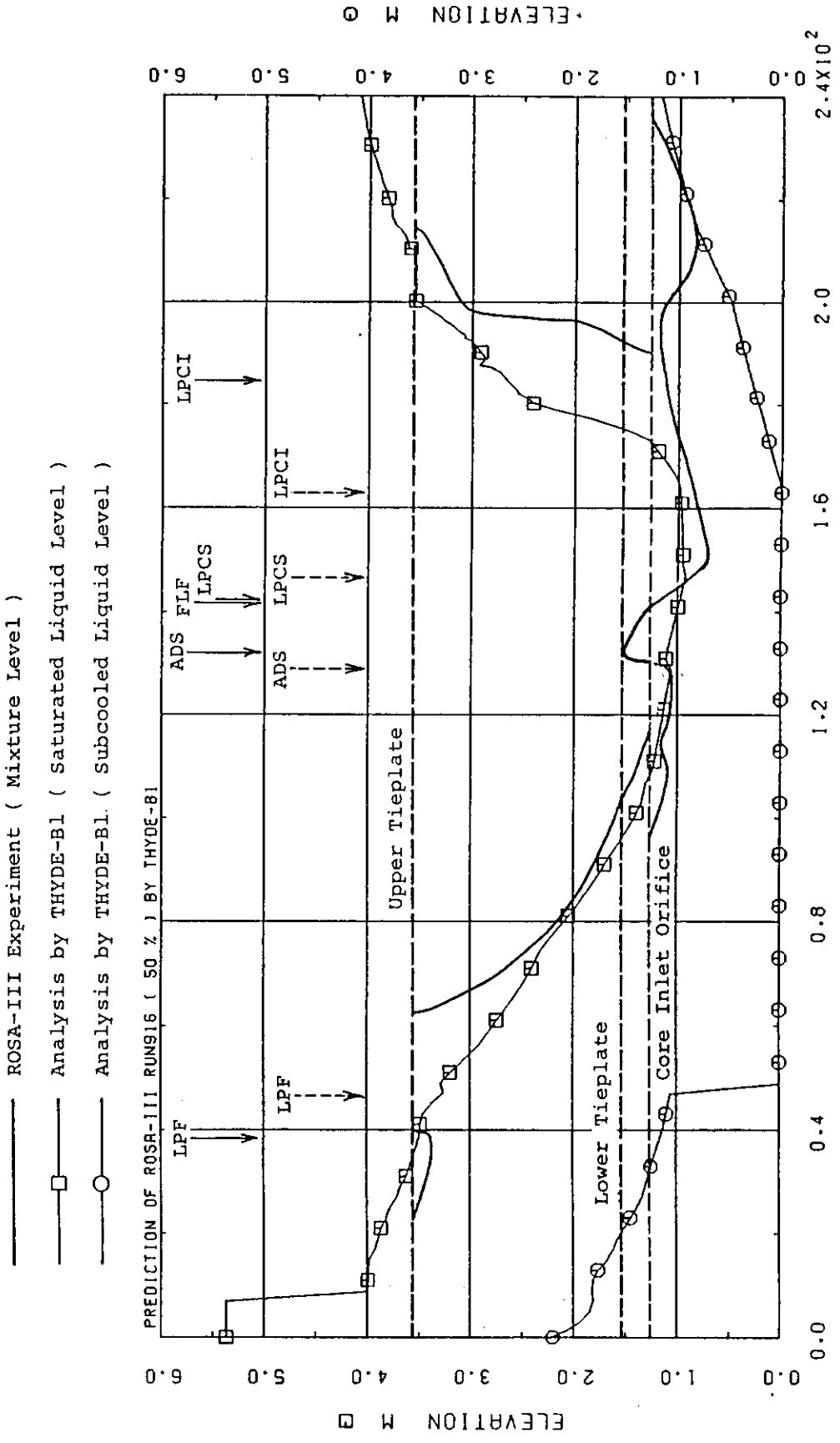

Fig. B.26 Measured vs. calculated core mixture levels - 50 % break test

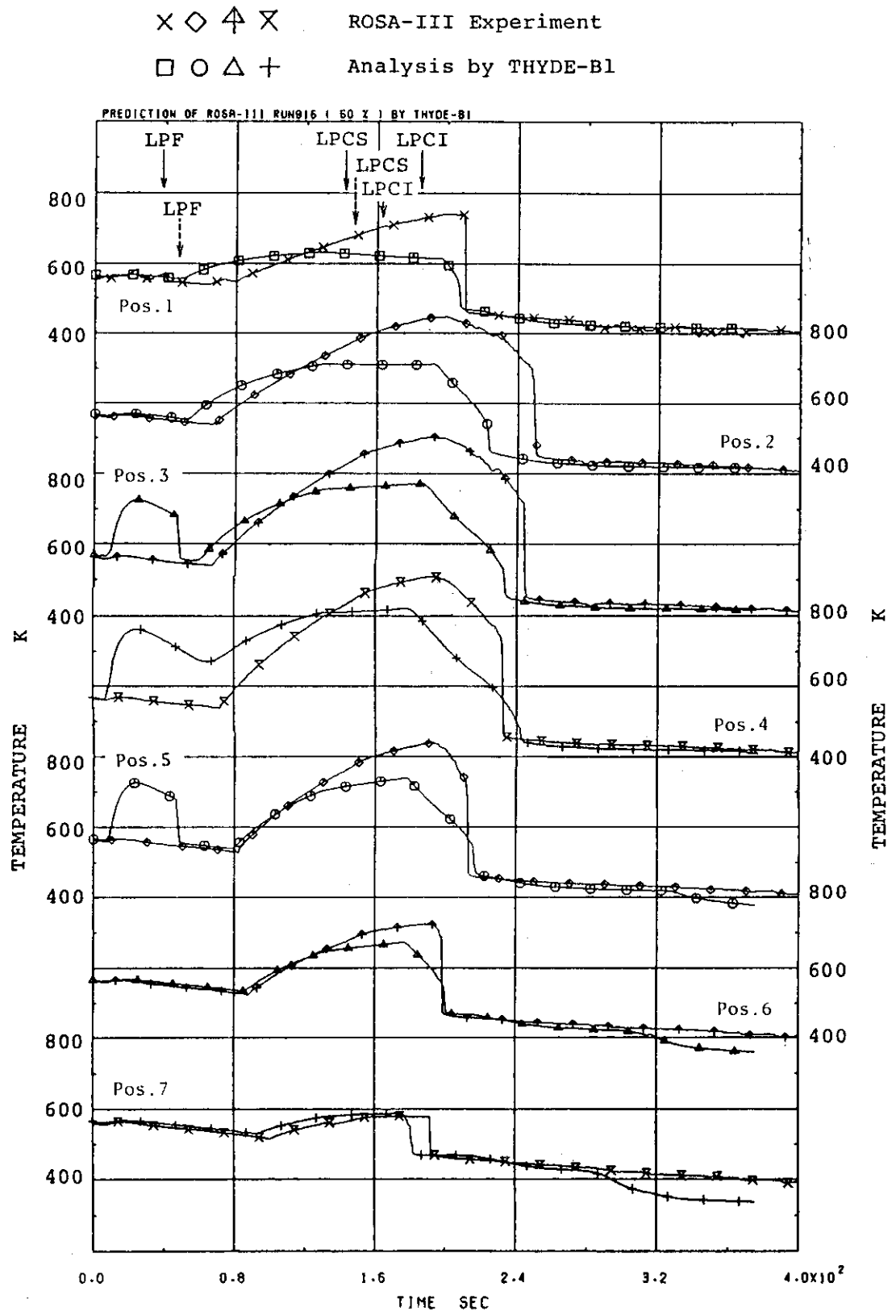

Fig. B.27 Measured vs. calculated peak-power rod temperatures - 50 % break test

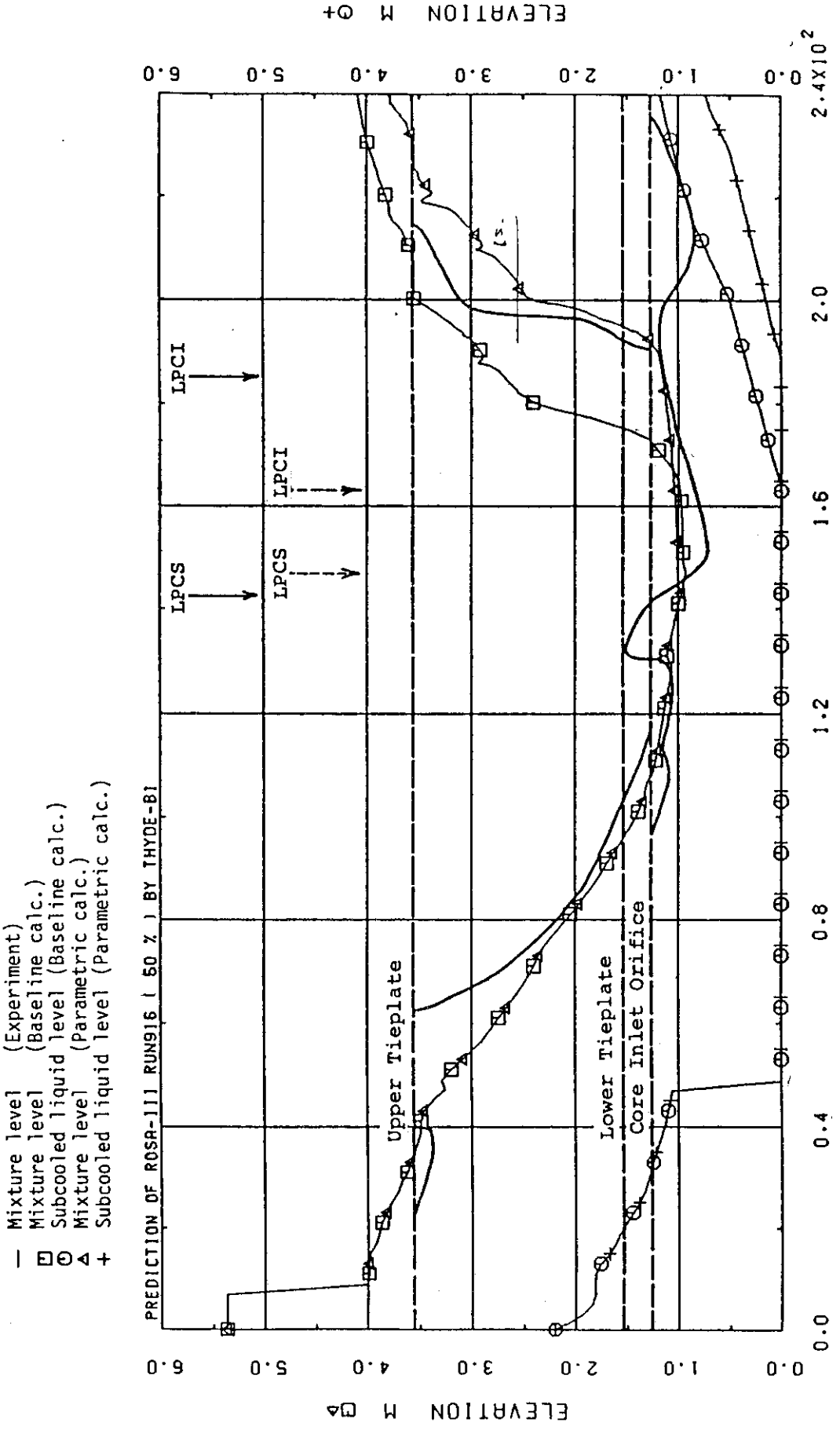

Fig. B.28 Core mixture level: baseline vs. parametric calculations
－ 50 % break test

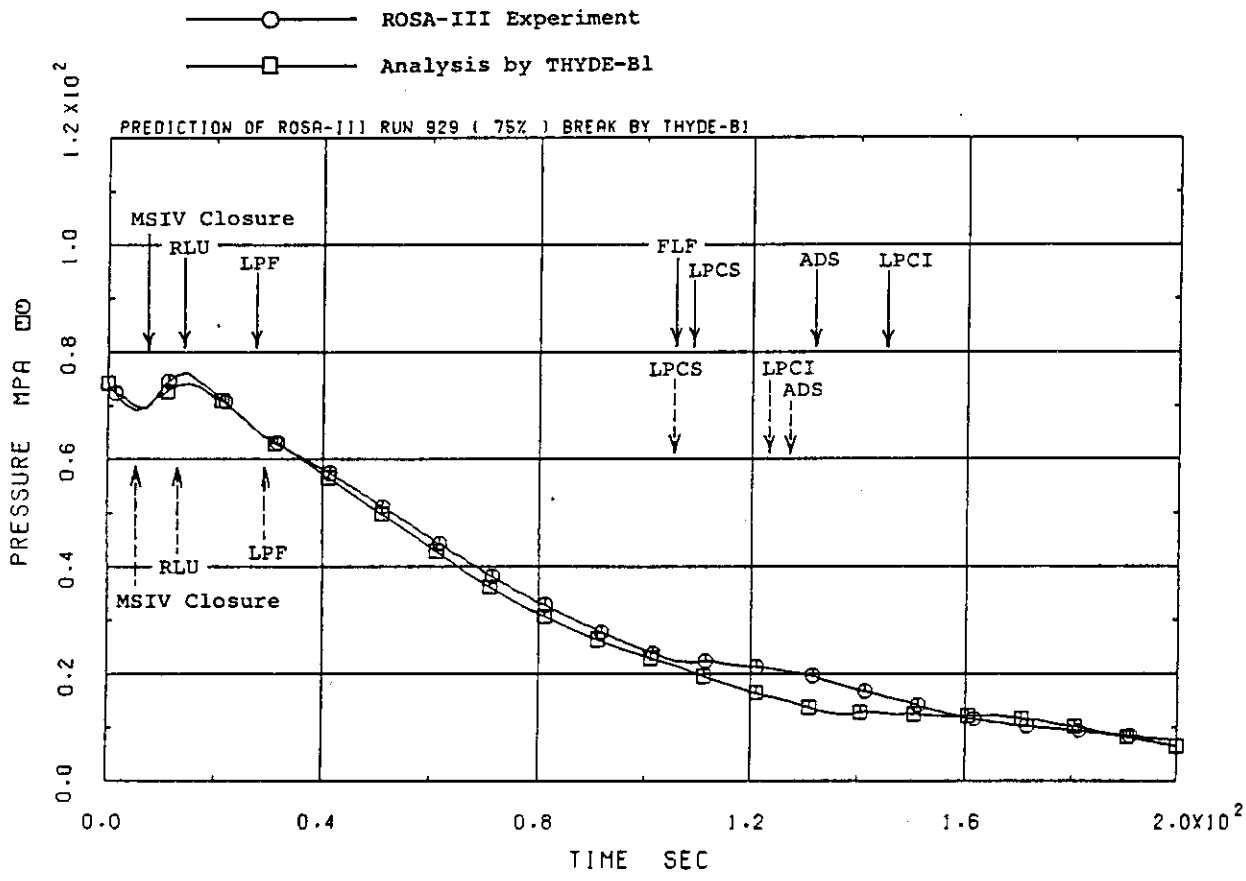

Fig. B.29 Measured vs. calculated system pressures - 75 % break test

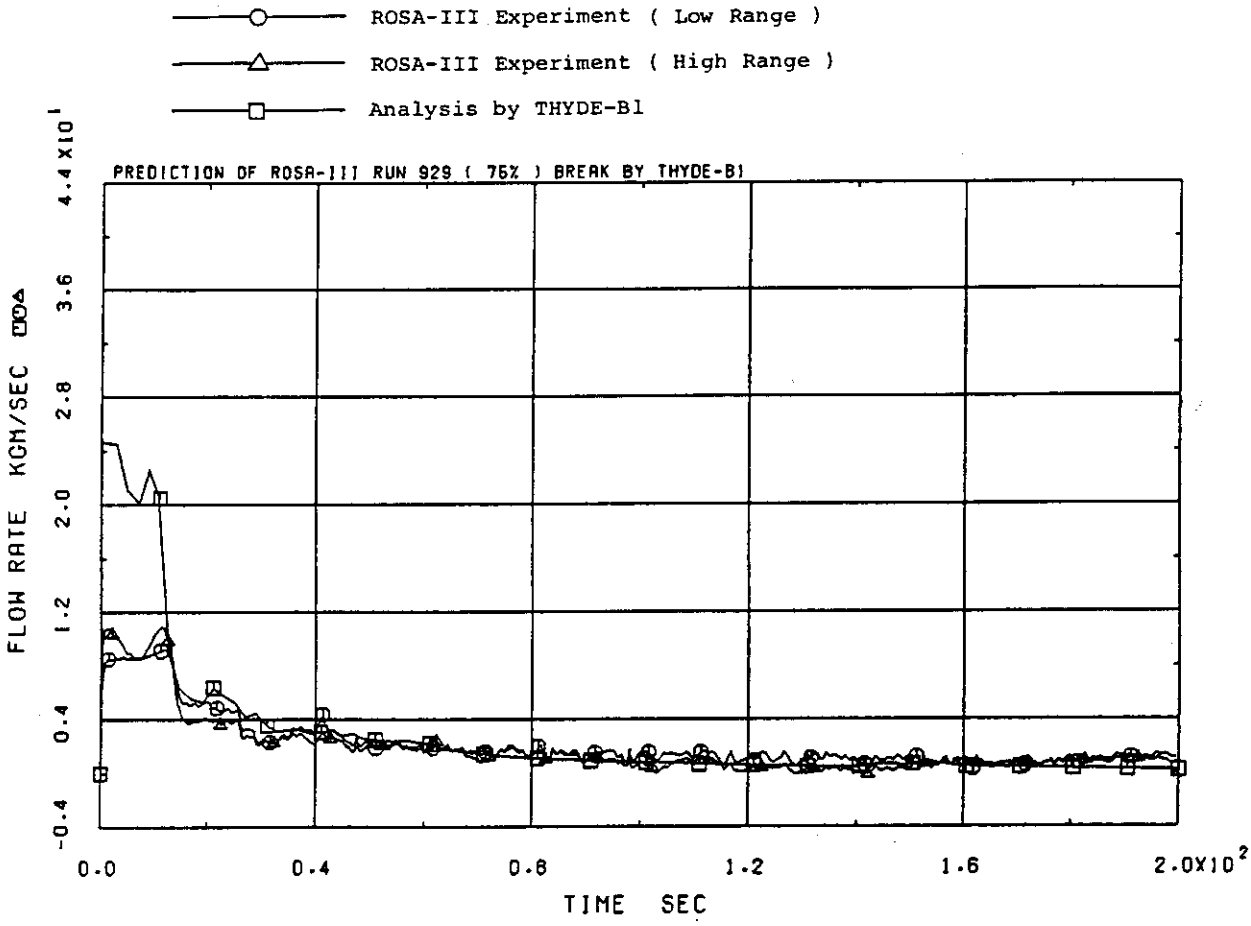

Fig. B.30 Measured vs. calculated break flow rates - 75 % break test

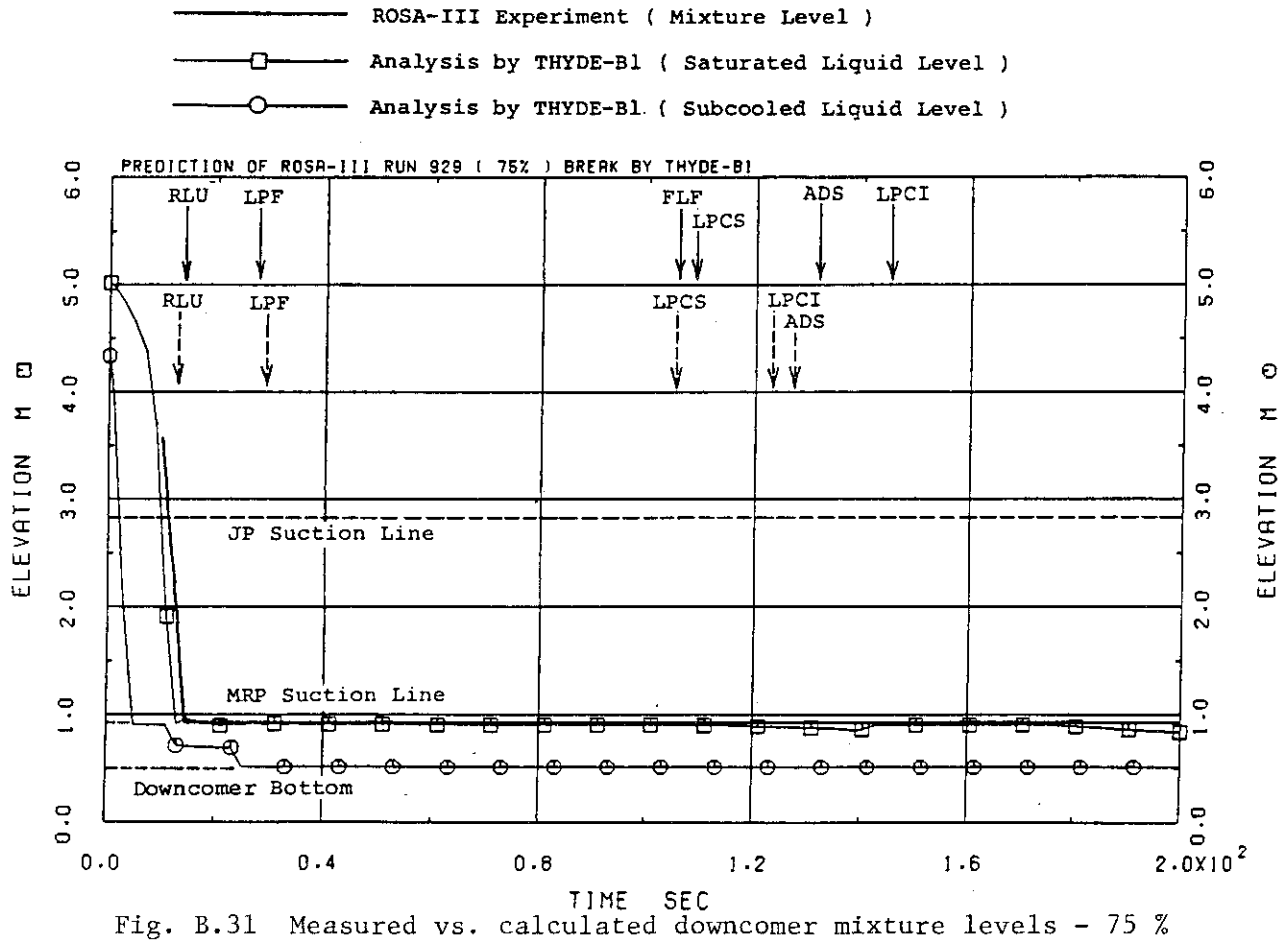

Fig. B.31 Measured vs. calculated downcomer mixture levels - 75 % break test

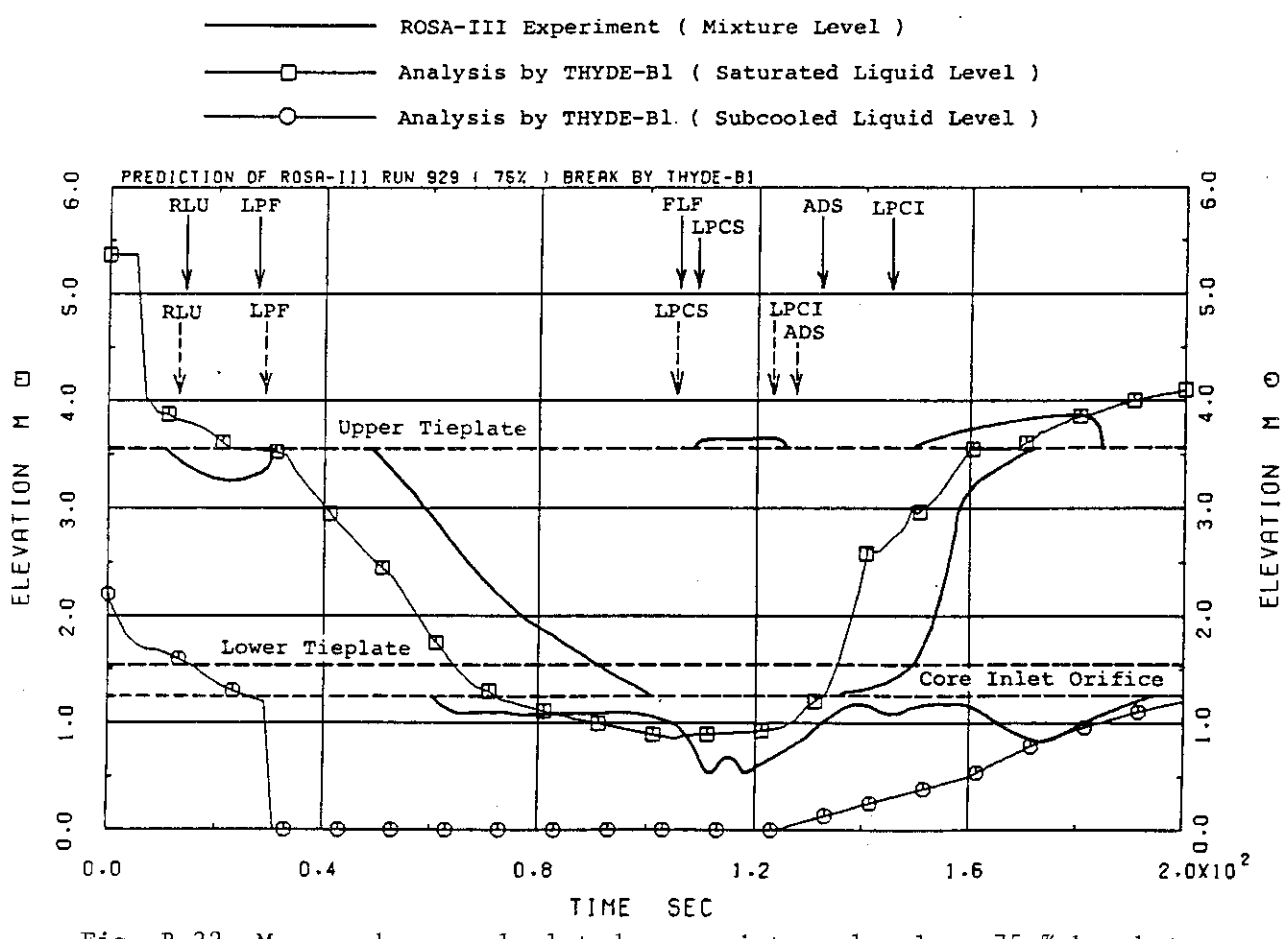

Fig. B.32 Measured vs. calculated core mixture levels - 75 % break test

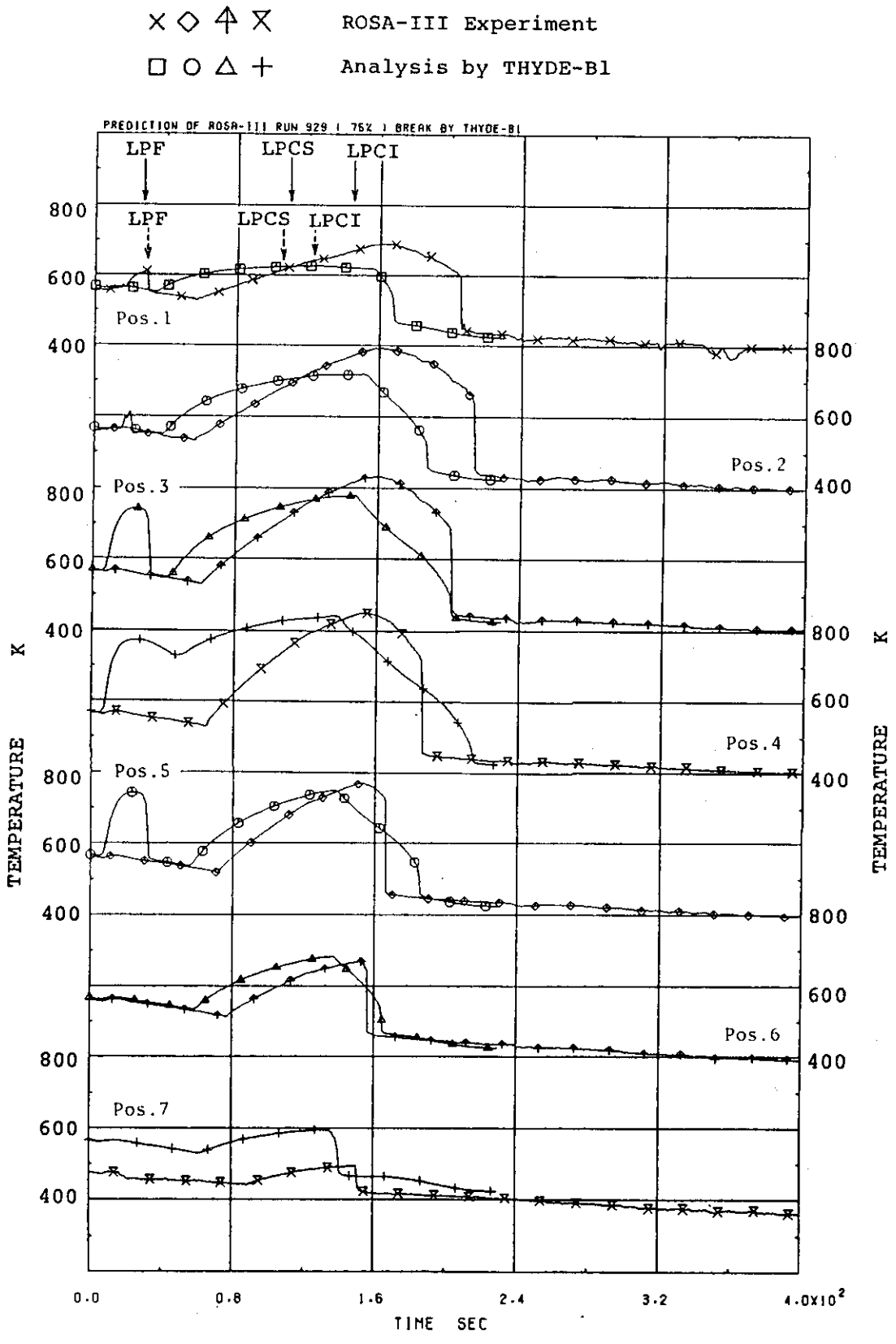

Fig. B.33 Measured vs. calculated peak-power rod temperatures - 75 % break test

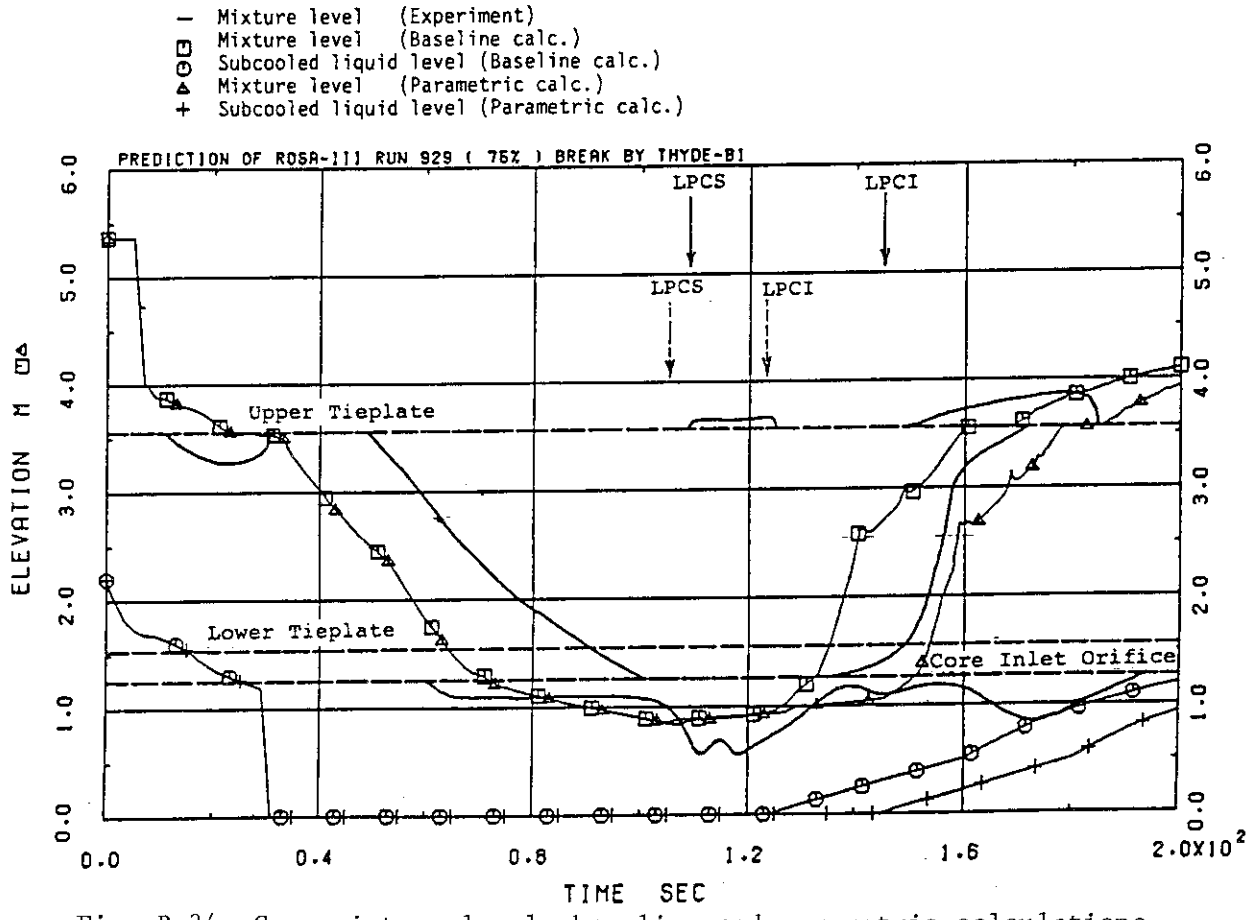

Fig. B.34 Core mixture level: baseline and parametric calculations - 100 % break test

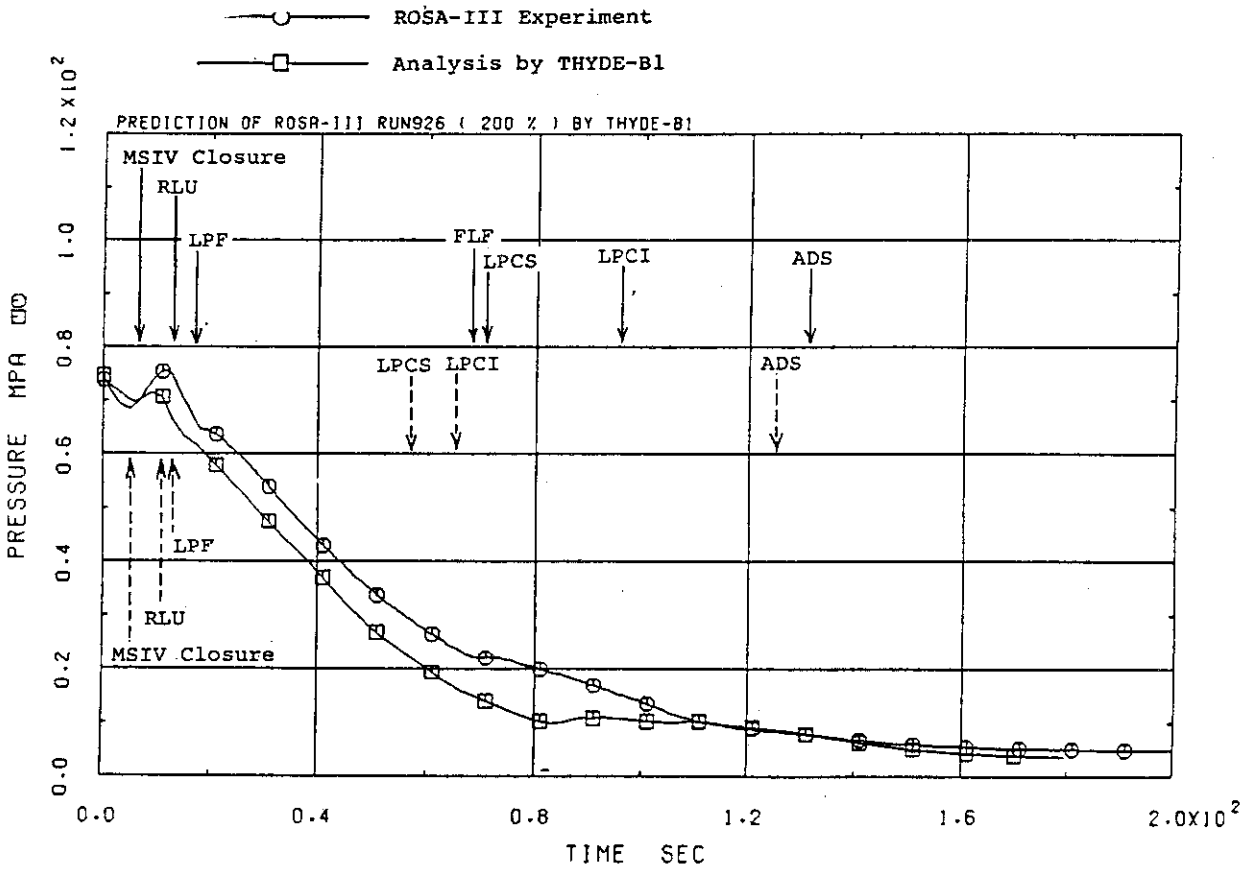

Fig. B.35 Measured vs. calculated system pressures - 200 % break test

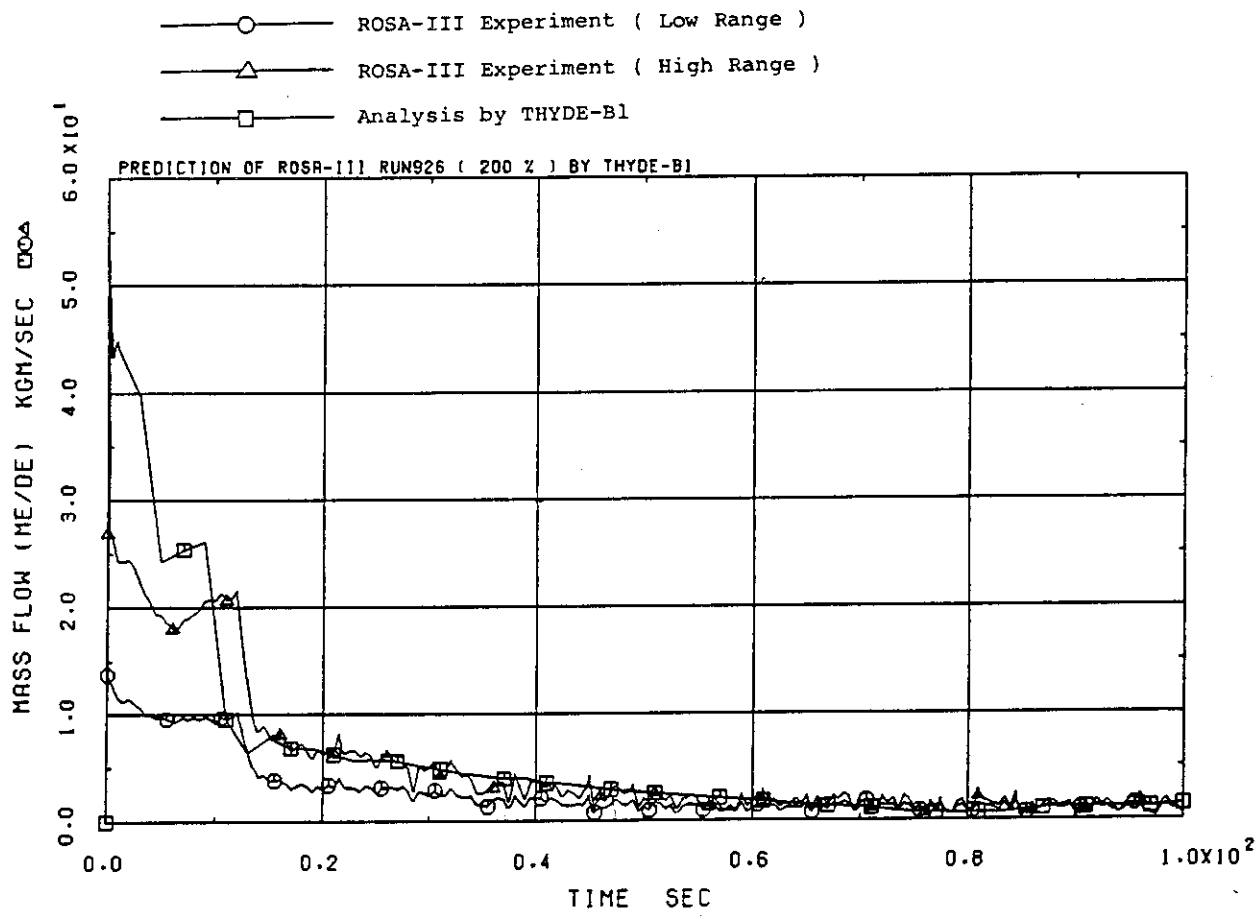

Fig. B.36 Measured vs. calculated break flow rates - 200 % break test

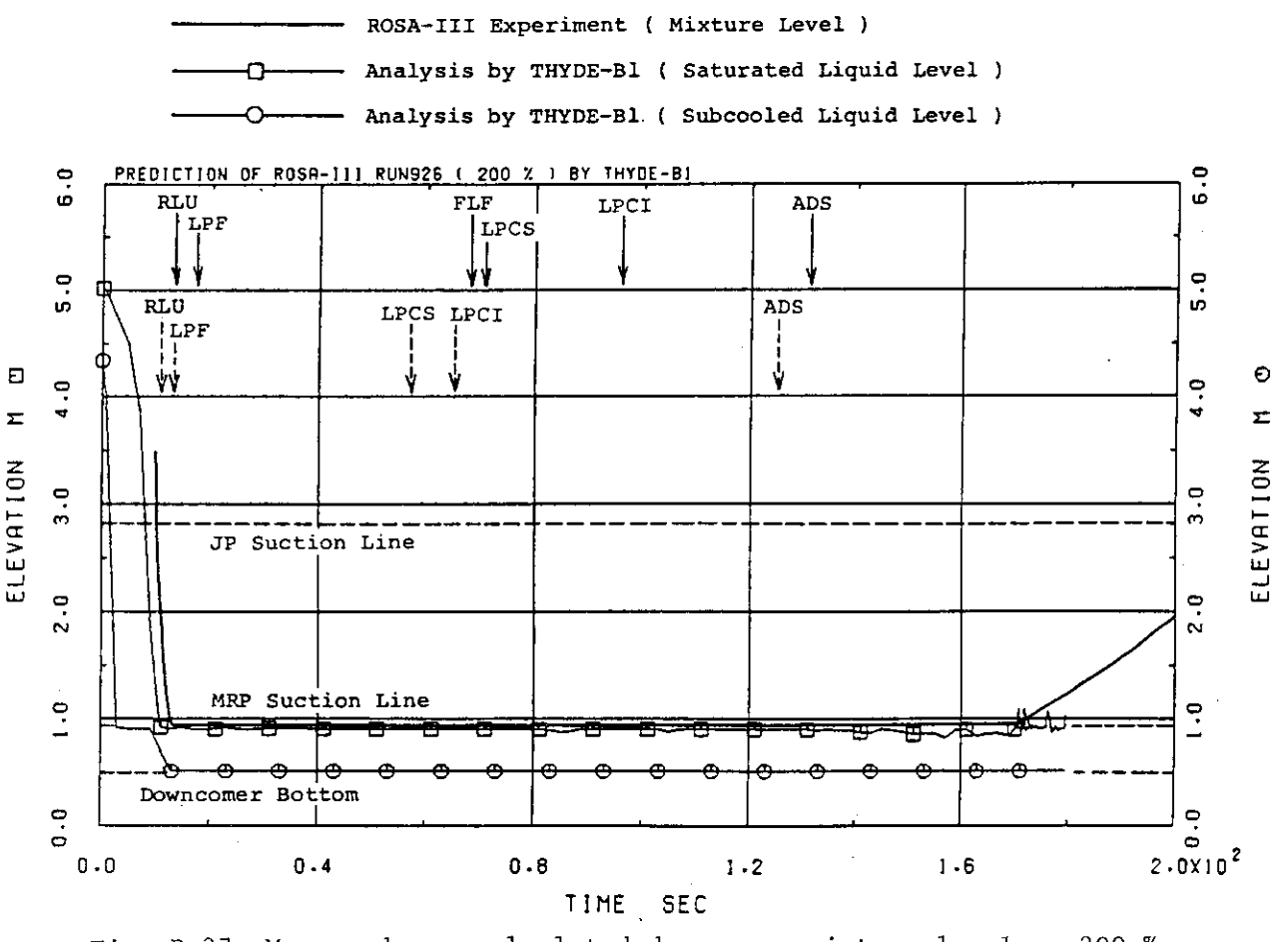

Fig. B.37 Measured vs. calculated downcomer mixture levels - 200 % break test

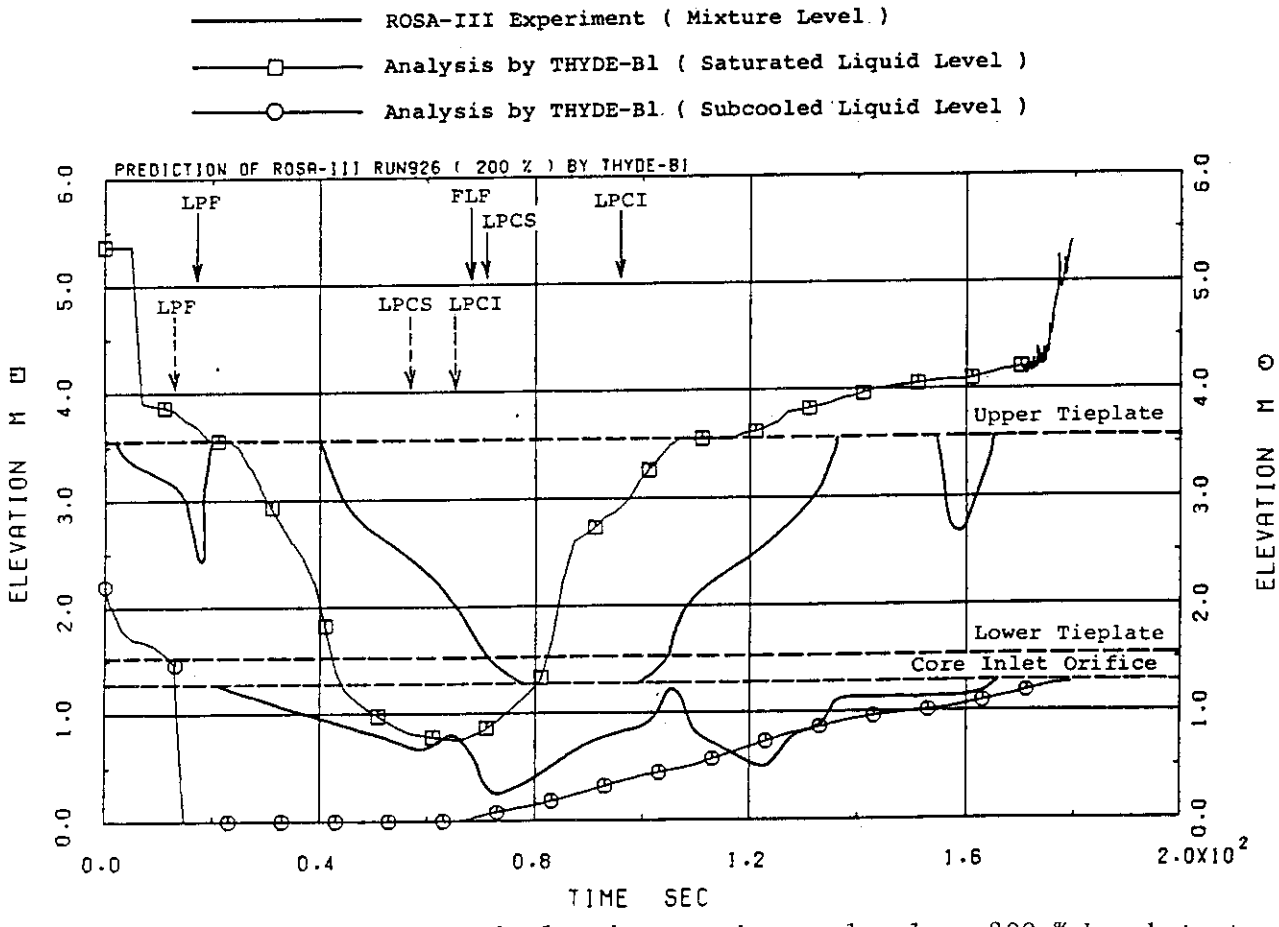

Fig. B.38 Measured vs. calculated core mixture levels - 200 % break test

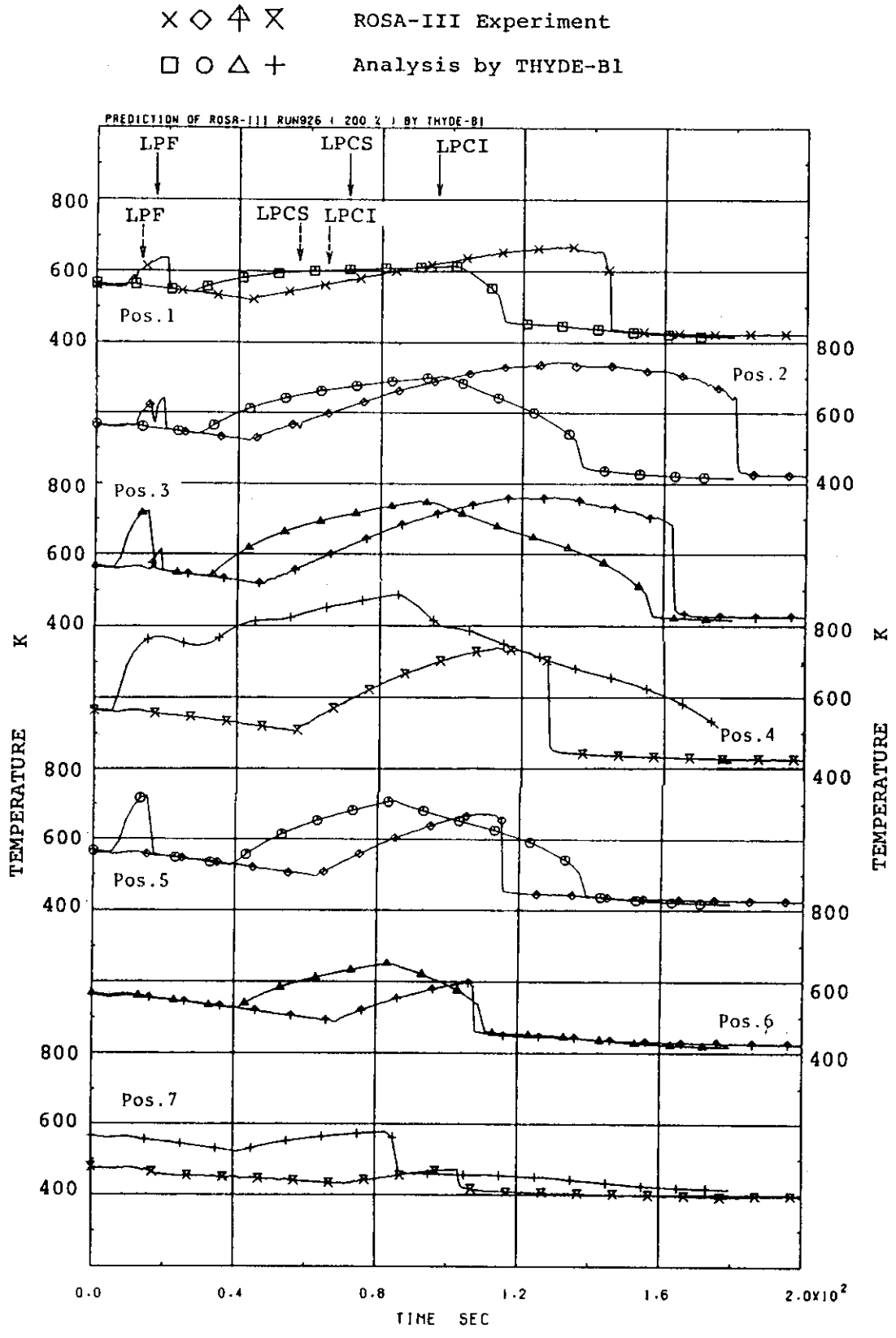

Fig. B.39 Measured vs. calculated peak-power rod temperatues - 200 % break test

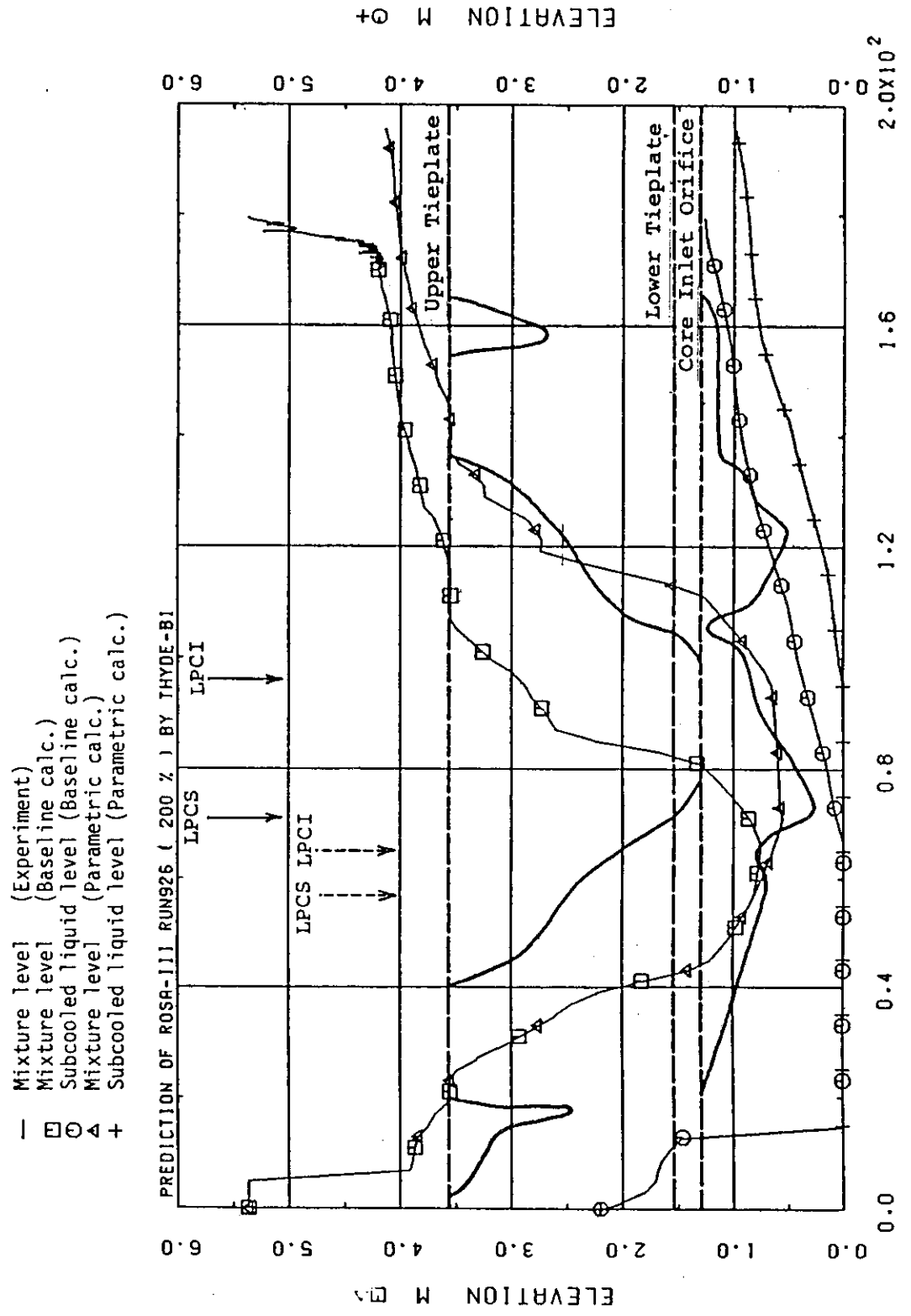

Fig. B.40 Core mixture level: baseline vs. parametric calculations
－ 200 % break test